Dipl.-Ing. Henrik Seefeldt

Flame retardancy of wood-plastic composites

BAM-Dissertationsreihe · Band 90
Berlin 2012

Die vorliegende Arbeit entstand an der BAM Bundesanstalt für Materialforschung und -prüfung.

Impressum

Flame retardancy
of wood-plastic composites

2012

Herausgeber:
BAM Bundesanstalt für Materialforschung und -prüfung
Unter den Eichen 87
12205 Berlin
Telefon: +49 30 8104-0
Telefax: +49 30 8112029
E-Mail: info@bam.de
Internet: www.bam.de

Layout: BAM-Referat Z.8

ISSN 1613-4249
ISBN 978-3-9815134-5-5

Flame retardancy of wood-plastic composites

vorgelegt von

Diplom-Ingenieur

Henrik Seefeldt

aus Berlin

Von der Fakultät III - Prozesswissenschaften

der Technischen Universität Berlin

zur Erlangung des akademischen Grades

Doktor der Ingenieurwissenschaften

Dr.-Ing.

genehmigte Dissertation

Promotionsausschuss:

Vorsitzender:	Prof. Dr. Walter Reimers
Berichter:	Prof. Dr.-Ing. Manfred H. Wagner
Berichter:	Prof. Dr. Michael Maskos

Tag der wissenschaftlichen Aussprache: 03.07.2012

Berlin 2012

D83

Zusammenfassung

Über das Brandverhalten von „Wood-plastic Composites“ (WPCs) und deren Flammschutz ist bislang wenig bekannt. Die Verwendung von WPCs ist in den vergangenen Jahren stetig gestiegen. Vor allem in ihrem Hauptanwendungsgebiet als Bodenbeläge verzeichnen WPC Materialien einen großen Marktanteil. Bis jetzt existiert jedoch noch keine Flammschutzlösung, die alle nötigen Anforderungen im Bauwesen erfüllt. Flammgeschützte Materialien sind jedoch vor allem für Innenanwendungen und im Bereich von Fluchtwegen unabdingbar. In dieser Arbeit werden zum einen grundlegende Mechanismen über das Brandverhalten von WPCs aufgeklärt. Zum anderen werden die Wirksamkeit und die Wirkungsweise verschiedener Flammschutzmitteln in WPC Materialien untersucht. Ein spezielles Augenmerk wird dabei auch auf Endprodukte aus WPC Materialien gelegt. WPC wurde dabei in seiner Hauptanwendung als Fußbodenbelag untersucht.

Das Brandverhalten wurde für Materialien und Produkte mit Hilfe von „Cone Calorimeter“ Untersuchungen und „Radiant Panel Tests“ bestimmt. Zudem wurden numerische Simulationen genutzt, um den Einfluss verschiedener thermischer Materialparameter auf das Brandverhalten zu erforschen. Des weiteren wurde das thermische Zersetzungsverhalten mittels thermogravimetrischer Methoden und spektroskopischen Untersuchungen ermittelt. Auf dessen Grundlage konnten Abbaumechanismen für WPC Materialen in Verbindung mit verschiedenen Flammschutzmitteln erstellt werden.

WPCs zeigen das gleiche Brandverhalten wie Holz, auf Grund des polymeren Anteils ist jedoch die Wärmefreisetzungsrate während der Verbrennung stark erhöht. Es konnte gezeigt werden, dass alle untersuchten Flammschutzmittel einen positiven Effekt auf das Brandverhalten von WPCs hatten. Beste Ergebnisse wurden durch Ammonium-Polyphosphat, Paxymer und expandierbaren Graphit erzielt. Expandierbarer Graphit war besonders in Verbindung mit rotem Phosphor sehr wirksam, da der Phosphor den gebildeten Rückstand stabilisierte. Neben dem Einfluss von Flammschutzmitteln konnte gezeigt werden, dass für WPC Fußbodendielen auch andere Einflussfaktoren, wie die Geometrie und der Feuchtigkeitsgehalt eine wichtige Rolle spielen. So weisen Hohlkammerprofildielen im Vergleich zu Vollprofilproben zwar eine verminderte Menge an brennbarem Material auf, die Flammenausbreitung ist jedoch stark erhöht.

Abstract

Up to now only little knowledge has been recorded about the fire behavior and flame retardancy of wood-plastic composites (WPCs). The use of WPCs has increased continuously in recent years. Especially in their main field of application as a decking material, WPCs present a big share of the market. To date no flame-retarded solution has been introduced for WPC materials that fulfils the necessary requirements. But flame-retarded materials are indispensable, especially for indoor use and the protection of escape routes. In this study basic knowledge about the fire behavior of WPCs is investigated first. Second, the effectiveness and mode of action of different flame-retardant additives is investigated. Special attention is drawn to products made of WPC material. Therefore WPC was further investigated in its main field of application as decking boards.

The fire behavior of materials and products was investigated by means of cone calorimeter measurements as well as radiant panel tests. Furthermore numerical simulations were carried out to study the effects of various thermal material properties on burning behavior. Thermal decomposition was studied using thermogravimetric methods and spectroscopic investigations. Against this background, models for thermal decomposition pathways were built for combinations of WPC material with different flame retardants.

WPCs show burning behavior similar to that of pure wood samples with an increased heat release rate due to polymeric fractions. It is shown that all investigated flame retardants had a positive effect on the burning behavior of WPCs. The best results were achieved by the flame retardants ammonium polyphosphate, Paxymer and expandable graphite. Especially in combination with red phosphorus, expandable graphite was highly effective because red phosphorus stabilized formed residue. Apart from the influence of flame retardants, other influencing factors like geometry and moisture content also played an important role concerning the flame retardancy of WPC decking boards. Indeed, hollow decking boards offer a reduced amount of combustible material, but their flame spread is increased in comparison to solid samples.

Content

1. Introduction

1.1. Preface

Composite materials are used in nearly every field of application to combine the positive attributes of different materials [1]. Wood-plastic composites (WPC) do the same. They combine two of the most widely used materials: wood and polyolefin polymers. WPCs consist of wood chips or wood flour used as a filler in a polymer matrix. The advantages are obvious. Thermoplastic polymers allow the use of the typical technologies to form thermoplastic materials, like extrusion or injection molding. In comparison to pure wood materials, more complex shapes can be formed. Wood chips or wood flour lend the compound higher stiffness and a natural look. Furthermore, wood presents a renewable material, which attracts special interest today in the interest of reducing the use of mineral-oil based polymers.

WPCs are used in nearly every field of application, but their main application is in construction engineering, with a main focus on decking for terraces and balconies. For decking material cost effectiveness is very important. For this reason mainly commodity polymers like polyethylene (PE) or polypropylene (PP) are used. For decking in outdoor use another important property of WPC material becomes relevant. Wood is prone to microbacterial degradation. Covered by polyolefin polymer, contact with water and biodegradating fungi are minimized and thus microbacterial degradation is reduced significantly.

Especially for construction engineering, fire poses a dangerous risk. In Germany alone, fire causes damage of around three billion euros each year, and more than 500 people lose their lives [2]. One big disadvantage of WPC material is its high fire risk due to the incorporation of polymeric material. The heating values of commodity polymers like PE or PP are more than two times higher than those of wood [3]. To reduce the fire risk in construction engineering, flame-retardant concepts are necessary. Concepts of flame retardancy are based on different approaches. They are divided into three categories: organizational, technical and constructional concepts. Organizational concepts describe organizational provisions like the creation of an escape plan. Technical concepts are based on technical fire protection installations like fire detectors, fireproof doors and so on. Constructional concepts of flame retardancy imply the reduction of the fire risk of materials and devices themselves. The work in this thesis is based on constructional concepts of flame retardancy. The fire risk of materials is reduced mainly by incorporating flame-retardant additives. The basic principles of flame-retardant additives are given in section 2.3. In the mean time flame retardants containing halogens have become ever less desirable due to toxicity and ecological risks [4, 5]. For this reason only non-halogenated flame retardants were used in this study.

1.2. Scope of the work

The goal of this thesis is to reduce the fire risk of WPC devices by using constructional concepts of flame retardancy. Therefore WPC materials with enhanced flame-retardant properties need to be investigated. Furthermore the mechanisms leading to enhanced material properties should be examined.

In a first step basic principles of WPC burning were investigated to obtain fundamental knowledge to build on the development of flame-retarded WPC material. In a second step various flame-retardant additives were tested in WPC material to increase flame-retardant properties. Furthermore, mechanisms of action of flame-retarded additives and their interaction with WPC material were investigated. The third part of this work focuses on a WPC product. Apart from investigations of enhanced material properties, other aspects were also explored, e.g. the influence of the geometry of WPC components needed to achieve a flame-retardant system. Decking boards were chosen as a product due to their main field of application.

2. Background

2.1. Combustion of polymers

To start combustion three components are necessary: fuel, oxygen and an external heat source to heat up a material. In many cases heat input is due to radiation. The heat input is than described by the external flux minus the energy loss due to reradiation and convection [6]. Heat input prior to ignition is explicitly given in *Formula 2.1*.

$$\dot{q}_{net} = \dot{q}_{ext} - \dot{q}_{loss} = \dot{q}_{ext} + \varepsilon\sigma(T_{sam}^4 - T_{amb}^4) - h_c(T_{sam} - T_{amb}) \tag{2.1}$$

In the formula ε describes the emissivity, σ the Stefan-Boltzmann constant, T_{sam} the sample surface temperature, T_{amb} the ambient temperature and h_c the surface convective heat transfer coefficient. Inside the solid material, the temperature distribution is described by the heat conduction equation, whereas κ displays thermal conductivity, C_v the heat capacity at constant volume and ρ the density. The heat conduction equation is given in *Formula 2.2*.

$$\frac{\partial T}{\partial t} = \left(\frac{\kappa}{C_v \rho}\right)^2 \frac{\partial^2 T}{\partial^2 x} \tag{2.2}$$

If the temperature inside the polymer is high enough it will start to decompose. The region of decomposition is called the pyrolysis zone. With progressive combustion the pyrolysis zone will move through the polymer. The products released during thermal decomposition depend strongly on the kind of polymer. They can be gaseous, or liquids and tar. Together with oxygen from the surrounding air they react exothermically, resulting in flaming combustion. Most of the reactions are radical chain reactions [7]. During combustion the entire amount of oxygen is consumed, so that the atmosphere at the pyrolysis zone is assumed to be inert. The heat input into the polymer during combustion expands to another part, indicating thermal feedback from the flame. Heat input after ignition is than represented by *Formula 2.3*.

$$\dot{q}_{net} = \dot{q}_{ext} - \dot{q}_{loss} + \dot{q}_{fla} \tag{2.3}$$

In addition, many polymers form a carbonaceous residue made of aromatic structures (*Figure 2.1*) [8]. Under inert conditions during flaming combustion the residue will increasingly transform into aromatics under the release of gaseous components that support flaming combustion. Under reactive conditions char becomes oxidized, resulting in glowing combustion. This occurs after the flames are already extinguished.

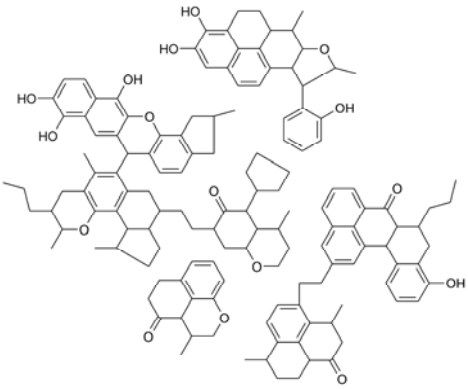

Figure 2.1: Carbonaceous residue formed during combustion of a char-forming polymer

For a char-forming polymer, mass loss during thermal decomposition is given by the rate constants of fuel and char production reactions (*Figure 2*) [9, 10]. The resulting mass loss rate can be determined using *Formula 2.4*.

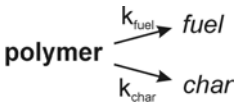

Figure 2.2: Simplified thermal decomposition reaction of char-forming polymers

$$\frac{\partial m_{sam}}{\partial t} = -k_{fuel} m_{sam} - k_{char} m_{sam} \tag{2.4}$$

It is assumed that the rate constants of pyrolysis have an Arrhenius form [6, 11] (*Formula 2.5*).

$$k = A \exp\left(\frac{-E_a}{RT}\right) \tag{2.5}$$

The only products of complete combustion are water and CO_2. If combustion is incomplete, additional CO, smoke and other gases are released. Incomplete combustion occurs, for example, if insufficient oxygen is available. Smoke is defined as a dispersion of solid or liquid particles in a gas flow of combustion products and air [12, 13]. CO is also released during glowing combustion of carbonaceous residue. The process of polymer combustion is summarized in *Figure 2.3*.

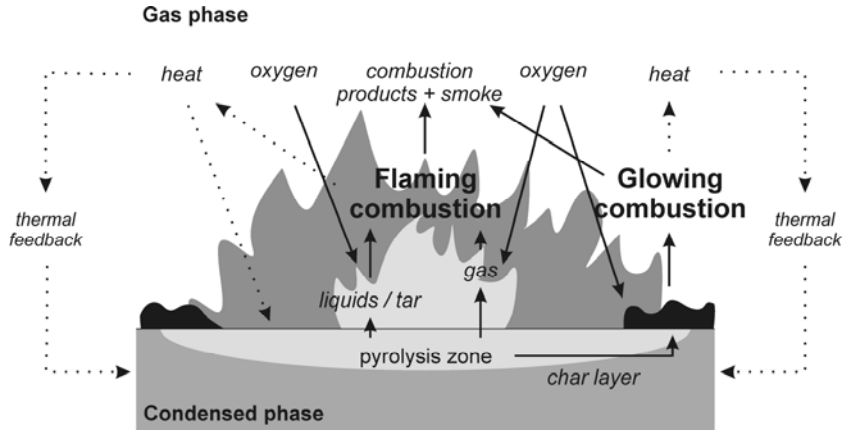

Figure 2.3: Schematic description of polymer combustion (heat transfer is plotted with dashed lines)

2.2. Large-scale fire propagation

In a large-scale real-term fire scenario, like a room fire, for example, more than one burning item is present. The progression of such a fire depends on the interaction of different combustible materials. In the simplest case, this means how much combustible material is available. The availability of heat and oxygen also plays an important role. The fire progression can be described by its temperature-time diagram. It is divided into five stages (*Figure 2.4*).

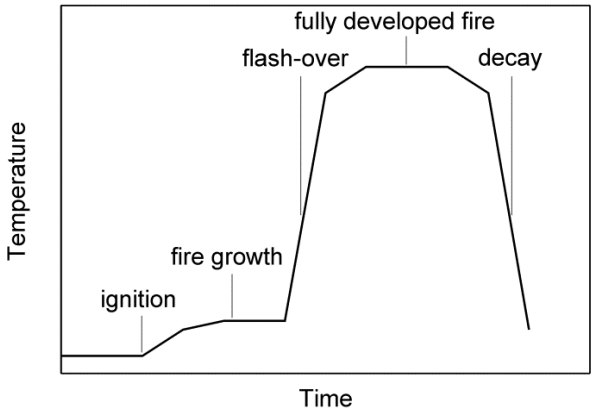

Figure 2.4: Schematic temperature-time diagram of a large-scale fire (for example, a room fire)

The first stage describes ignition. For this an external heat source is necessary. The first stage is followed by fire growth. The burning materials generate additional heat, which is used to ignite other objects. The growing fire generates more and more heat so that high amounts of pyrolysis gases are formed. The ignition of these pyrolysis gases induces a flashover. The fire spreads fast to all combustible material. Afterwards the fire is fully

developed. The fully developed fire remains as long as combustible material and oxygen is sufficient. If either of them decreases the fire decreases as well [14].

2.3. Flame retardancy of polymers

The aim of flame retardancy is to avoid the origin of a fire or to slow down fire propagation. Concepts of flame retardancy based on delaying the flashover so that it is still possible to extinguish the fire easily. Extinguishing can then be realized by firefighters or other people or other means like sprinklers. Flame retardants act during ignition or during fire growth. In later fire stages flame retardancy has hardly any advantage. If the whole room is burning it does not matter whether or not a single object is flame-retarded.

Flame retardants can act in the gas phase or in the condensed phase and their mechanism can be of physical or chemical nature [15-17].

The formation of a protective barrier is the main concept of flame retardancy in the condensed phase [18]. Barrier formation provides protection against heat transfer to underlying material [19, 20]. Furthermore a good barrier can also prevent the release of fuel gases. Some materials already form carbonaceous residue by themselves [21]. Flame retardants can enhance this formation or initiate residue formation in non-charring polymers. Carbonaceous residue also decreases the fire load by storing combustible material. Apart from aromatic structures, glassy residue also can be formed, as is typical for borates [22, 23].

Another flame retardant concept is to reduce the thermal feedback of the flame. Endothermic reactions can dissipate energy and cool down combustion. The release of water from metal hydroxides is one example for an endothermic reaction [24-26]. In addition, the release of incombustible gases dilutes the flame gases, reducing combustion efficiency [27, 28]. These effects are not so strong that large amounts of these additives are necessary. Typical filler contents of metal hydroxides of about 60 wt.% can achieve sufficient flame retardancy [29].

For polymer burning, heat transport phenomena play an important role. A change in the thermal conductivity and specific heat of the materials can also have a positive influence. An increase in thermal conductivity can delay ignition by removing heat from an irradiated surface and conducting it to underlying material.

A reduction of the heat of combustion is realized by flame inhibition [30]. Highly reactive radicals are the engine of combustion. Trapping these radicals can prevent combustion or at least slow combustion down. Effective radical trappers include halogens, but other additives like phosphorous compounds [31-33] also show good performance. Flame retardants also influence combustion products and smoke. Radical trapping inhibits radical chain reactions during combustion. This leads to an increase in products of incomplete combustion like smoke and CO.

Often the combination of different flame retardants or the combination of flame retardants and other additives achieves synergistic effects [34]. The best flame-retarded systems often contain more than one flame retardant.

2.4. Material fundamentals

All of the WPCs used in this work are made of a mixture of native woods and PP. Wood consists of three main ingredients: cellulose, polyose and lignin [35, 36]. Cellulose is made of D-glucopyranose units which are linked together (*Figure 2.5*). The degree of polymerization is about 9000 to 15000. Cellulose molecules have the tendency to form intra- and intermolecular hydrogen bonds. This supports the formation of crystalline regions. Most wood-derived cellulose is highly crystalline. Polyose is also composed of chains of sugar molecules, but it has a much lower degree of polymerization — about 100 to 200 on average. Lignin consists of a highly complex aromatic structure of phenylpropane units. A possible structure is given in *Figure 2.5* [37].

During thermal decomposition, in addition to water, CO and CO_2 biomass forms a broad range of decomposition products [38-40]. Cellulose forms fragments of their chains, which can be larger like levoglucosan or smaller fragments of cellulose monomers. Many other decomposition products are found as well, like methanol and furan derivatives [41, 42]. Lignin mainly decomposes into methoxy phenols which can easily recombine to form aromatic residue [43]. Lignin is mainly responsible for the formation of residue in biomass.

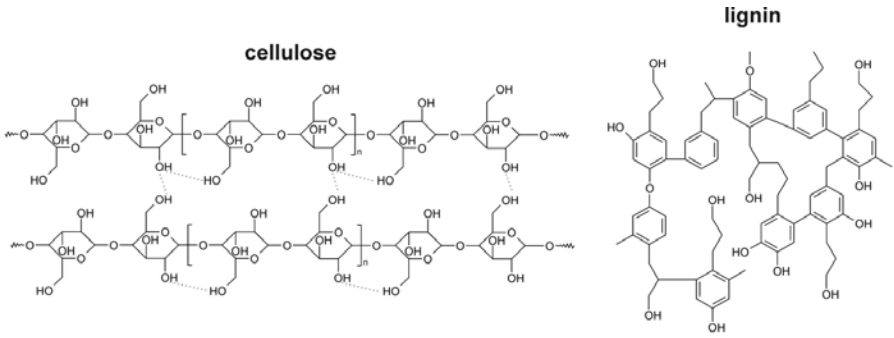

Figure 2.5: Chemical structure of two cellulose chains and possible chemical structure of lignin (some possible intra- and intermolecular hydrogen bonds inside cellulose are designated with dashed lines)

Often talc is added to WPC material to increase the cost-benefit ratio. Talc ($Mg_3Si_4O_{10}(OH)_2$) is a mineral filler which also shows flame-retardant effects. It is able to release water at high temperatures and increases the amount of residue, thus building a thermal barrier [44-46]. But in comparison to other mineral fillers like aluminum trihydroxide or magnesium hydroxide, the amount of water released is small.

Some of the flame retardants used in this work are common flame retardants for polymers like ammonium polyphosphate (APP), red phosphorus (RP) and expandable graphite (EG). They are already well established for polymers. The chemical structure of APP is shown in *Figure 2.6*. It is a typical agent of an intumescent system. Together with a blowing agent and a carbonization agent it is able to form cross-linked structures which increase the amount of residue [47-53]. As a carbonization agent polyamide 6 or pentaerythritol is often used [54, 55]. In contrast, in WPC no additional carbonization agent is necessary because wood is able to take on this function. In addition, the release of ammonia acts to dilute

flame gases. Red phosphorus (RP) is present in amorphous polymerized P_4 tetrahedrons. Apart from this form, phosphorus can also appear in white, black or violet modifications [56]. In flame retardancy RP can act in the gas phase by radical trapping and in the condensed phase. In combination with oxygen it forms phosphates which are able to cross-link carbonaceous structures [57-60]. Expandable graphite (EG) is a flame retardant which acts physically by creating a layer of expanded graphite worms on the top of a sample. The structure of EG is shown in *Figure 2.6*. It consists of graphite layers in which a blowing agent is incorporated (here, sulfuric acid). While heating up, sulfuric acid outgases and expands the graphite layers to form a protective barrier of graphite worms [61-65].

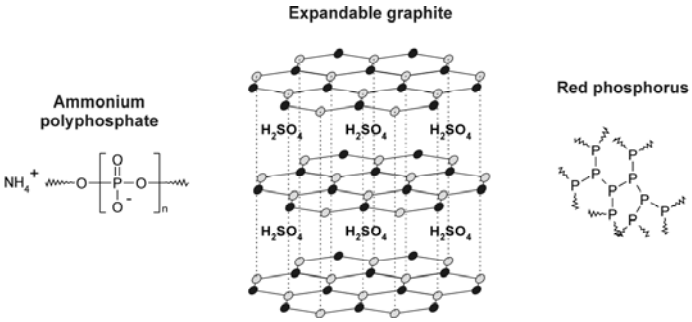

Figure 2.6: Chemical structure of ammonium polyphosphate, schematic description of expandable graphite and possible chemical structure of red phosphorus

In this work other flame retardants were used which are new and have not been studied before. They are commercially available and listed here under their trade name. The first one is called Disflamoll TP LXS 51064 (Dis) and is available from Lanxess. It is based on a salt of an ammonium phosphonate ester. Its chemical structure is given in *Figure 2.7*. The flame retardant was developed to protect wood. To flame-retard WPC, wood was impregnated with Dis solution before processing.

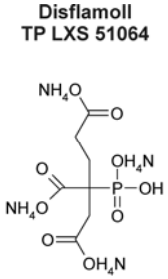

Figure 2.7: Chemical structure of Disflamoll TP LXS 51064

Another flame retardant investigated in this work is Paxymer (Pax). Pax is a mixture of different ingredients. Chemical analysis showed that Pax contains red phosphorus,

polydimethylsiloxane, magnesium hydroxide and calcium hydroxide. Struktol SA 0832 (Str) is a char-forming flame retardant based on nitrogen. Spectroscopic measurements identified peaks of melamine and borates inside the flame retardant.

2.5. Methods

2.5.1. Thermogravimetry

Thermogravimetric analysis (TG) is used to study the thermal decomposition of polymeric material. TG measures the change in the sample mass as a function of temperature or time [66]. Measurements can be performed under different atmospheres. Using nitrogen as a purge gas, TG measurements refer to pyrolysis that occurs under inert conditions. By use of synthetic air, thermo-oxidative decomposition is investigated. Measurements under air were also used to investigate the thermal stability of formed residues. Therefore the sample was first pyrolyzed under inert conditions. Afterwards purge gas was switched to a reactive atmosphere to oxidize carbonaceous residue.

2.5.2. Fourier-transform infrared spectroscopy

A Fourier-transform infrared spectrometer (FTIR) consists of four main parts. The first part is a beam source which emits an infrared light beam. Afterwards the beam is split with an interferometer into its single wavelengths and then measured one at a time. When the beam hits a sample they interact. Infrared light is able to activate chemical bond vibrations. FTIR uses these phenomena to identify chemical compositions of unknown samples. After the beam leaves the sample, wavelengths which were used to activate chemical bond vibrations are now missing from the spectrum of the beam. Detection of the beam enables the chemical composition of the sample to be inferred. But the beam is still split into its single wavelengths which are measured one at a time. Therefore the technique of Fourier transformation is used to convert the wavelengths back to spectra. Accordingly, the last part of a FTIR is a processor which Fourier transforms the measured data. FTIR can be used in different scenarios. In transmission mode the beam passes through the whole sample and is detected on the other side. Attenuated total reflection (ATR) reflects the beam at the surface.

FTIR is often coupled with TG (TG-FTIR) to identify decomposition products released during TG experiments [67].

2.5.3. Differential scanning calorimetry

During a differential scanning calorimetry (DSC) measurement a sample is exposed to a temperature profile and measured in comparison to an inert reference [66]. Due to exothermic or endothermic processes inside the sample, for example phase changes, there is a difference between the heat flow inside the sample and the reference. Heat flow is plotted over temperature to gain insight into the chemical and physical phenomena inside the sample at different temperatures. DSC is also able to determine the heat capacity of a material. Therefore the measurement needs to be compared to a reference with a known heat capacity.

2.5.4. Hot disc

Hot discs use the transient plane source method to measure the thermal conductivity of a sample. In this method a sensor is placed between two samples of the same material. The sensor serves simultaneously as a continuous plane heat source and a temperature monitor. While heating up, the sensor measures the temperature increase inside the sample over time. The change in temperature over time is used to calculate the thermal conductivity of the material measured.

2.5.5. Cone Calorimeter

The cone calorimeter simulates a well ventilated fire under a fixed external heat flux [68, 69]. The heat flux can vary between 0 and 100 kWm^{-2} to simulate different fire scenarios. 35 kWm^{-2} is equivalent to a burning wastepaper basket, and 70 kWm^{-2} simulates a fully developed fire. A scheme of a cone calorimeter is shown in *Figure 2.8*.

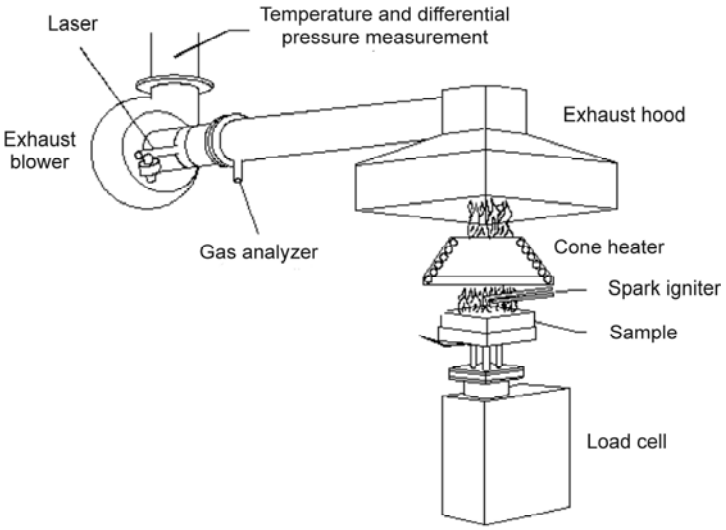

Figure 2.8: Schematic description of the assemblies of a cone calorimeter

An exhaust blower ensures that the ventilation of the sample is constant at a defined value. The sample is placed under a conic heater to induce external heat flux. The formed pyrolysis gases of the sample are ignited by a spark igniter. This ensures good reproducibility in the time to ignition. The combustion products of the burning samples are trapped by an exhaust hood. Here further analyses are made. The main parameter measured is the heat release rate (HRR). The measurement of the HRR relies on the measurement of the consumed oxygen during a combustion. The heating value per consumed mass of oxygen is constant within an error of 5% for nearly all polymers and amounts to about 13.1 kJg_{O2}^{-1} [70, 71]. The reason is that most of the polymers consist of

almost only hydrogen and carbon, and during a complete combustion water and carbon dioxide are the only reaction products. In incomplete combustions carbon monoxide is formed as well. But the difference in oxygen consumption in comparison to complete combustion is within the margin of error. The flow rate of the exhaust gas is analyzed by temperature and differential pressure measurements. The oxygen concentration in the exhaust gas is measured by a paramagnetic oxygen analyzer. The values need to be corrected by taking into account that the exhaust gas is diluted by carbon dioxide and carbon monoxide. Further on, values of carbon monoxide are important data on their own (CO production and total CO production). Released smoke (smoke release rate and total smoke release) and the weight of the burning sample are also analyzed. The smoke is measured by the absorption of transmission of a laser beam and mass is detected by a load cell. Another important output datum is the effective heat of combustion (EHC). It results from dividing HRR by the mass loss rate.

2.5.6. Pyrolysis combustion flow calorimeter

A pyrolysis combustion flow calorimeter (PCFC) is based on the combustion principle of a polymer. In a first step the material is pyrolized under inert conditions, and in a second step the decomposition products are oxidized [72-75]. Pyrolysis occurs in an oven with a constant heating rate and a nitrogen atmosphere. Afterwards the decomposition products are conducted to another oven with an atmosphere of 20 vol.% oxygen and 80 vol.% nitrogen. These are combusted and the HRR is measured by the oxygen consumption method, as in the cone calorimeter. Apart from measurement of HRR, results are the total heat evolved (THE) and the amount of residue formed after the experiment.

2.5.7. Radiant panel test

Radiant panel test (RPT) is a test to characterize the burning properties of flooring materials [76]. It simulates fire propagation in a corridor which is already burning on one side. RPT measurements can be used to classify flooring materials [77]. Samples are exposed to an external flux and ignited by an additional burner on one side. Measurement results are the distance of fire propagation. Furthermore the temperature inside the RPT is measured with a thermocouple.

2.5.8. Scanning electron microscopy

Scanning electron microscopy (SEM) is able to take pictures of samples with very high magnification. Light microscopy is limited in its magnification by the wavelength of visible light. SEM uses an electron beam with a much shorter wavelength. During the measurement electrons are shot onto a sample and interact with the sample. Different interactions can occur. Electron beams can break other electrons of the sample out of their shells (secondary electrons). Electrons of the beam can be scattered back, or electrons of the sample can be lifted to higher energetic levels. If they fall back to their origin they emit the x-ray radiation typical for their energy level. The detection of secondary and back-scattered electrons is used to build a picture of the sample. X-ray radiation is used to

determine the composition of the sample (EDX) because every element emits its typical spectrum.

2.5.9. Fire Dynamics Simulator

Fire dynamics simulator [78-80] (FDS) is a computer program which is based on computational fluid dynamics to simulate the evolution of fires. It is normally used to simulate fires on a large scale, for example room fires, but other approaches also use FDS for small-scale fire simulation [81].

To simulate fire scenarios the according geometries need to be set up and the thermal properties of the materials used need to be parameterized. Combustibles can be solids, liquids and gases. In solid material, heat conduction is calculated by a one-dimensional heat conduction equation. Convection and other hydrodynamic behavior of gases and liquids are calculated by solving the Navier-Stokes equation by using large eddy simulations. The fuel gas production rate of solids and liquids goes back to an Arrhenius approach. The combustion of exposed fuel gases is realized in FDS by a mixture fraction model. The mixture fraction model combines fuel and oxygen conservation in a single equation

3. Experimental

3.1. Sample compositions of WPC material

All WPC formulations investigated in this study are based on a mixture of native woods and a polymer matrix made of PP. Apart from PP, polymer matrix also contains different additives like color pigments and process stabilizers. Flame-retarded WPC formulations contain additional flame-retardant additives. On the one hand, WPCs with single flame retardants were investigated; on the other, WPCs with combinations of different flame retardants. A list of all investigated WPC material compositions with and without single flame retardants is given in *Table 3.1*. Apart from the influence of different flame retardants, the effect of talc on combustion and the impact of different amounts of wood were also investigated. Numbers in brackets indicate the amount of wood, or, if listed after an additive, the amount of the given additive.

Table 3.1: Composition of WPC materials without and combined with a single flame retardant

	Wood / wt.%	**PP / wt.%**	**Talc / wt.%**	**Flame retardant / wt.%**
WPC(50)	50	50	-	-
WPC(60)	60	40	-	-
WPC(70)	70	30	-	-
$WPC(55)_{talc}$	55	40	5	-
$WPC(50)_{talc}$	50	45	5	-
$WPC(50)_{talc(10)}$	50	40	10	-
WPC-APP	50	35	-	15
WPC_{talc}-APP	50	30	5	15
WPC_{talc}-EG	50	30	5	15
WPC_{talc}-RP	50	40	4.5	5
WPC_{talc}-Str	50	30	5	15
WPC-Dis(3)	60	37	-	3
WPC-Dis(10)	53	37	-	10
WPC-Pax	49.2	40	-	10.8

WPC formulations with combinations of flame retardants are presented in *Table 3.2*. It gives three formulations for combinations of EG and APP, and one combination of APP and RP as well as EG and RP. Subscript numbers indicate the ratio of flame retardants to each other.

Table 3.2: Composition of WPC materials with combined flame retardants

	Wood / wt.%	PP / wt.%	Talc / wt.%	EG / wt.%	APP / wt.%	RP / wt.%
WPC_{talc}-EG_1APP_3	50	30	5	3.75	11.25	-
WPC_{talc}-EG_1APP_1	50	30	5	7.5	7.5	-
WPC_{talc}-EG_3APP_1	50	30	5	11.25	3.75	-
WPC_{talc}-APP_3RP_1	50	30	5	-	7.5	2.5
WPC_{talc}-EG_3RP_1	50	30	5	7.5	-	2.5

Samples were either extruded or flat-pressed by Werzalit (Germany), or injection-molded at the Technische Universität Berlin (TU Berlin, Germany). WPC(70) was an exception. It is a commercially available WPC fabricated by Megawood sold in the form of solid decking boards. The samples were cut to dimensions of the according measurements. Flat-pressed samples are formulations containing Dis and Pax, whereas samples with combinations of different flame retardants as well as WPC_{talc}-APP, WPC_{talc}-EG and WPC_{talc}-RP were injection-molded. Samples of residual compositions were extruded. WPC_{talc}-APP was also manufactured by extrusion.

3.2. Sample properties of WPC decking boards in end-use conditions

Apart from studying the fire behavior of WPC material, investigations on decking boards made of WPC were also carried out. For decking boards, the effect of geometry plays an additional role. Decking boards are available in solid and hollow geometries. Both geometries were extruded. The decking boards are shown in *Figure 3.1*. The solid geometry is called S1 and the hollow geometry H1. Exact dimensions are given in *Figure 3.2*. Dimensions in *Figure 3.2* are already based on samples for cone calorimeter measurements, where a 100 x 100 mm slab was cut out of the decking board while maintaining the original height.

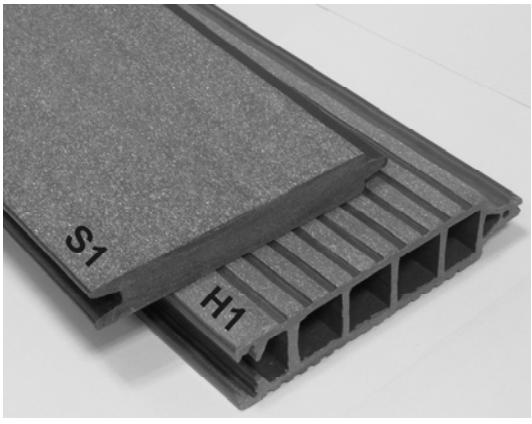

Figure 3.1: Investigated WPC decking boards in the solid (S1) and hollow (H1) forms

For investigations on the effect of the hollow form, additional samples with variations in the dimensions of cavities were created. First the height of cavities was varied, and then the width of cavities. The samples were extruded as solid geometries and afterwards the cavities were milled out of the samples (geometries H2 – H7). In addition, a solid sample (S2) with the same initial mass as H2 was created. The material composition of these samples was WPC(70). The samples and their dimensions are given in *Figure 3.2*.

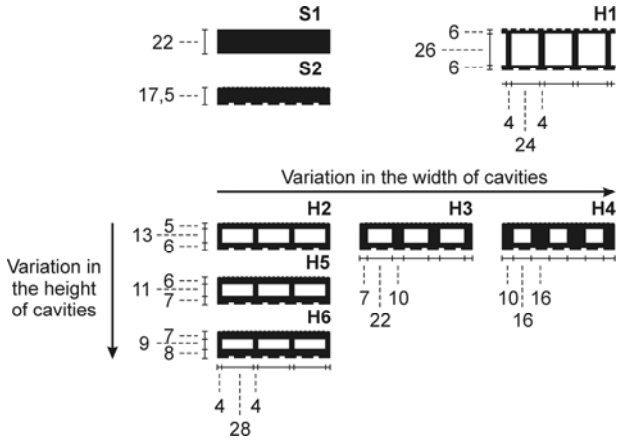

Figure 3.2: Geometries of WPC decking boards used in cone calorimetric measurements

To increase the slip resistance of WPC decking boards, surfaces of timber pilings often contain incorporated bars. The impact of surface profiles was tested on plates with thicknesses of 5 mm including surface bars. The exact dimensions of surface bars are given in *Figure 3.3*. Additional investigations were carried out on plates without surface profiles but varied thicknesses (3, 4 and 5 mm).

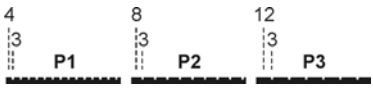

Figure 3.3: Samples for investigations of the impact of surface profiles

Apart from investigations of the effects of different geometries of WPC decking boards, the influence of different moisture contents was also studied. Therefore in a first step the samples were dried in an oven at 363 K. Afterwards they were inserted into a water bath of 368 K until they absorbed a defined amount of water. The moisture content of the samples were 5 wt.%, 10 wt.% and 16 wt.% as well as a completely dry sample.

3.3. Measurement parameters

3.3.1. TG/TG-FTIR

TG measurements (TGA SDTA 851 Mettler Toledo) entailed heating from room temperature up to 1173 K at a heating rate of 10 $Kmin^{-1}$. The gas flow rates of the corresponding gases were 30 $mlmin^{-1}$. All specimens were milled to powder before testing. Sample masses were 5 mg to enable isothermal heating inside the sample. The samples were measured in an alumina pan. For coupling with FTIR (Nexus 470, Nicolet), decomposition gases released in TG were conducted with a transfer line to the FTIR spectrometer. The transfer line was heated up to 523 K and the gas cell of the FTIR spectrometer was heated up to 533 K to avoid condensation of the decomposition products.

3.3.2. FTIR measurements in the condensed phase

FTIR investigations (Nexus 470, Nicolet) of the condensed phase were carried out in transmission mode. The samples were placed in a heatable cell (Linkam cell 600) and measured over varying temperatures. To enable transmission, WPC samples were pressed into thin films. For this a heatable press (Graseby Specac) was used. Samples were pressed at 423 K for 3 min. For measurements of the pure flame retardant Dis, a solution of Dis was dropped onto a KBr window and dried at room temperature. FTIR measurements had a temperature ranging from room temperature up to 770 K. Heating rates were 10 $Kmin^{-1}$. Samples were tested in inert atmosphere under nitrogen with a gas flow rate of 100 $mlmin^{-1}$.

3.3.3. DSC

DSC measurements (DSC Seiko 7020) were performed in a temperature range from 193 K to 493 K. Samples were milled to power before testing and the sample masses for DSC measurements were 3 mg. The samples were tested in alumina pans. For measurements of heat capacity sapphire was used as a reference material.

3.3.4. Hot disc

The sensor of the hot disc (Hot Disk Transient Plane Source TPS 2500 apparatus, Hot Disk AB) was placed between two plates with the same material composition and dimensions of 100 x 100 x 3 mm.

3.3.5. PCFC

The pyrolyzer from PCFC (Fire Testing Technology) was heated at a heating rate of 1 Ks^{-1} up to a maximum temperature of 1020 K. The atmosphere inside the pyrolyzer consisted of pure nitrogen. Afterwards the decomposition gases were combusted in an atmosphere of 20 vol.% oxygen and 80 vol.% nitrogen. The temperature inside the combustor was 1170 K. Samples were tested as powders with sample masses of 3 mg in alumina pans.

3.3.6. Cone calorimeter

Cone calorimeter tests (Fire Testing Technology) were carried out according to the standard ISO 5660 [82]. All specimens were tested under an irradiation of 50 kWm^{-2}. For further investigations additional tests were carried out at 35 and 70 kWm^{-2}. The sample size was 100 to 100 mm with different sample heights [83]. Height of injection moulded samples amounted 5 mm whereas extruded samples had heights of 3 mm and flat pressed samples of 9 mm. The distance between the cone heater and the specimen was 25 mm and the exhaust blower had a flow rate of 24 ls^{-1}. The unexposed side of the sample was wrapped in aluminum foil and laid horizontally under the cone heater. A layer of ceramic wool was placed underneath the sample to prevent strong heat flow from the sample to the sample holder. All samples were conditioned before testing for at least one week at 298 K and 50% humidity.

Samples forming aromatic residue show afterglow effects after the fire extinguishes. Afterglow makes it difficult to recognize the end of burning. The time of flame-out was defined as the point of zero smoke release rate. For a few samples this criteria was not practical due to minimal smoke emission. For these samples the time of flame-out was defined as the point of a critical mass loss rate. The critical mass loss rate was determined from samples with sufficient smoke emission and amounted to 0.02 gs^{-1}.

3.3.7. RPT

RPTs (Custom Scientific) comply with the DIN EN ISO 9239-1:2002 standard [76]. Samples were measured in end-use geometries as hollow or solid decking boards. The dimensions of the specimens were 1050 x 230 mm. For decking boards with widths less than 230 mm, two boards were connected according to their end-use geometry. Specimens were conditioned at 298 K and 50% humidity for at least one week before testing. External heat flux during the measurement was 10.9 kWm^{-2} after 110 mm and dropped down to the end of the sample. The burner was fed with a propane gas flow of 0.026 ls^{-1}.

3.3.8. SEM

SEM (FEI) images were recorded with a secondary electron detector using an acceleration voltage of the primary electron beam of 10 kV. For EDX measurements the acceleration voltage was increased to 15 kV to increase the production of x-ray radiation. Before the measurements all samples were sputtered with gold to enable sufficient electrical conductivity.

4. Burning of WPC material

4.1. Thermal properties and decomposition of WPC and its individual components

As already mentioned in section 2.1, burning depends strongly on the thermal properties of a material, which are responsible for heat conduction and thermal decomposition. This chapter gives an overview of the thermal properties of the investigated WPC material and its individual components: wood and PP.

Thermal conductivity of WPC(60) at room temperature amounted to 0.35 $Wm^{-1}K^{-1}$ (*Table 4.1*). By comparison, the thermal conductivity of PP was measured to be 0.26 $Wm^{-1}K^{-1}$, which correlates well with values in the literature [84]. Measurements of the thermal conductivity for wood mixture used in WPC(60) would cause errors due to the finely chopped structure. Therefore the thermal conductivity of a pine plate measured perpendicular to the grain is given. The thermal conductivity of wood depends strongly on its spatial orientation [85]. It increases while measured along the grain. In contrast, the thermal conductivity of WPC material does not depend on orientation, because the wood particles inside the material are orientated isotropically. For the burning rate and time to ignition thermal conductivity plays an important role. High thermal conductivity increases the time to ignition and reduces the burning rate. If a sample is heated with an external heat source, it is easy for materials with high thermal conductivity to conduct heat away from the claimed section, which reduces the local temperature and thus increases the time to ignition and reduces the burning rate.

Table 4.1: Thermal conductivity of WPC material and individual components at 293 K

Material	**Thermal conductivity / $Wm^{-1}K^{-1}$ ± 0.02**
WPC(60)	0.35
PP	0.26
Pine	0.18

Figure 4.1 gives the heat capacity of WPC(60) and its individual components. Values of WPC(60) lie between those of wood and PP. At room temperature the heat capacity of WPC(60) amounts to 1.2, of PP 1.7 and of wood 0.7 $Jg^{-1}K^{-1}$. Values increase with increasing temperature. Furthermore PP and WPC(60) show a strong increase between 400 and 440 K due to the melting of the polymer. High heat capacity offers advantages because it reduces the heating rate of the material. Higher amounts of energy are necessary to increase the temperature of the material and the decomposition temperature is reached later.

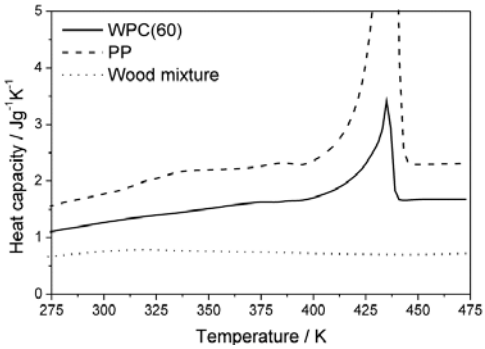

Figure 4.1: Heat capacity of WPC material and individual components as a function of temperature

Thermal decomposition is measured with TG experiments (*Figure 4.2*). PP starts to decompose at about 670 K in a single step and forms hardly any residue. The residue obtained in the TG experiment was 0.5 wt.%. Wood starts to decompose much earlier, at about 490 K. Due to its composition of different ingredients, the decomposition of wood is divided into two steps. The first step is attributed to decomposition of polyose and the second to the decomposition of cellulose. Lignin decomposes during both polyose and cellulose decomposition [86]. The mass and mass loss rate (MLR) of a TG experiment is given in *Figure 4.2*. The theoretical thermal decomposition of wood ingredients is designated by a dotted line. The residue obtained in the TG experiment from a mixture of different woods used in the WPCs was 15.3 ± 0.5 wt.%.

The thermal decomposition of WPC consists of steps from wood and from PP. MLR curves in *Figure 4.2* are calibrated such that the amount of wood and PP is the same for measurements of single components as for wood and PP inside WPC(60). For wood no change in thermal decomposition was found. PP decomposition shows a slight shift in the peak of MLR. Pure PP has its peak in MLR at 732 K, while PP in WPC(60) shows a value of 740 K. This shift is due to a physical interaction with the formed residue of wood. The residue forms a barrier around the undecomposed PP and therefore reduces the heat flow to the PP. Furthermore the peak of MLR of pure PP is increased in comparison to PP in WPC(60). The polymer matrix in WPC materials contains additives that substitute PP and therefore reduce its content inside the sample. WPC(60) forms 10.8 ± 0.5 wt.% of residue.

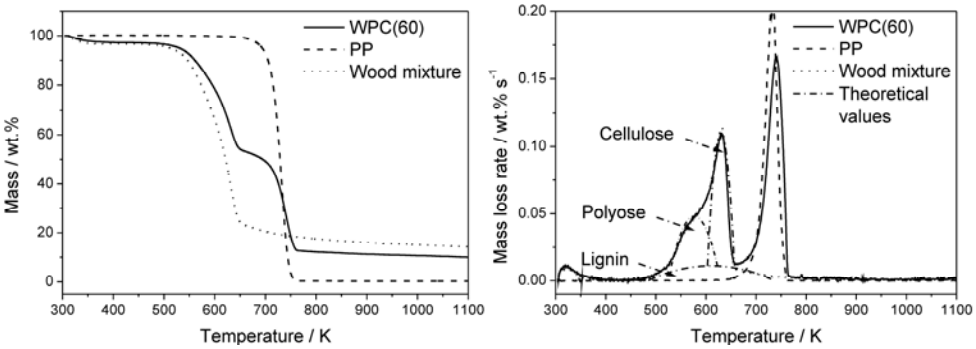

Figure 4.2: TG experiments: mass (left) and mass loss rate (right) for WPC(60), PP and wood. Theoretical decomposition of components of wood (lignin, polyose and cellulose) is marked in the mass loss rate curve.

4.2. Fire behavior of WPC and its individual components

The fire behavior of WPC material and its individual components was tested with the cone calorimeter. Wood and PP exhibit totally different fire behavior. The burning of PP shows only a single peak in its HRR curve (*Figure 4.3*). After ignition at about 26 s the HRR increases until it reaches the peak of heat release rate (pHRR). The evolved heat accelerates combustion and pyrolizes more and more material. The HRR drops after all PP is consumed. Due to the high heating values of PP of 42.9 $MJkg^{-1}$ (measured with PCFC), the pHRR is very intense. In contrast to PP combustion, wood releases much less energy that contributes to combustion (9.9 $MJkg^{-1}$ measured with PCFC). Furthermore, wood forms residue. The formation of residue leads to the typical burning behavior of char-forming polymers. It shows one peak at the beginning and one peak at the end of burning (*Figure 4.3*). Residue forms a thermal barrier which decreases the HRR. The more residue is formed, the more the HRR is reduced. Decay after 1.pHRR is caused by formation of residue. The rise at the end is due to the backing material underneath the sample [87]. Here the backing material was ceramic wool with low heat conductivity. When the burning front approached the back of the sample, heat was trapped inside the sample. The pyrolysis zone became broader and more fuel gases were formed during thermal decomposition. With use of other backing materials with high heat conductivity the last pHRR vanished.

WPC material exhibits the burning behavior of wood with an increased heat output. (Released heat of WPC(60) in PCFC was 22.6 $MJkg^{-1}$). It has two pHRRs as well (*Figure 4.3*), which are caused by the same effects as in wood combustion. Burning can be described as resembling many small wooden wicks in a PP melt. A look at the EHC displays two peaks as well, one at the beginning and one at the end. Burning, and especially the burning of wood, depends strongly on external conditions like heating rate and temperature [38, 86, 88]. Pyrolysis under low heating rates evolves mainly water, CO_2 and small fragments of molecules. An increase in the heating rate allows the formation of larger molecule fragments which have a higher heating value. At the beginning of burning the heating rate inside the WPC material is high. Accordingly the EHC shows higher values. The heating rate inside the WPC material dropped down after a protective char layer was formed. This resulted in a decrease in the EHC as well. The second peak of EHC (pEHC) has two causes. First, the heating rate inside the material rose because of the backing

effect. Second, at this time the fire gradually extinguished and oxygen from the surrounding air was able to come in contact with the formed residue. This resulted in char oxidation. The values of EHC for char oxidation are higher than for flaming combustion. Values of char oxidation are shown at the end of the measurement in *Figure 4.3*.

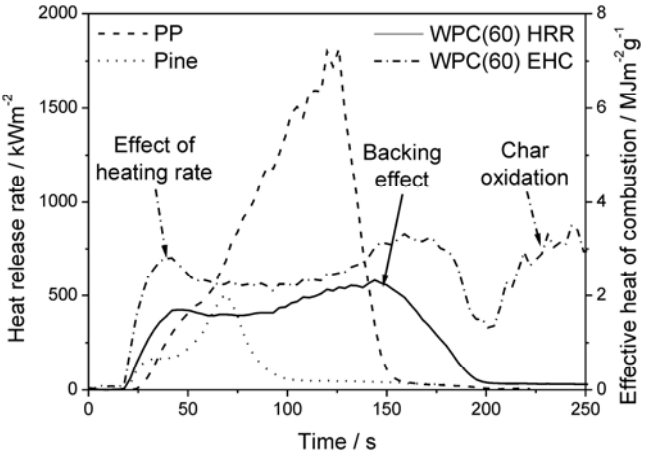

Figure 4.3: HRR of cone calorimeter measurements at an irradiance of 50 kWm^{-2} for WPC(60), PP and pine wood. For WPC(60) the EHC is given as well.

The sample thickness of the investigated WPC material was 3 mm. The burning behavior also depends on the sample thickness. Further investigations of varied sample thicknesses were carried out using the material WPC(70). Samples with increased sample thicknesses display different burning behavior at the end of the cone calorimeter test, whereas burning at the beginning is not affected. On the one hand the last pHRR decreases for increased sample thicknesses; on the other hand the amount of residue increases for increased sample thicknesses (*Figure 4.4*). For comparison the 1.pHRR, which presents a parameter at the beginning of the fire test, shows no dependency at all on sample thickness. The reason for changes at the end of burning lies in the formation of an increased amount of residue, which provides increased protection of the underlying material and thus reduces the last pHRR. The residue shows a varied chemical composition depending on the depth. Secondary decomposition processes of the formed residue also depend on barrier protection. Residue on the top consists almost entirely of aromatic structures, whereas residue at the bottom still contains many end groups. Furthermore, for thicker samples cracking becomes more important. The volume of the charred residue is decreased in comparison to unburned WPC material. The result is cracking of the residue (*Figure 4.4*). Cracking deteriorates the formed barrier so that heat and mass transport through the residue increase. Without cracking, samples would extinguish once the charred residue reaches a sufficient thickness.

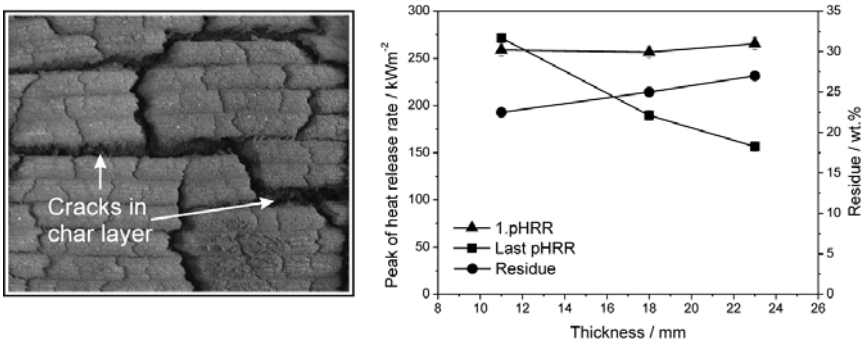

Figure 4.4: Influence of sample thickness — left: residue after cone calorimeter measurement of WPC(70) with sample thickness of 23 mm, right: cone calorimeter measurement of WPC(70) with different sample thicknesses

4.3. Influence of material composition

Investigations of fire behavior in section 4.2 were performed on WPC(60), which is based on a mixture of native woods and a polymer matrix made of PP. In this part the influence of variation in wood species and matrix polymers as well as the influence of the ratio between wood and polymer fraction is investigated. Furthermore studies were carried out concerning the influence of adding talc.

Wood shows a strong variation in chemical composition depending on the kind of species. Different species show different ratios of cellulose to polyose to lignin. Lignin is mainly responsible for the formation of residue, whereas cellulose and polyose are mainly responsible for the evolution of heat during flaming combustion. The cellulose and polyose are often combined as holocellulose to represent the complete share of polysaccharides. Apart from the wood mixture used in the WPC samples, five different wood species were studied. These are the native woods oak, pine, spruce, maple and beech. Oak represents the wood with the highest lignin content, and the lowest content of holocellulose. Lignin content decreases in the following order: oak > pine > spruce > maple > beech [37, 89]. *Table 3.2* gives the results of PCFC measurements. Best results were obtained from wood species with high lignin contents. Oak releases the least heat and forms the highest amount of residue. At the opposite end of the spectrum, beech releases the highest amount of energy and forms the least residue. The wood mixture used in WPC for this study showed THE of 9.9 $MJkg^{-1}$ and residue of 14.7 wt.%. These results could be further increased by using woods that have higher lignin content. But results for different wood species vary only marginally by comparison with results for PP and PE. Both PE and PP release about four times more heat than wood and do not form any residue. Most heat evolved during the combustion of WPC relies on the polymeric component inside the material. Furthermore the use of PE or PP makes no difference. Both achieve similar results. Polymers like PVC show strong enhancement of their fire properties. Due to its chemical structure it is able to form residue on its own and the THE is reduced by a factor of four in comparison to PP and PE [90-92]. Furthermore PVC is able to inhibit the flame during combustion. But PVC contains halogens which were released during combustion. Halogens are problematic because of their effects on health and the environment [4]. Therefore only halogen-free flame-retarded solutions were used in this thesis.

Table 3.2: PCFC measurements of different wood species and matrix polymers (total heat evolved and residue)

Sample	**THE / MJkg^{-1} ± 0.3**	**Residue / wt.% ± 0.4**
Wood mixture	9.9	14.7
Oak	9.6	16.8
Pine	10.4	14.9
Spruce	10.6	12.1
Maple	11.2	12.8
Beech	12.1	10.6
PP	42.9	0
PE	43.1	0
PVC	9.2	17.7

Due to the high difference in fire properties between wood and commodity polymers, the ratio between wood and polymer matrix inside the WPC has a much greater influence than substitution of wood with other species or PP with other commodity polymer types. On this account the variation in the wood/PP ratio was now investigated by means of cone calorimeter measurements. As already expected, WPC burns more vigorously with decreasing wood content and increasing PP content. The THE as well as the first and last pHRR increase with decreasing wood content (*Figure 4.5*). Residue formation shows the opposite behavior, decreasing with decreasing wood content because the formation of residue goes back to the wood content. Cone calorimeter measurements showed that WPCs with different wood contents exhibit a linear dependency on the amount of wood, at least in the range of 50 wt.% to 70 wt.% of wood. Residue, THE and peaks of HRR were the only differences in cone calorimeter measurement. The shape of all HRR curves was the same for all investigated materials.

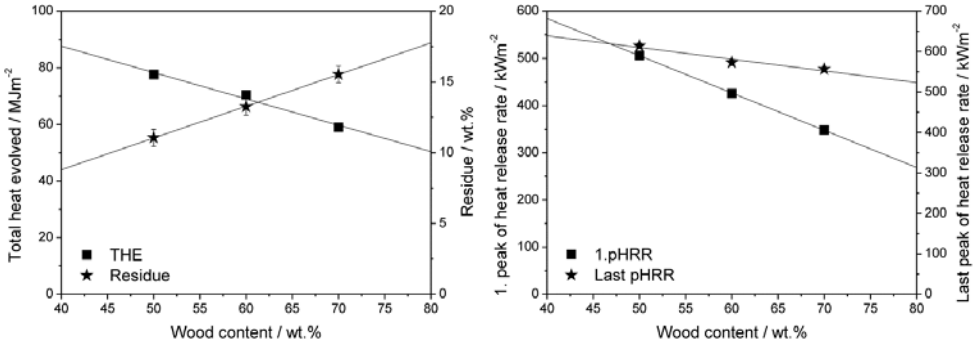

Figure 4.5: Comparison of the cone calorimetric values THE, residue, 1.pHRR and last pHRR for WPCs with different wood content

Addition of talc to WPC material resulted in only marginal differences in burning behavior in comparison to WPC without talc. Two samples with different talc content were analyzed by means of cone calorimetric measurements and TG experiments. Differences in the burning behavior of $WPC(55)_{talc}$ and $WPC(50)_{talc(10)}$ in comparison to WPC(60) are a reduction in fire load and an increase in the amount of residue. Reduction of the fire load is attributed to the substitution of combustible material with talc. Residue is increased from 13.3 ± 0.9 wt.% (WPC(60)) to 21.6 ± 0.9 wt.% ($WPC(55)_{talc}$) and 25.7 ± 0.9 wt.% ($WPC(50)_{talc(10)}$) in cone calorimetric measurement. The increase is due in part to the talc that remains in the residue. Furthermore talc prevents char from further decomposition processes by forming a shell around it. It is seen by comparing SEM pictures of the residue of WPC(60) and $WPC(50)_{talc(10)}$ (*Figure 4.6*). A decrease in the secondary decomposition processes of charred residue is the reason for the non-linear increase in residue through the addition of talc. An increase in residue from WPC(60) to $WPC(55)_{talc}$ is much greater than from $WPC(55)_{talc}$ to $WPC(50)_{talc(10)}$, although in each step 5 wt.% of talc was added.

TG experiments showed that talc undergoes no chemical interaction with WPC material. Decomposition temperatures remained the same as for WPC(60). All interactions between WPC and talc are of a physical nature.

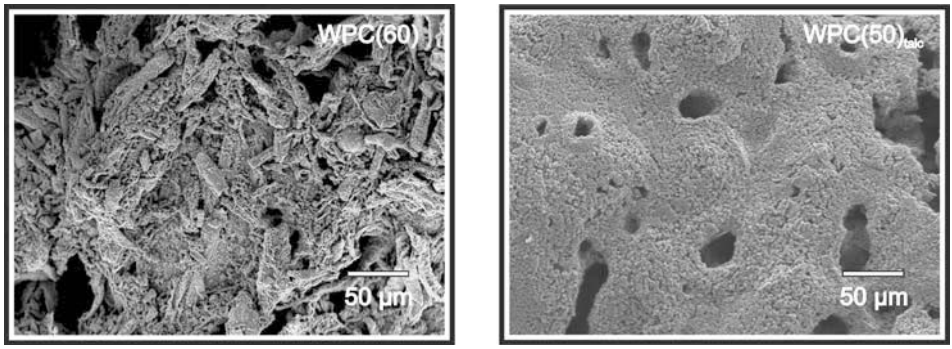

Figure 4.6: SEM images of residues of WPCs with and without talc

4.4. Simulation of the influence of material properties on WPC burning

The influence of different material properties on the burning behavior of WPC was studied using numerical simulations. Therefore cone calorimeter tests were simulated by the use of FDS. Different material properties were varied to investigate their impact on WPC burning.

4.4.1. Burning model and input parameters

In the simulation WPC is subdivided into five components to realize realistic burning behavior. The wood content consists of cellulose + lignin and polyose + lignin. Both parts are responsible for the formation of residue. Furthermore they contribute to the formation of fuel gas (*Figure 4.7*). The wood content constitutes 50 wt.% of the investigated WPC. PP decomposes only to volatile products which contribute to fuel gas production. WPC material contains 45 wt.% of PP. To focus on material compositions close to WPCs inside the market, 5 wt.% of talc was added in the simulation as well. Talc is an inert material and remains unchanged in the simulation inside the residue. An additional 2 wt.% of water was added to WPC in the simulation. Due to the additional amount of water all other fractions needed to be reduced accordingly. Water releases water vapor to act as a heat sink.

WPC	Fraction / wt.%		
cellulose + lignin	33.05	→	gas + char
polyose + lignin	15.95	→	gas + char
PP	44.1	→	gas
talc	4.9	→	inert
water	2.0	→	water vapor

Figure 4.7: Decomposition scheme of WPC components

Parameters for material properties are given in *Table 4.3*, *Table 4.4* and *Figure 4.8*. *Table 4.3* presents density, thermal conductivity and heat capacity, whereas temperature-dependent functions of heat capacity are given in *Figure 4.8*. For WPC material all values were measured. Measurements of heat capacity were carried out with DSC. For thermal conductivity values of WPC(60) from section 4.1 were used. Because all values are based on measurements of WPCs, no differentiation is made for the different components. These parameters were equal for all components of the WPC material.

Table 4.3: Input parameters for WPC(50)$_{talc}$ and its formed residue (values without reference were measured)

	Density / gcm^{-3}	**Thermal conductivity / Wm^{-1}K^{-1}**	**Heat capacity / Jg^{-1}K^{-1}**
WPC(50)$_{talc}$	1.2	0.35	C_p(T)
Char	0.3 [93]	0.1 [93]	C_p(T)

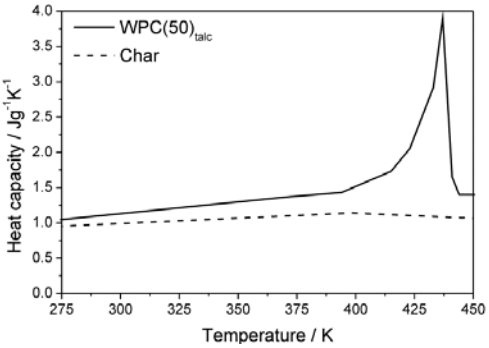

Figure 4.8: Measurements of heat capacity for WPC(50)$_{talc}$ and char as input parameters for simulation. Values obtained by DSC.

Parameters in *Table 4.4* are separated for the different components of WPC material. The heat of combustion was derived from PCFC measurements. For both cellulose + lignin and polyose + lignin the values for wood combustion from section 4.3. were used. Heat of combustion of PP is reduced in comparison to the values from section 4.3. due to the fact that, apart from PP, color pigments and other additives are also incorporated into polymer content. They reduce the amount of combustible material and therefore also reduce the heat of combustion of the polymer content. The value was determined by the PCFC measurement of WPC material, taking only the heat derived from PP into account. This is possible because wood and PP decompose under nitrogen in separate decomposition steps. Talc and water do not contribute to heat output during combustion. Instead water removes energy from the system by setting a heat of reaction. This is due to the ability of water to act as a heat sink. Arrhenius parameters of water evaporation were taken from the literature. Talc is an inert material which stays unchanged during combustion. The Arrhenius parameters for the decomposition of cellulose + lignin, polyose + lignin and PP were derived from TG measurement of WPC(50)$_{talc}$. Thereby it was assumed that all of these components decompose in one single decomposition step. The amount of residue formed was obtained from the TG measurement as well. The formation of residue of PP is again attributed to additional additives inside the PP content.

Table 4.4: Input parameters for components of WPC(50)$_{talc}$

	Heat of combustion / MJkg^{-1}	Heat of Reaction / MJkg^{-1}	Residue / wt.%	A	E / Jmol^{-1}
Cellulose + lignin	9.9	-	20	$4.0 \cdot 10^{12}$	$1.8 \cdot 10^{5}$
Polyose + lignin	9.9	-	20	$5.7 \cdot 10^{6}$	$1.01 \cdot 10^{5}$
PP	36.1	-	5	$2.0 \cdot 10^{20}$	$3.2 \cdot 10^{5}$
Talc	-	-	100	-	-
Water	-	2.26	-	10^{22} [78]	$1.62 \cdot 10^{5}$ [78]

Figure 4.9 gives the TG measurement of WPC(50)$_{talc}$ used to determine the Arrhenius parameters. For comparison, a simulation of the TG measurement with FDS is given. Both curves show a strong relation. The greatest difference lies in the continuous mass loss after the main decomposition steps have occurred (T > 800 K). The continuous mass loss relies on further decomposition processes inside the formed residue that were not included in the material model of the simulation.

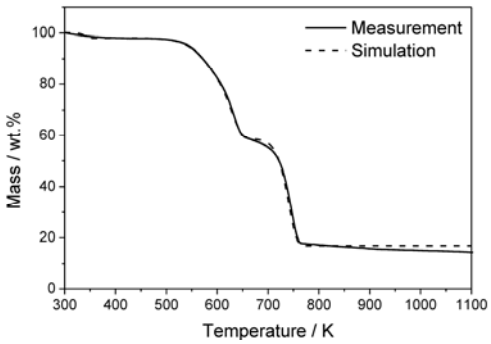

Figure 4.9: Simulation of TG experiment for WPC(50)$_{talc}$ in comparison to TG measurement

4.4.2. Simulation results

The simulated HRR of WPC(50)$_{talc}$ in the cone calorimeter in comparison to the measured HRR is given in *Figure 4.10*. At the beginning both curves are closely related, although the pHRR of the simulation is increased in comparison to the measurement. But after about 1200 s the correlation decreased. Burning after 1200 s is dominated by cracking of the charred residue. The sample burns almost only out of cracks in the residue. Cracking of the residue cannot be simulated with FDS. Here the residue forms a continuous layer above the undecomposed sample. After a sufficient thickness of the residue layer is reached, the sample extinguishes before all combustible material is consumed.

Simulation of the cone calorimeter experiment is used to study the impact of different material properties. Further simulations were carried out featuring variations in the heat capacity and thermal conductivity of WPC material and its formed residue. The heat of combustion of individual components of WPC was varied as well. The impact of the different properties is studied by comparing the pHRR values from the different simulations. PHRR is often used as a simplification of the HRR. Additionally, here it occurs at the beginning of the simulation where no error due to residue formation appears.

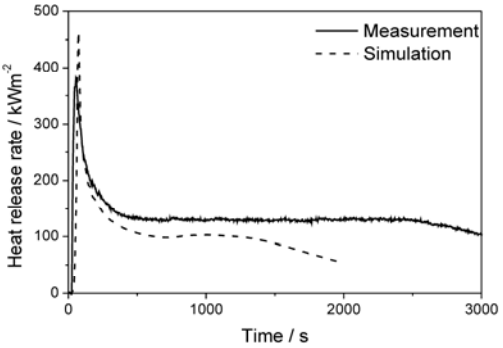

Figure 4.10: Comparison of HRR of cone calorimetric measurement of WPC(50)$_{talc}$ and simulated cone calorimetric measurement

Figure 4.11 gives the pHRR as a function of the different thermal properties of WPC material. All parameters were varied by 50%, 75%, 150% and 200% in comparison to the input parameters in section 4.4.1. The greatest impact is on the heat capacity of WPC material as well as the heat of combustion of PP content. Back in section 4.3. it was concluded that the high heat of combustion of PP presents one of the main problems for WPC combustion. A reduction in the heat of combustion of PP produces a strong decrease in the pHRR measured in the cone calorimeter. In addition, an increase in the heat capacity of WPC also yields a strong reduction in pHRR. Due to higher heat capacities the decomposition of the material is slowed down, because more energy is necessary to heat up the material. PHRR is not only decreased for increasing heat capacity, furthermore pHRR is shifted to later times, too. PHRR occurs at 40, 55, 68, 98 and 128 s for samples with 50%, 75%, 100%, 150% and 200% of initial heat capacity, respectively. Reducing the thermal conductivity of the residue also achieves positive effects. But its impact is diminished by the heat capacity of WPC and the heat of combustion of PP. The heat capacity of the formed residue, the thermal conductivity of WPC, and the heat of combustion of wood content show only a minor impact in cone calorimeter simulations.

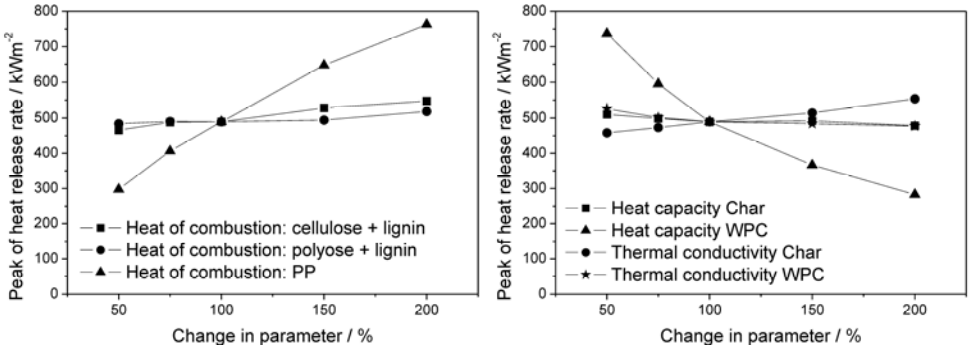

Figure 4.11: Change in pHRR by changing different parameters in a simulated cone calorimeter experiment

4.5. Conclusion of chapter 4

Chapter 4 focused on investigations on non-flame-retarded materials to draw conclusions about the general burning behavior of WPC samples. Burning behavior was studied by using the cone calorimeter, PCFC and SEM. Investigations of thermal decomposition were carried out by TG. Furthermore, numerical simulations of cone calorimeter tests were performed to investigate the influence of different thermal properties on burning behavior.

The main components of the investigated WPC material, wood and PP, show completely different burning behavior. PP burns more vigorously than wood, because it forms no residue and its heat of combustion is about four times higher than that of wood. WPCs offer the same burning behavior than wood, but release much more heat due to polymeric content. Accordingly, burning properties increase linearly with increasing wood content and decreasing PP content. In contrast to variations in the ratio of wood to PP, substituting wood with other wood species or substituting the PP matrix with PE has only minor effects. The incorporation of talc also influences the burning behavior of WPCs only slightly. But talc covers the formed residue and prevents it from undergoing further decomposition processes. The thermal decomposition of wood and PP inside WPC occur independently of each other. Only the decomposition temperature of PP is shifted to slightly higher temperatures due to the formation of residue from wood. Numerical simulations showed that the heat of combustion of PP and the specific heat of the WPC material had the greatest influence on burning behavior.

5. Flame retardancy of WPC material

This chapter relates investigations on WPC materials in which different flame-retardant additives were added to samples with standard geometries. Some of these were common flame retardants and others new flame retardants that have not been investigated before. The common flame retardants were combined to achieve synergistic effects. All samples were studied to examine their mechanisms of action and interaction with WPC material as well as their fire behavior.

5.1. WPC material combined with common flame retardants

5.1.1. WPC + ammonium polyphosphate

Figure 5.1 provides the TG and DTG curves of WPC-APP and WPC(50) measured under nitrogen. TG experiments show a strong increase in residue for the flame-retarded sample. 10.4 ± 0.5 wt.% for WPC(50) was raised to 25.1 ± 0.5 wt.% for WPC-APP. Additional TG measurements under combination of nitrogen and air show that the residue of WPC-APP is not only increased in quantity, it also offers higher resistance against thermo-oxidative decomposition. TG measurements first decomposed WPC under nitrogen and then oxidized the residue formed under air. For WPC(50) residue oxidation took place from 670 K to 760 K. For WPC-APP the end temperature was shifted to 1030 K, amounting to an increase of 270 K.

Furthermore TG data in *Figure 5.1* present a shift in cellulose decomposition for WPC-APP. The maximum MLR of cellulose decomposition was shifted from 632 K for WPC(50) to 578 K for WPC-APP. During thermal decomposition APP forms polyphosphoric acid. Acids are able to catalyze the decomposition of cellulose through hydrolysis [94, 95]. In general cellulose decomposes over different pathways [42, 96]. Apart from hydrolysis it also decomposes by random pyrolytic scissions. The change in thermal decomposition due to hydrolysis is accompanied by an increase in the amount of residue formed. But the increase in residue due to hydrolysis cannot explain the entire increase observed in the measurement.

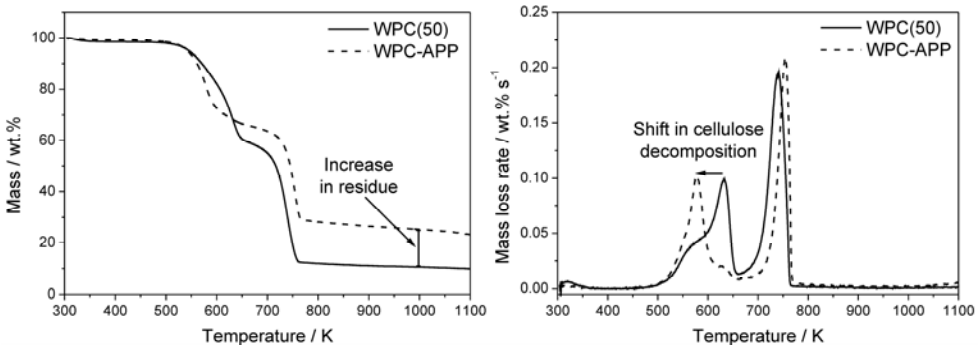

Figure 5.1: Comparison of mass (left) and mass loss rate (right) in TG experiment for WPC(50) and WPC-APP

Released products from TG-FTIR measurements under nitrogen confirm the change in thermal decomposition. *Figure 5.2* gives the gas-phase spectra of released products at 560 K and the product release rates of CO_2, water, NH_3 and carbon acids. The spectra show peaks of typical products for wood pyrolysis. These are, in particular, species containing OH, C-H, C-O and C=O groups, as well as CO_2, water and ammonia. OH-groups appear between 3470 and 3650 cm^{-1}, C-H between 2700 and 3100 cm^{-1}, C-O between 1050 and 1320 cm^{-1} and C=O between 1650 and 1850 cm^{-1}. Thereby peaks of C=O at higher wavelengths (1750 – 1850 cm^{-1}) belong to carbon acids, and peaks at lower wavelengths (1650 – 1750 cm^{-1}) belong to ketones or aldehydes. CO_2 appears at 2250 – 2400 cm^{-1} and ammonia shows absorption bands at 966 and 930 cm^{-1}. Peaks of water have been eliminated from the spectra because they would cover other decomposition products.

Product release rates of WPC-APP in comparison to WPC(50) show an increased release of water and a decreased release of CO_2 and carbon acids. These observations confirm the catalyzation of cellulose decomposition. Hydrolysis is associated with an increased release of water in comparison to other decomposition pathways. Release of CO_2 and carbon acids are mainly related to random pyrolytic scissions, and because these decomposition pathways are less preferred, the release of CO_2 and carbon acids is decreased in the thermal decomposition of WPC-APP. The release of ammonia goes back to the decomposition of APP itself. It is released during formation of polyphosphoric acid. Ammonia starts to release at 500 K.

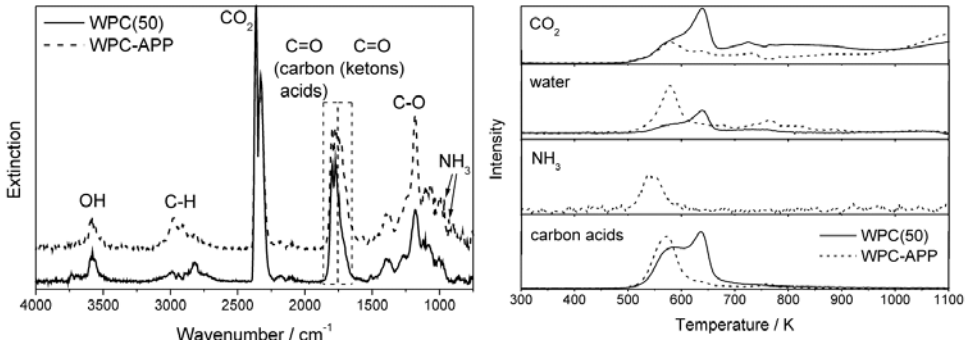

Figure 5.2: Comparison of released products during TG-FTIR measurements for WPC(50) and WPC-APP (left: spectra of decomposition products at 560 K [peaks of water have been eliminated], right: product release rates of CO_2, water, NH_3 and carbon acids)

Figure 5.3 presents FTIR measurements of WPC-APP in the condensed phase. The spectrum at room temperature shows vibrations of undecomposed WPC material. Peaks at 1592, 1503, 1250, 1160 and 1063 cm^{-1} belong to wood and peaks at 1458, 1377 and 894 cm^{-1} belong to PP. During heating the peaks of wood and PP vanish and P=O (1276 cm^{-1}), P-O-P (1085 cm^{-1}) and P-O bonds (883 cm^{-1}) are formed. P=O, P-O-P and P-O are attributed to the formation of polyphosphates during the thermal decomposition of APP. Polyphosphates are able to react with wood. In detail, OH-groups of polyphosphates react by eliminating water from OH-groups in wood. The reaction between polyphosphates

and wood leads to a cross-linked residue structure which was seen in the spectra of FTIR investigations. The formed residue of WPC-APP consists of typical aromatic structures netted by polyphosphates. Cross-linkage of the residue species formed is the main reason for the increase in residue observed in the TG experiment. Furthermore, the residue is stabilized and shows increased stability during thermo-oxidative decomposition.

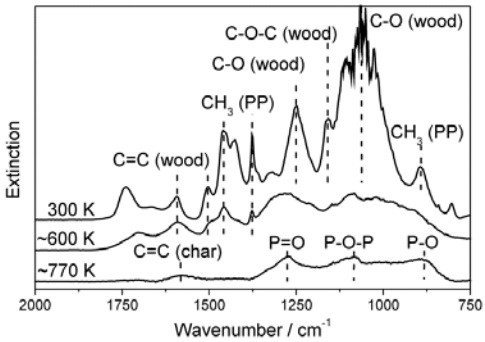

Figure 5.3: FTIR measurements of condensed phase for WPC-APP at different temperatures

The decomposition of cellulose in the presence of APP and the cross-linking of formed residue are summarized in *Figure 5.4*. To confirm the decomposition process, detected gaseous decomposition products from measurements are marked with solid squares, and detected condensed-phase decomposition products are marked with dashed squares. Cross-linking also occurs in polyose and lignin, but for better clarity the figure shows only cellulose.

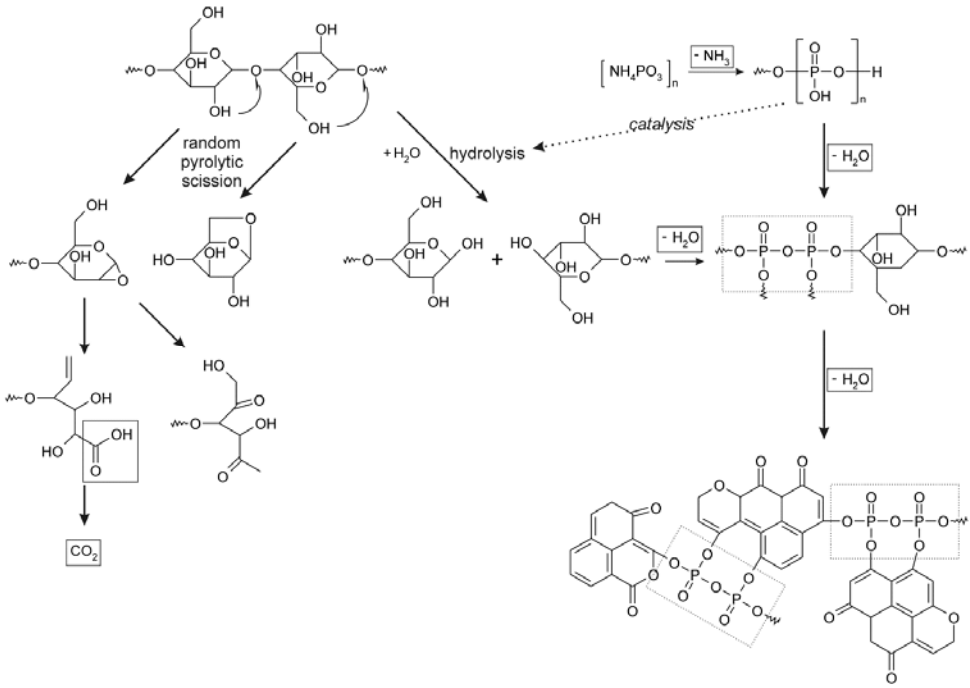

Figure 5.4: Main decomposition mechanism of cellulose in presence of APP and formation of cross-linked residue. (Solid squares: detected gaseous decomposition products, dashed squares: detected condensed decomposition products)

Exposed to an external heat flux in the cone calorimeter, WPC-APP showed a strong reduction in HRR in comparison to WPC(50) (*Figure 5.5*). First pHRR is reduced to 47% and last pHRR is reduced to 53% (*Table 5.1*). The reduction in the HRR of WPC-APP is due to the cross-linkage of cellulose. The residue in cone calorimeter measurements offers an increase in the amount as well. A value of 11.1 wt.% for WPC(50) rises to 28.8 wt.% for WPC-APP. The residue of WPC-APP provides a better barrier, reducing the intensity of burning. Furthermore, cross-linking stores combustible material in the residue and thus reduces the amount released to the gas phase. Substitution of PP with the flame retardant APP also reduces the amount of combustible material. Both effects are seen in reduced values of THE (*Table 5.1*). Substitution of highly combustible PP also contributes to a reduction in the HRR.

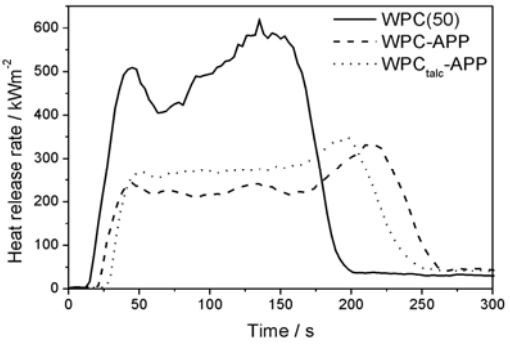

Figure 5.5: Cone calorimeter measurements at an irradiance of 50 kWm^{-2} for WPC(50), WPC-APP and WPC$_{talc}$-APP

Figure 5.5 and *Table 5.1* present the cone calorimetric results of an APP-retarded WPC containing talc. The HRR of WPC$_{talc}$-APP shows slightly worse results than WPC-APP, although 5 wt.% of PP are substituted with incombustible talc. The residue of WPC$_{talc}$-APP is increased in comparison to WPC-APP, but the increase is only 1.5 wt.%. Due to incorporation of 5 wt.% talc, residue was expected to increase by about 5 wt.% as well. It is concluded that APP interacts with talc. The reaction between APP and talc lowers the effectiveness of APP in cross-linking the WPC residue and causes a slight increase in HRR. Reactions between talc and APP have also been reported in the literature [97]. Talc and APP can form silicon diphosphate (SiP_2O_7), silicon oxymonophosphate ($Si_5O(PO_4)_6$), magnesium tetrapolyphosphate ($Mg_2P_4O_{12}$) and magnesium ultraphosphate ($Mg_2P_4O_{11}$). Formed phosphates do not contribute to the cross-linking of wood.

Table 5.1: Values of cone calorimeter measurement at an irradiance of 50 kWm^{-2} for WPC(50), WPC-APP and WPC$_{talc}$-APP (samples were plates of 3 mm thickness)

	THE / MJm^{-2} ± 0.4	**Residue / wt.% ± 0.5**	**1.pHRR / kWm^{-2} ± 5**	**Last pHRR / kWm^{-2} ± 20**	**TCOP / g ± 0.02**
WPC(50)	77.6	11.1	506	614	0.5
WPC-APP	54.3	28.8	239	324	1.4
WPC$_{talc}$-APP	54.4	30.3	264	326	0.5

For further investigations with varied heat fluxes WPC$_{talc}$-APP was chosen, because it presents better correlation with the WPC formulations on the market and offers better comparability with other flame-retarded formulations investigated in this study. Further investigations were carried out on injection-molded samples with different geometries. The strongest dependency on the applied heat flux was observed for 1.pHRR (*Table 5.2*). At the beginning only a small amount of residue is formed which acts as thermal barrier. The increase in external heat flux is passed directly to unburned material and increases the

HRR. After the formation of a barrier the dependency on external irradiation becomes smaller. Results for the last pHRR show less dependency on external heat flux than 1.pHRR. The THE and residue are affected only marginally by variation in external irradiation.

Table 5.2: Values of cone calorimeter measurements for $WPC_{talc}APP$ and $WPC(55)_{talc}$ at different irradiations (samples were plates of 5 mm thickness)

	Heat flux / kWm^{-2}	**THE / MJm^{-2} ± 4**	**Residue / wt.% ± 0.7**	**1.pHRR / kWm^{-2} ± 5**	**Last pHRR / kWm^{-2} ± 10**	**TCOP / g ± 0.06**
$WPC(55)_{talc}$	35	131	24.2	245	461	0.6
$WPC(55)_{talc}$	50	128	24.2	340	472	0.7
$WPC(55)_{talc}$	70	131	22.9	498	507	0.9
WPC_{talc}-APP	35	111	33.0	172	199	0.8
WPC_{talc}-APP	50	111	33.2	244	242	1.0
WPC_{talc}-APP	70	109	31.3	365	272	1.2

5.1.2. WPC + expandable graphite

Figure 5.6 shows the mass and MLR of TG experiments for EG alone and WPC_{talc}-EG in comparison to $WPC(55)_{talc}$. The mass loss of EG starts at 470 K, due to the decomposition of sulfuric acid. Parallel FTIR measurements showed peaks of SO_3 and SO_2 (at 1068, 1103, 1242, 1381 and 2900 cm^{-1}). The decomposition of sulfuric acid causes a mass loss of about 25 ± 0.9 wt.%. After the main mass loss step, EG showed a slight continuous mass loss. Under nitrogen graphite is normally stable up to high temperatures. Decomposition is caused by impurities within the material. The main mass loss step of EG occurred even before decomposition of the WPC material. Therefore EG is able to act before ignition of the WPC sample.

The release of sulfuric acid is also seen in WPC_{talc}-EG in a slight mass loss at about 500 K. Furthermore, WPC_{talc}-EG showed a slight change in thermal decomposition in comparison to $WPC(55)_{talc}$. The mass loss of cellulose is partly shifted to lower temperatures. The reason for this shift in thermal decomposition is, again, acid-induced catalysis. Sulfuric acid from EG catalyzes the decomposition as in APP. But due to the small amount of sulfuric acid inside the sample, the decomposition of cellulose is shifted only in part. WPC_{talc}-EG yielded increased values for residue in comparison to $WPC(55)_{talc}$. The residue of WPC_{talc}-EG at 1000 K amounted to 25.8 ± 0.5 wt.% and the residue of $WPC(55)_{talc}$ to 17.1 ± 0.5 wt.%. The increase is due to the expanded graphite that remained in the residue after expansion.

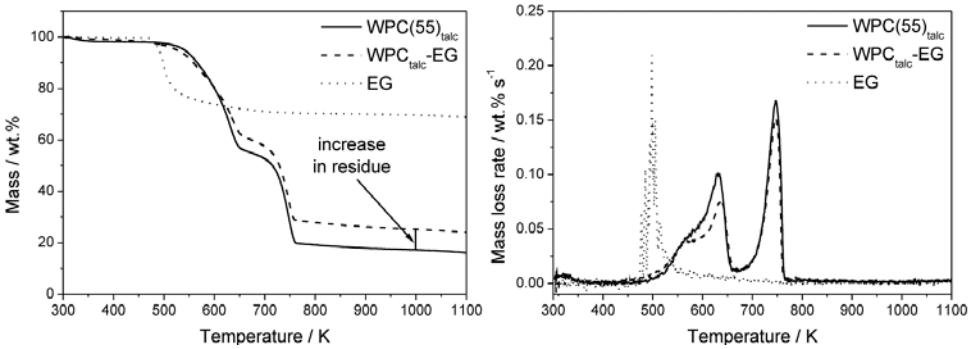

Figure 5.6: TG experiment: mass (left) and mass loss rate (right) for WPC(50), WPC_{talc}-EG and EG alone

During fire tests in the cone calorimeter WPC_{talc}-EG showed the formation of wormlike structures of expanded graphite (*Figure 5.7* right). Expanded graphite worms were found inside the residue of WPC. The residue structure of WPC_{talc}-EG is loose and many pieces dropped off from the sample. Most of these pieces were caught by an additional alumina tray to correct the sample mass (*Figure 5.7* left).

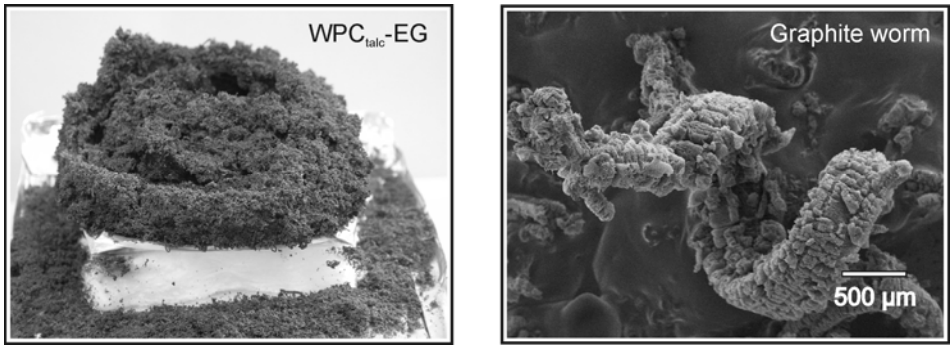

Figure 5.7: Residue of WPC_{talc}-EG after cone calorimeter measurement (left) and SEM image (10 kV, SE detector) of expanded graphite worm from the residue of WPC_{talc}-EG

The HRR showed reduced values in comparison to $WPC(55)_{talc}$ at the beginning of measurement (*Figure 5.8*), but after about 200 s the HRR of WPC_{talc}-EG strongly increased. The last pHRR of WPC_{talc}-EG measured under an irradiation of 50 kWm^{-2} is about 50 kWm^{-2} higher than for $WPC(55)_{talc}$, whereas 1.pHRR decreases by about 250 kWm^{-2} (*Table 5.3* compared to *Table 5.2*). At the beginning expanded graphite worms formed an effective barrier on top of the sample and reduced the HRR. But with progressive combustion, the barrier became increasingly ineffective. The residue exhibited a loose structure. It is easy for evolved decomposition products to break holes in the residue, which worsens its properties as a thermal barrier. The reason for the loose residue structures lies in the expansion of EG. This expansion goes along with a strong increase in its volume.

Expanding graphite causes pressure on the formed residue of the WPC and disrupts it. Disruption increases over time because more and more EG begins expanding. Disruption also causes a strong error in values of the last pHRR and the amount of residue formed.

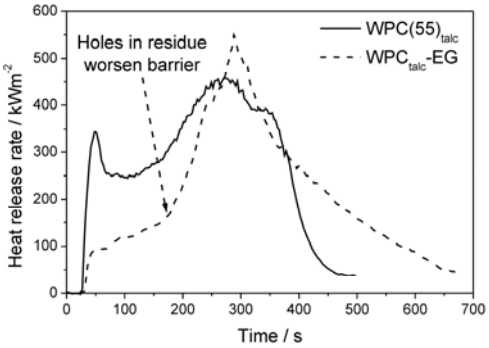

Figure 5.8: HRR of cone calorimeter measurements for WPC(55)$_{talc}$ and WPC$_{talc}$-EG at an irradiance of 50 kWm^{-2}

The residue of WPC$_{talc}$-EG is increased in comparison to WPC(55)$_{talc}$ in cone calorimeter experiments. An increase in residue was already observed in TG analysis and was attributed to the expanded graphite that remains in the residue. The THE and TCOP showed no change at all. They are similar to those for WPC(55)$_{talc}$ and show no change in dependency on external irradiation. WPC$_{talc}$-EG generally shows only a limited correlation with external heat flux. The difference in 1.pHRR between irradiations of 35 and 70 kWm^{-2} is only 23 kWm^{-2}. This small difference is related to the good barrier properties of expanded graphite worms, which prevent heat flow to underlying unburned material even at high external irradiations. At the end of the test these good barrier properties are lost and increase the dependency on external irradiation.

Table 5.3: Values of cone calorimeter measurements at different irradiations for WPC$_{talc}$-EG

Heat flux / kWm^{-2}	**THE / MJm^{-2} ± 4**	**Residue / wt.% ± 1.7**	**1.pHRR / kWm^{-2} ± 5**	**Last pHRR / kWm^{-2} ± 70**	**TCOP / g ± 0.1**
35	123	25.1	86	323	0.9
50	127	27.7	91	527	1.0
70	120	29.5	109	511	0.8

5.1.3. WPC + red phosphorus

The thermal decomposition of WPC$_{talc}$-RP showed no change in comparison to WPC(55)$_{talc}$ (*Figure 5.9*). Thermal decomposition begins at the same temperature as unprotected material, and no shift in wood or PP decomposition was detected. Parallel FTIR

measurements from evolved decomposition products showed the spectra of polyphosphates (peaks at 882, 1085 and 1275 cm^{-1}). Polyphosphates originate from phosphor species which were released from WPC_{talc}-RP to the gas phase and recombine at the gas cell to form polyphosphates.

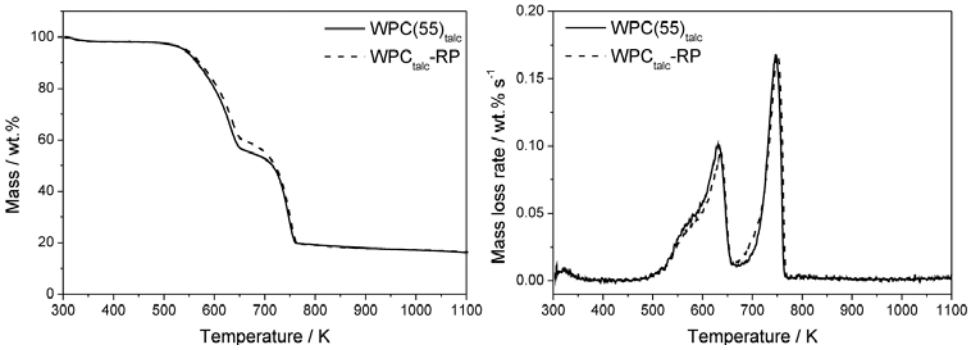

Figure 5.9: TG experiment under nitrogen: mass (left) and mass loss rate (right) for $WPC(55)_{talc}$ and WPC_{talc}-RP

The residue after the TG experiment on WPC_{talc}-RP under nitrogen showed only a small increase in quantity in comparison to $WPC(55)_{talc}$ (*Table 5.4*). But residue after the TG experiment on WPC_{talc}-RP under air increased by more than 100%. Values of WPC_{talc}-RP are even higher if measured under air than if measured under nitrogen, although residue is oxidized when it comes in contact with air at high temperatures. The increase in residue depends on the availability of oxygen. Together with oxygen phosphorus is able to form phosphates. Phosphates are able to cross-link charred residue, as was already observed for APP. In TG measurement under nitrogen the only oxygen available originates from the WPC material itself. Cellulose and polyose, especially, contain oxygen that becomes available for formation of phosphates during the thermal decomposition of wood. But due to small quantities the increase in residue is small. During TG measurement under air oxygen is sufficiently available.

Table 5.4: Residue of TG experiment under nitrogen and air at 1000 K for $WPC(55)_{talc}$ and WPC_{talc}-RP

	Nitrogen / wt.% ± 0.2	**Air / wt.% ± 0.2**
$WPC(55)_{talc}$	17.1	10.1
WPC_{talc}-RP	17.7	21.7

Cone calorimeter results of WPC_{talc}-RP show only marginal improvements in comparison to $WPC(55)_{talc}$. The heat release rate is decreased only marginally (*Figure 5.10*). 1.pHRR and

last pHRR are lowered by around 10% (*Table 5.5*). During burning WPC_{talc}-RP showed strong deformation of the sample. The sample swelled, decreasing the distance between the sample surface and cone heater. This increases the applied heat flux on the sample and worsens the results for the HRR. Therefore an additional pHRR occurred at the time of the sample's strongest swelling (240 s). Swelling occurs when pyrolysis gases are trapped inside the sample. This is probably due to a change in melt viscosity. If the viscosity is too high, the sample is not able to deform under the pressure of trapped gases; if the viscosity is too low, trapped pyrolysis gases can easily escape by breaking holes inside the melt.

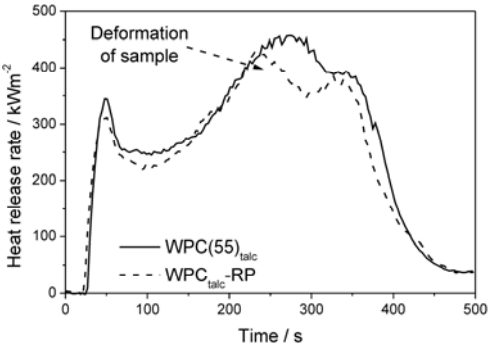

Figure 5.10: Cone calorimeter measurement of $WPC(55)_{talc}$ and WPC_{talc}-RP at an irradiance of 50 kWm^{-2}

Values of residue and TCOP indicate condensed-phase and gas-phase mechanisms of RP as already expected due to measurements of thermal analysis. Residue is increased by about 1 - 1.5 wt.% in comparison to $WPC(55)_{talc}$ (*Table 5.5* compared to *Table 5.2*). TCOP is about 12 times higher. The gas-phase mechanism is always accompanied by a strong increase in TCOP. It is concluded that most of RP was released to the gas phase because of the small increase in residue. Dependency on the external heat flux shows the same results as were observed for WPC without flame retardants. 1.pHRR and last pHRR increase with increasing heat flux.

Table 5.5: Values of cone calorimeter measurements at different irradiations for WPC_{talc}-RP

Heat flux / kWm^{-2}	**THE / MJm^{-2} ± 1.8**	**Residue / wt.% ± 0.5**	**1.pHRR / kWm^{-2} ± 5**	**Last pHRR / kWm^{-2} ± 20**	**TCOP / g ± 0.1**
35	120	25.7	229	319	8.5
50	120	25.2	307	431	8.6
70	119	24.3	446	418	9.2

5.2. WPC materials with combinations of common flame retardants

The goal of combining different flame retardants is to increase their potential in flame retardancy. One approach is to combine flame retardants that act over different mechanisms. APP and EG present flame retardants which act mainly in the condensed phase, whereas RP shows mainly gas-phase activity.

5.2.1. Combination of gas-phase and condensed-phase mechanisms

First WPC material containing APP and RP was manufactured. Cone calorimeter tests of WPC_{talc}-APP_3RP_1 showed the expected gas-phase and condensed-phase mechanisms. Residue is increased by about 25% in comparison to $WPC(55)_{talc}$ and TCOP is about six to eight times higher (*Table 5.6* in comparison to *Table 5.2*). By comparing the results with those of WPC with single flame retardants, WPC_{talc}-APP_3RP_1 yielded less residue than WPC_{talc}-APP. But taking into account that WPC_{talc}-APP contains twice the amount of APP, which is mainly responsible for residue formation, the residue-forming tendency of WPC_{talc}-APP_3RP_1 is actually increased. The formation of TCOP and therefore gas-phase action is slightly increased in comparison to WPC_{talc}-RP, again, by taking into account that WPC_{talc}-APP_3RP_1 contains only half the amount of RP. In sum it is concluded that APP and RP act slightly synergistically concerning the gas-phase and condensed-phase mechanisms. The increase in the condensed-phase mechanism is probably due to physical interactions inside the material. The change in melt viscosity, which was due to the RP inside the material, may act beneficially for barrier formation.

Table 5.6: Values of cone calorimeter for WPC_{talc}-APP_3RP_1 measured at three different irradiations

Heat flux / kWm^{-2}	**THE / MJm^{-2} ± 1.8**	**Residue / wt% ± 0.4**	**TCOP / g ± 0.03**	**1.pHRR / kWm^{-2} ± 5**	**Last pHRR / kWm^{-2} ± 10**
35	112	30.2	5.1	179	208
50	107	30.0	5.6	260	250
70	104	29.2	5.9	367	284

The main flame-retardant action of WPC_{talc}-APP_3RP_1 appears in the condensed phase. This is concluded from the HRR which gives similar results as for WPC_{talc}-APP (*Figure 5.11*). Values of the 1.pHRR and last pHRR lie in the same range (*Table 5.6* compared with *Table 5.2*). But the HRR of WPC_{talc}-APP_3RP_1 also shows a pHRR between 250 s and 350 s depending on the applied heat flux (*Figure 5.11*). The additional pHRR is, again, related to the deformation of the sample. It already occurred for WPC_{talc}-RP as well and is attributed to the RP inside the sample. Different irradiations showed only a slight dependency between THE and residue. The strongest dependency on external heat flux was observed for 1.pHRR. The reason for this is the same as was discussed back in section 5.1.1 for WPC_{talc}-APP. The main flame-retardant action of WPC_{talc}-APP_3RP_1 occurs in the

condensed phase. Barrier formation increases with time; therefore at the beginning where 1.pHRR occurs, it offers only limited protection.

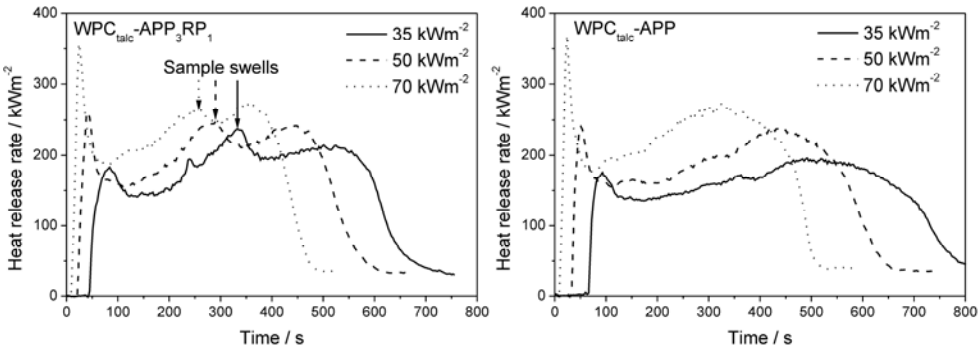

Figure 5.11: Cone calorimeter measurements for WPC$_{talc}$-APP$_3$RP$_1$ in comparison to WPC$_{talc}$-APP at 3 different irradiations (sample thickness 5 mm)

In a second approach, samples containing EG and RP were manufactured. WPC$_{talc}$-EG$_3$RP$_1$ presents a combination of a gas-phase and condensed-phase mechanism as well.

During the cone calorimeter test the samples bent upwards for more than 2 cm to form half of a hollow sphere that left a hollow space underneath the sample. The residue after the cone calorimeter test of WPC$_{talc}$-EG$_3$RP$_1$ is shown in *Figure 5.12*.

Figure 5.12: Residue after cone calorimeter measurement for WPC$_{talc}$-EG$_3$RP$_1$ measured under an irradiation of 50 kWm^{-2}

Both condensed-phase and gas-phase mechanisms were observed in the fire tests. Residue is increased by about 35 % and the values of TCOP are about 6 times higher in comparison to WPC(55)$_{talc}$ (*Table 5.7* compared to *Table 5.2*). Comparing the residue amounts with those of WPC containing single flame retardants shows that neither WPC$_{talc}$-EG nor WPC$_{talc}$-RP is able to reach the amount of residue formed from WPC$_{talc}$-EG$_3$RP$_1$ (*Table 5.7* compared to *Table 5.3* and Table *5.5*). It is concluded that the strong increase in

the amount of residue relies on a synergistic effect between EG and RP, leading to additional storage of phosphorus inside the residue. In parallel, the release of phosphorus to the gas phase is reduced in comparison to other flame-retarded systems containing RP. Values of TCOP are less than those of WPC_{talc}-APP_3RP_1, although both samples contain the same amount of RP (*Table 5.7* compared to *Table 5.6*). Furthermore, values of TCOP and the amount of residue observed in the cone calorimeter show a strong dependency on external irradiation. TCOP increases with increasing irradiation, whereas the amount of residue decreases.

Table 5.7: Values of cone calorimeter measurement for WPC_{talc}-EG_3RP_1 at three different irradiations

Heat flux / kWm^{-2}	**THE / MJm^{-2} ± 4**	**Residue / wt.% ± 0.5**	**1.pHRR / kWm^{-2} ± 5**	**Last pHRR / kWm^{-2} ± 10**	**TCOP / g ± 0.1**
35	105	33.0	119	201	3.6
50	105	31.9	137 ± 15	233	4.6
70	108	30.5	179	312	5.3

It was already discussed in section 5.1.3. that RP is able to increase the amount of residue by cross-linking wood. But therefore it needs to come in contact with oxygen to form phosphates. Oxygen can originate from only two sources. The first source is WPC material on its own, and the second source is the surrounding air. In general it is agreed that pyrolysis occurs under inert conditions and no oxygen comes in contact with the sample. The cross-linking of wood in WPC_{talc}-RP was only related to the oxygen released from decomposing WPC material. But this yields only a small increase in residue and cannot explain the strong increase for WPC_{talc}-EG_3RP_1. Here the flame-retardant impact of EG is strong enough to decrease the flames so that oxygen from the surrounding air is able to come in contact with the material while burning. Measurements of WPC_{talc}-EG already indicate high potential for the flame retardancy of EG as it achieves a very low 1.pHRR. Oxygen enables the formation of phosphates, which cross-link the residue and increase its amount. Furthermore cross-linked residue embeds the expanded graphite worms and prevents the residue from being disrupted. Disruption was observed for WPC_{talc}-EG and attributed to the expansion of EG. Preventing disruption is also beneficial for the formation of more phosphates. Non-disrupted residue is able to decrease the flames so that oxygen still can come in contact with the pyrolysis zone. TG measurements under nitrogen and air confirmed that oxygen from the surrounding air is responsible for the formation of phosphates (*Table 5.8*). If measured under air, the formation of residue is clearly increased for samples containing RP in comparison to samples without RP, but not for measurements under nitrogen.

Table 5.8: Residue of TG experiment under nitrogen and air at 1000 K

	Nitrogen / wt.% ± 0.2	**Air / wt.% ± 0.2**
WPC_{talc}-EG_3RP_1	22.1	20.9
WPC_{talc}-EG	26.0	14.9
WPC_{talc}-RP	17.6	21.7

The formation of phosphates with oxygen from the surrounding air also explains the strong dependency of TCOP and the amount of residue on external irradiations. Higher external heat fluxes result in increased burning and thus less oxygen is able to come in contact with the sample. Therefore the amount of phosphorus released to the gas phase increases with increasing heat flux, and the amount of phosphorus stored in the residue decreases, respectively.

The HRR curves of WPC_{talc}-EG_3RP_1 for three different irradiations are shown in *Figure 5.13*. After the 1.pHRR all samples showed an early slope to the last pHRR. The slope is caused by the swelling of the sample, because the sample gets closer to the heater. Furthermore HRRs confirm the effects discussed above. The 1.pHRRs lie between the values of WPC_{talc}-EG and WPC_{talc}-RP. The last pHRRs of WPC_{talc}-EG_3RP_1 are reduced in comparison to those of WPCs with a single RP and single EG. Reduction is based on the increased amount of residue and the avoidance of its disruption. Dependency on external irradiation is also observed in the HRR. Measurements under 35 and 50 kWm^{-2} achieved similar results, whereas the HRR measured under 70 kWm^{-2} is clearly increased, especially for the last pHRR. The difference between measurements under 70 kWm^{-2} to those measurements under 35 and 50 kWm^{-2} were attributed to the reduced formation of phosphates because less air comes in contact with the pyrolysis zone.

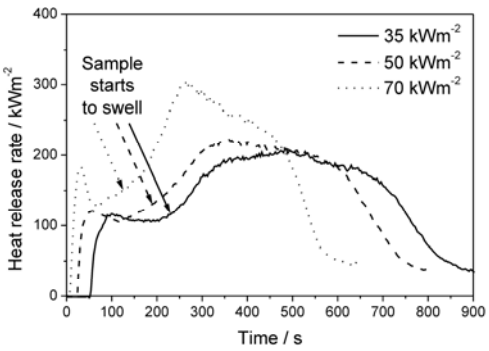

Figure 5.13: Cone calorimeter measurements for $WPC_{talc}EG_3RP_1$ at three different irradiations

5.2.2. Combination of two different condensed-phase mechanisms

In previous investigations on combining flame retardants with gas-phase and condensed-phase mechanisms, the best results were achieved for WPC_{talc}-EG_3RP_1. The good performance was based on the stabilization of the formed residue. Embedding expanded graphite worms in a cross-linked matrix is especially effective. In contrast, gas-phase action seems less important. APP is able to cross-link residue as well. Therefore now different formulations of combinations of APP and EG were fabricated to systematically study the impact of APP on residue stabilization. Three samples with different ratios of APP to EG were investigated.

Cone calorimeter tests showed disrupted residues for WPC_{talc}-APP_1EG_3 and WPC_{talc}-APP_1EG_1. WPC_{talc}-APP_3EG_1 was the only sample where disruption was avoided (*Figure 5.14*). A ratio of three to one for APP to EG is necessary to embed expanded graphite and avoid disruption. Without showing disruption, strong swelling was observed for WPC_{talc}-APP_3EG_1.

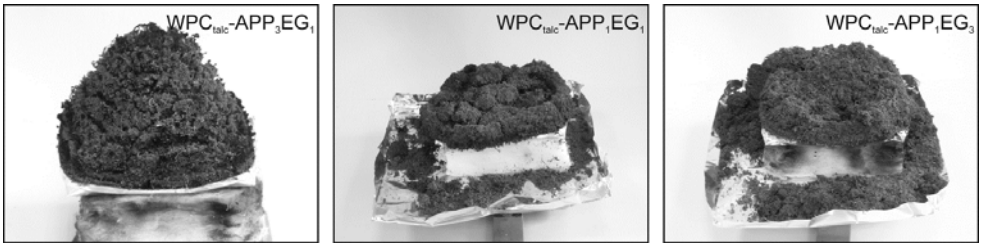

Figure 5.14: Residue after cone calorimeter measurement for WPC_{talc}-APP_3EG_1, WPC_{talc}-APP_1EG_1 and WPC_{talc}-APP_1EG_3 at an irradiation of 50 kWm^{-2}

Figure 5.15 and *Figure 5.16* present a comparison of the 1.pHRR and the last pHRR for WPCs with different ratios of mixtures of APP and EG. The 1.pHRR decreases for increasing amounts of EG and decreasing amounts of APP for all measured irradiations. At the beginning of burning expanded graphite worms present better protection of underlying material than cross-linked residue due to APP. The reason is that EG is able to protect the sample earlier. The expansion of EG occurs even before ignition, whereas APP acts only in a burning or degrading sample. The decrease in 1.pHRR for increasing amounts of EG and decreasing amounts of APP shows a disproportionately strong relation. The decrease in 1.pHRR by substituting APP with EG shows a saturation concentration. Expanded graphite worms form a layer on top of the burning sample. If enough graphite worms are present to form a continuous barrier, a further increase in their amount will yield only minor improvements.

With increasing amounts of EG and decreasing amounts of APP, the dependency on the external heat flux is reduced. For samples containing only APP, the difference in 1.pHRR for measurements under 35 and 70 kWm^{-2} amounted to over 100%. The difference decreases with incorporation of EG. For samples containing 3.75, 7.5, 11.25 and 15 wt.% EG, the decrease is 89%, 71%, 59% and 27%, respectively. In general, thermal barriers reduce the dependency on external heat flux.

This has also been reported in other studies [49]. Although both flame retardants EG and APP act by forming thermal barriers, the expansion of EG occurs much earlier than cross-linking of APP. Therefore the impact of the barrier at the beginning of burning when the 1.pHRR occurs is much higher for EG than for APP.

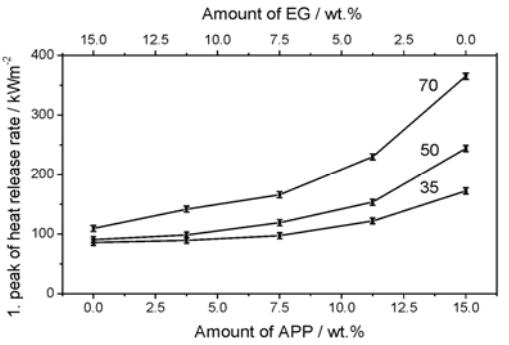

Figure 5.15: Comparison of 1.pHRR of WPC containing different ratios of APP and EG at different irradiations (numbers indicate the applied heat flux)

The last pHRR decreases for decreasing amounts of EG and therefore shows a relation opposite from the 1.pHRR. There are two main reasons for the observed behavior. Disruption of the residue increases with increasing amounts of EG, because a higher amount of expanded graphite worms assists disruption. Simultaneously, the addition of APP acts counter to disruption. Expanded graphite worms were embedded in a cross-linked residue and the residue was therefore stabilized.

Disruption of the residue causes an increased error in the last pHRR. Therefore no analysis of dependency on external radiation was possible.

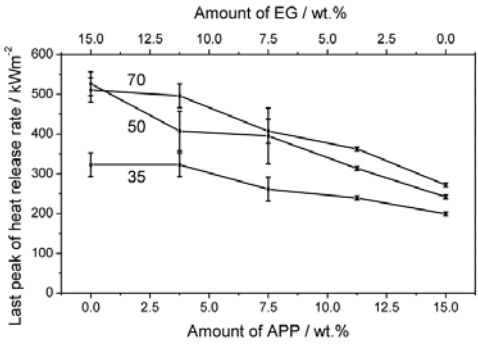

Figure 5.16: Comparison of last pHRR of WPC containing different ratios of APP and EG at different irradiations (numbers indicate the applied heat flux)

5.3. WPC materials with new flame retardants

5.3.1. WPC + Disflamoll TP LXS 51064

Dis constitutes a new, commercially available flame retardant for wood materials. Apart from studying the impact of Dis on the flame retardancy of WPC material, a mechanism for the thermal decomposition of flame-retardant molecules was also investigated. Investigations for pure flame retardant were carried out on a solution of Dis containing 59 wt.% of water. *Figure5.17* shows the mass and MLR of a TG experiment on Dis solution under nitrogen. It shows two main steps of mass loss. The first mass loss step ranged from 300 K up to 480 K and the second mass loss step started at 480 K and ended at 650 K. After the second mass loss step the flame retardant showed a continuous mass loss up to the end of the experiment. The amount of pure flame retardant residue after 650 K amounted to 54.5 ± 0.5 wt.%. The residue mass was corrected by subtracting the amount of released water from the solution.

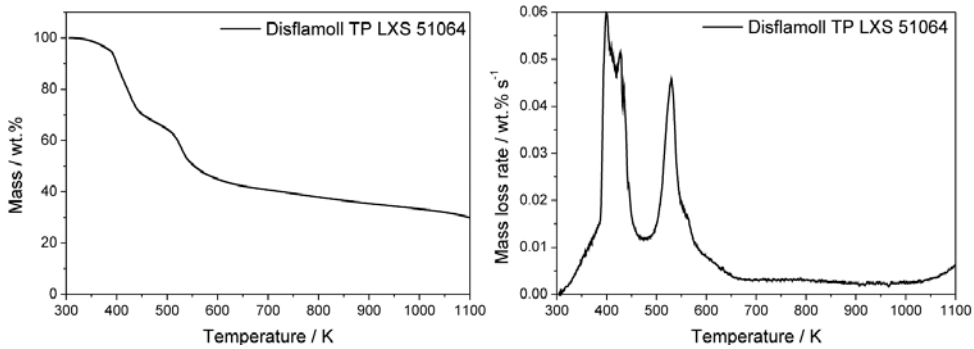

Figure 5.17: TG experiment under nitrogen: mass (left) and mass loss rate (right) curve of Disflamoll TP LXS 51064

Parallel FTIR measurements of gaseous decomposition products (*Figure5.18*) identified the first mass loss step, which was due mainly to the evaporation of water. Additional ammonia is released. Water shows broad absorption bands between 1250 and 2100 cm^{-1} and between 3400 and 4000 cm^{-1}. Absorption bands of ammonia are located between 715 and 1250 cm^{-1} with two strong peaks at 930 cm^{-1} and 966 cm^{-1}. Furthermore, an additional peak of ammonia occurs at 3332 cm^{-1}. During the second mass loss step water and ammonia are released as well. The release of CO_2 (2250 – 2395 cm^{-1} and 669 cm^{-1}) was also detected, and small peaks of C=O double bonds were identified between 1690 and 1820 cm^{-1}. The absorption bands of water are eliminated in the spectra of 580 K as well as in the spectra of 870 K, because they would cover the peaks of C=O double bonds. The release of CO_2 and C=O also occurred for the continuous mass loss after the second mass loss step.

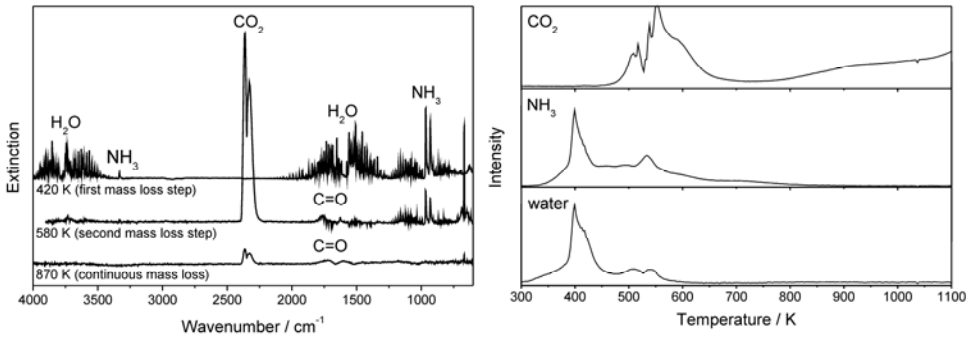

Figure 5.18: TG-FTIR spectra of Dis at different temperatures (peaks of water are eliminated in the spectra at 580 and 870 K, because they would cover peaks of C=O)

Investigations of the condensed phase are shown in *Figure5.19*. The spectrum at room temperature shows the peaks of undecomposed flame retardant. Peaks of ammonium carboxylate salt are identified at 1445 and 1560 cm^{-1}, while associated carbon acids show peaks at 1400 and 1695 cm^{-1}. A P-C bond was identified at 910 cm^{-1}. Additional water from the solution shows broad absorption bands between 2500 and 3700 cm^{-1}, which are not shown in *Figure5.19*. Upon heating up to temperatures of around 600 K the peaks of ammonium carboxylate salt vanish and the peaks of free and associated carbon acids increase. This correlates well with the results of evolved gas analysis, where the release of water and ammonia was detected. While heating up further to temperatures of around 750 K, peaks of phosphates dominate the spectra (1090, 1270 and 1400 cm^{-1}). Furthermore the formation of intermediary anhydrides was observed for wave numbers at around 1780 cm^{-1}. The P-C bond remained stable over the entire temperature range.

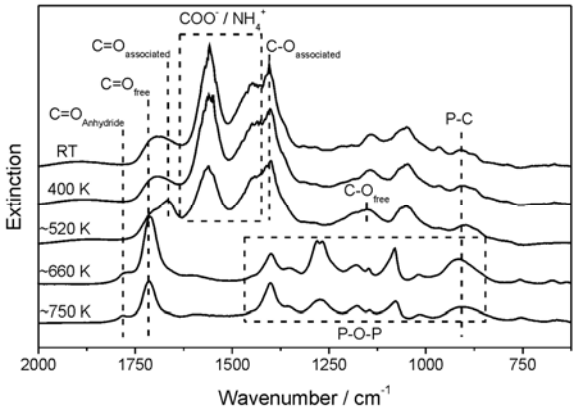

Figure 5.19: FTIR measurements of condensed phase for Dis at different temperatures

The presented investigations of the gas and condensed phases lead to the decomposition model of the flame retardant Dis presented in *Figure5.20*. In the figure all measured

gaseous decomposition products are designated by solid squares, and all measured condensed-phase products by dashed squares. In a first step ammonia is released under the formation of phosphonic acid. Additional ammonia and water are released to form a thermodynamically favorable five-member anhydride ring through a ring-closing reaction. Afterwards decomposition continues under the further release of ammonia and propanic acid. The release of propanic acid was concluded from the molecule of Dis and detected carbonyl bonds in the gas phase. But other decomposition products containing carbonyl bonds are also possible, like, for example, formic acid. After decomposition of the flame retardant molecules the decomposition products are able to recombine under the formation of polyphosphate structures. Under continuous heating, polyphosphate structures decompose in further reactions due to the continuous mass loss in the TG measurement. The amount of residue in the TG experiment amounted to 54.5 wt.% after the second mass loss step. Calculations of the residue from the decomposition model before the formation of polyphosphates amounted to 54 wt.%, which fits very well with the measurement.

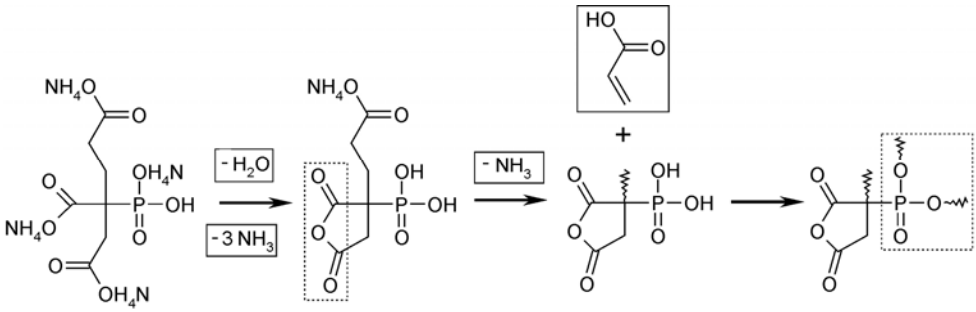

Figure 5.20: Decomposition mechanism of Dis molecules

Flame-retarded WPC materials were tested with two different amounts of Dis. *Figure5.21* gives the results of TG analysis. Flame-retarded samples, again, show a shift in cellulose decomposition to lower temperatures as was also observed for WPC-APP in section 5.1.1. This shift is attributed to the formation of phosphonic acid and its catalysis of cellulose decomposition over hydrolysis. But in contrast to WPC-APP, cellulose decomposition is shifted only in part. WPC-Dis forms lower amounts of acid than APP due to a lower content of phosphorus inside the flame retardant. Additionally, the amount of flame retardant inside WPC-Dis is less than in WPC-APP. Dependency on the amount of flame retardant is also seen for WPC with different amounts of Dis. In WPC-Dis(3) cellulose decomposition is shifted less than in WPC-Dis(10). The maximum of mass loss of cellulose decomposition was shifted by about 45 K for WPC-Dis(3) and about 55 K for WPC-Dis(10). The decomposition of PP shows no change. The addition of Dis is accompanied by an increase in the formed residue. Residue at 1000 K amounted to 14.5 ± 0.5 wt.% for WPC-Dis(3) and 19.2 ± 0.5 wt.% for WPC-Dis(10). WPC(60) showed a residue of only 10.8 wt.%.

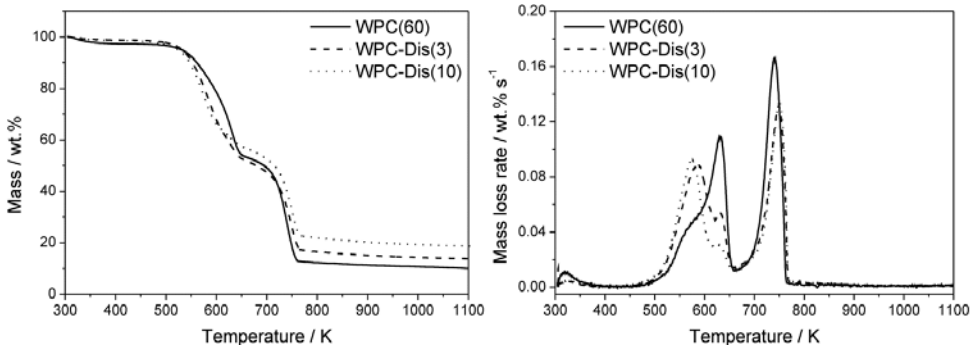

Figure 5.21: TG (left) and DTG (right) curves of WPC combined with different amounts of Disflamoll TP LXS 51064

The resultant phosphate structures after decomposition of the flame retardant are able to cross-link the residue from wood combustion. The same effect was observed for APP. *Figure5.22* shows a possible structure of the formed residue for WPC-Dis in comparison to WPC-APP. The difference in both residues lies in the cross-linking points. In both cases phosphates are responsible for cross-linking. In principle every phosphorus atom is able to form three cross-linking points. In the Dis molecule one bond is already occupied due to the stable P-C bond. In APP two bonds are occupied because of its polyphosphate structure. Here only one bond is left for cross-linking the residue.

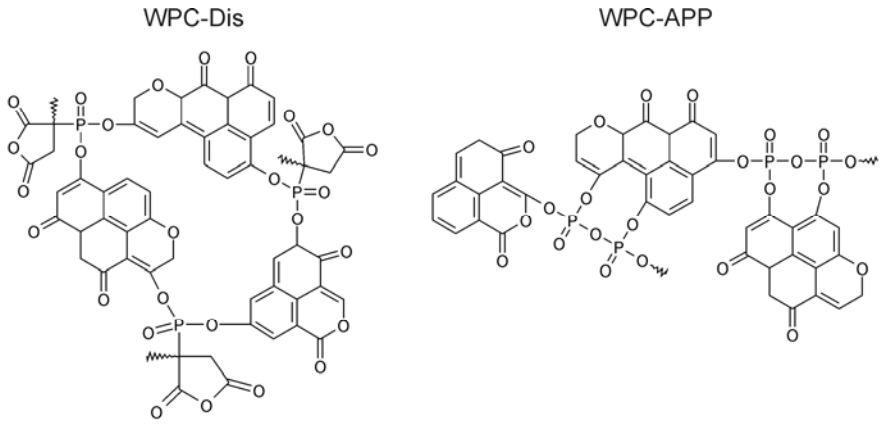

Figure 5.22: Residue of WPC-Dis in comparison with residue of WPC-APP

Figure5.23 gives a comparison of the amount of residue formed during a TG experiment. On the left the residue is plotted over the amount of phosphorus inside the sample. Dis is much more effective in increasing the residue, for the reasons described above. In APP two possible cross-linking points of a phosphorus atom are occupied by bonds with other phosphates. In Dis only one bond is occupied. But plotted over the amount of flame retardant, the residue gives a linear correlation for the two different flame retardants. For

Dis phosphorus works more effectively, but the amount of phosphorus inside the flame retardant is lower. It amounted to 9.2 wt.%. In comparison APP has a phosphorus content of 32 wt.%. Furthermore, more flame retardant was added to WPC-APP than to WPC-Dis samples.

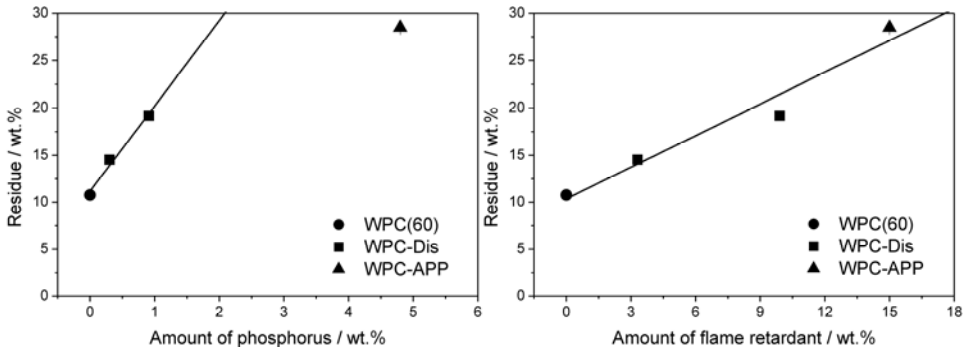

Figure 5.23: Comparison of the amount of residue at 1000 K for WPC-Dis and for WPC-APP in a TG experiment (left: values are plotted over the amount of phosphorus in the sample, right: values are plotted over the amount of flame retardant in the sample)

The HRR of WPC-Dis(3) and WPC-Dis(10) is plotted in *Figure5.24*. It is decreased in comparison to WPC(60). Dis acts mainly over the condensed-phase mechanism through barrier formation. Therefore it is typical that the flame-retardant protection increases over time. The 1.pHRR is reduced only marginally for flame retardant samples (*Table5.9*). The main reduction is observed for the last pHRR. Apart from the condensed-phase mechanism, Dis is also able to act by means of flame gas dilution with the release of incombustible gases, in particular water vapor, CO_2 and ammonia. But the flame-retardant impact of flame gas dilution is small because of the small amount of flame retardants inside the sample. Flame retardants that act mainly through flame gas dilution require much higher amounts [98].

The difference in HRR between WPC-Dis(3) and WPC-Dis(10) is negligible, even though WPC-Dis(10) contains a much higher amount of flame retardant. An increase in the amount of flame retardant did not show any further improvement. The condensed-phase mechanism was achieved by increasing the amount of residue. Dis shows a strong increase in residue by the addition of 3 wt.% (*Table5.9*), but 10 wt.% of flame retardant yields only a slight further increase in residue formation in the cone calorimeter. This indicates the reason for the negligible difference in the HRR observed in the cone calorimeter. The values for residue in the cone calorimeter measurement contrast with those from the TG experiments. TG showed a linear increase in the amount of residue formed. Dis shows different performances in different fire scenarios.

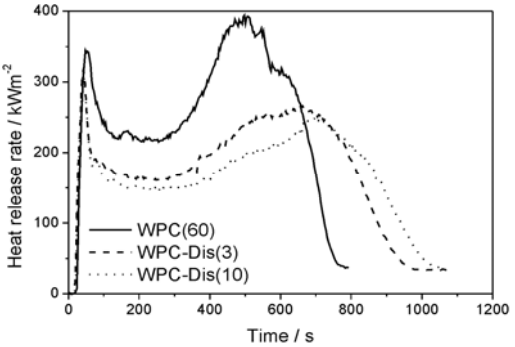

Figure 5.24: Cone calorimeter measurement for WPC(60), WPC-Dis(3) and WPC-Dis(10) at an irradiance of 50 kWm^{-2} (sample thickness = 9 mm)

Table 5.9: Values of cone calorimeter measurements for WPC-Dis(3) and WPC-Dis(10) in comparison with WPC(60) at an irradiance of 50 kWm^{-2}

	THE / MJm^{-2} ± 3	**Residue / wt.% ± 0.2**	**1.pHRR / kWm^{-2} ± 10**	**Last pHRR / kWm^{-2} ± 10**
WPC(60)	191	16.4	347	391
WPC-Dis(3)	179	22.9	323	263
WPC-Dis(10)	175	25.2	311	252

5.3.2. WPC + Paxymer

Thermal analysis of WPC-Pax showed no change in the decomposition temperatures of WPC components. But an increase in residue for WPC-Pax during a TG experiment under nitrogen was observed (*Table5.10*). Increase in residue is 15.1 wt.% and is therefore higher than the amount of flame retardant which was added (10.8 wt.%). Pax displays a complex system with different components. Therefore different interactions occur. RP and metal hydroxides tend to react and form phosphates [58]. These phosphates exist in a great number of formulations. The most common ones are orthophosphates and pyrophosphates ($Mg_3(PO_4)_2$, $Ca_3(PO_4)_2$ and $Mg_2P_2O_7$, $Ca_2P_2O_7$). Metal phosphates stay in the residue and increase its amount. But formation of metal phosphates alone is not able to explain strong increase in residue. This can only rely on promotion of char formation. As already mentioned in section 5.1.3., RP is also able to form phosphates that cross-link wood residue. This is accompanied by an increase in the amount of residue. But for the formation of these phosphates oxygen is necessary. Additional ingredients may present an oxygen source and thus enhance the amount of residue by cross-linking wood species. Another possibility is a reaction of polydimethylsiloxane with OH-groups of wood. Polydimethylsiloxane also tends to react with RP. Reaction of polydimethylsiloxane with wood and RP would form networks and cross-linking is therefore possible, too.

Further investigations of evolved gases showed that not all of the red phosphorus remains in the residue. Part of it is released to the gas phase as well. TG-FTIR measurements showed peaks of phosphor species in the spectra of decomposition products (878, 1091 and 1284 cm^{-1}). Therefore Pax is able to show flame-retardant mechanisms in the condensed phase and in the gas phase.

Table 5.10: Residue at 1000 K of TG experiment under nitrogen for WPC-Pax

Sample	**Mass / wt.% ± 0.2**
WPC(60)	10.8
WPC-Pax	25.9

Cone calorimeter measurements show both the condensed-phase and gas-phase mechanisms. The amount of residue for WPC-Pax is more than doubled in comparison to WPC(60) and the CO production is raised from 1.0 to 6.3 g (*Table5.11*). The THE shows a decrease of 16%. It is caused by substitution of combustible material with the flame retardant Pax, as well as flame inhibition and enhanced storage of combustible material in the residue due to cross-linking.

Table 5.11: Values of cone calorimeter measurement for WPC(60) and WPC-Pax at an irradiance of 50 kWm^{-2}

	THE / MJm^{-2} ± 3	**Residue / wt.% ± 0.7**	**1.pHRR / kWm^{-2} ± 5**	**Last pHRR / kWm^{-2} ± 10**	**TCOP / g ± 0.2**
WPC(60)	191	16.4	347	390	1.0
WPC-Pax	161	34.5	168	142	6.3

Flame-retardant mechanisms result in a strong reduction in the HRR for WPC-Pax in comparison to WPC(60) (*Figure5.25*). Reduction already occurs at the 1.pHRR. The peak is reduced by more than 50% from 347 to 168 kWm^{-2}. During the cone calorimeter test WPC-Pax shows swelling, which worsens the results for the HRR. Swelling has already been observed before for other samples containing red phosphorus, and is probably due to a change in the melt viscosity of the sample. Swelling caused an additional pHRR with its maximum at 570 s. The last pHRR is reduced as well. The reduction at the end is caused mainly by the condensed-phase mechanism and enhancement of residue formation.

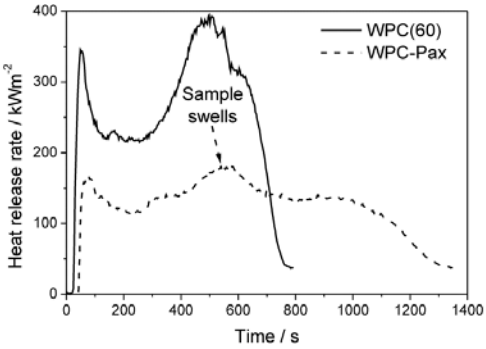

Figure 5.25: Cone calorimeter measurement at an irradiance of 50 kWm^{-2} for WPC(60) and WPC-Pax

5.3.3. WPC + Struktol SA 0832

The pure flame retardant Str decomposes in two decomposition steps (*Figure5.26*). The first step starts at 400 K. Parallel FTIR measurements identified only the release of water (broad absorption bands between 1250 and 2100 cm^{-1} and between 3400 and 4000 cm^{-1}). The second decomposition step starts at about 500 K. It goes back mainly to the release of pyrimidine derivatives (*Figure5.27*). Pyrimidine derivatives are formed from melamine, which is part of the flame retardant.

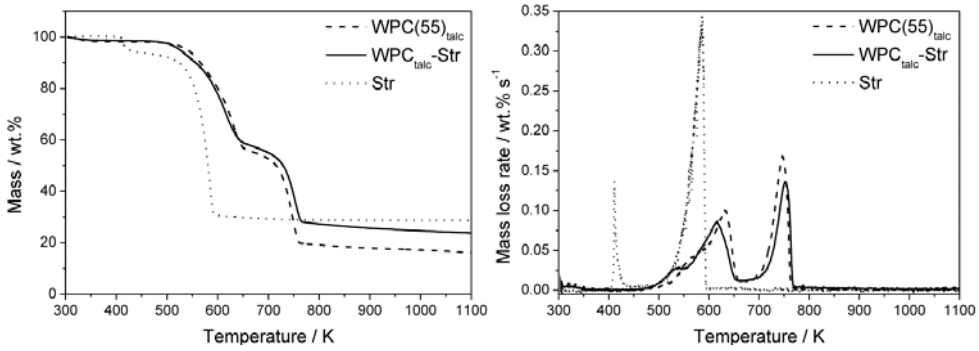

Figure 5.26: TG (left) and DTG (right) curve for WPC$_{talc}$-Str, WPC(55)$_{talc}$ and pure Str

Decomposition of WPC material combined with Str showed only small differences in comparison to WPC(55)$_{talc}$ (*Figure5.26*). Part of the cellulose decomposition is shifted to lower decomposition temperatures. But this shift is only marginal. The biggest difference is an increase in the formed residue. The residue of WPC(55)$_{talc}$ amounted to 21.6 ± 0.9 wt.%, whereas WPC$_{talc}$-Str forms 24.9 ± 0.9 wt.% of residue. The decomposition of PP is not affected at all.

In combination with WPC material, Str no longer forms pyrimidine derivatives. Here the release of ammonia was detected (*Figure5.27*). The release of ammonia is accompanied by with the formation of an acid. Acid is responsible for the cross-linkage of wood species,

which leads to the observed increase in residue. Furthermore formed acid shifts the decomposition of cellulose to lower temperatures, as was already reported for WPC-APP in section 5.1.1. But acid formation occurs at higher temperatures than in WPC-APP. *Figure5.27* gives the product release rates of ammonia and ketones for WPC_{talc}-Str. Ketones are typical products of wood decomposition. The formation of ammonia starts at temperatures where wood decomposition has already begun. Therefore interaction between the formed acid and cellulose is limited and cellulose decomposition is shifted to only marginally lower temperatures.

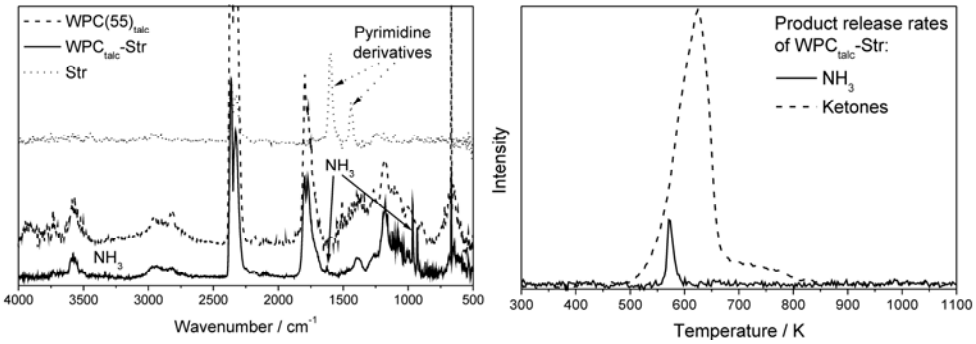

Figure 5.27: Evolved gas analysis for $WPC(55)_{talc}$, WPC_{talc}-Str and pure Str: FTIR spectra at 578 K (left) and product release rates of WPC_{talc}-Str for NH_3 and ketones (right)

The cone calorimeter results of WPC_{talc}-Str were improved in comparison to non-flame-retarded materials. The HRR is reduced for the first and last pHRR (*Figure5.28*). The main flame-retarded impact is a condensed-phase mechanism due to an increase in the amount of residue. WPC_{talc}-Str achieved performance similar to WPC_{talc}-APP. Parameters like THE, residue, 1.pHRR and last pHRR showed nearly the same values. The only difference was observed for TCOP. WPC_{talc}-Str showed the lowest CO release of all investigated materials (*Table5.12*).

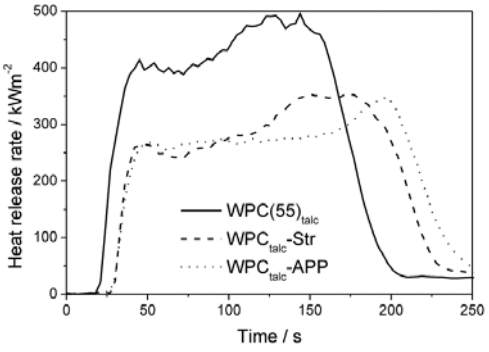

Figure 5.28: Cone calorimeter measurements at 50 kWm^{-2} for WPC_{talc}-Str in comparison with WPC_{talc}-APP

Table 5.12: Values of cone calorimeter measurements at different irradiations for WPC_{talc}-Str

Heat flux / kWm^{-2}	THE / MJm^{-2} ± 0.8	Residue / wt.% ± 0.5	1.pHRR / kWm^{-2} ± 5	Last pHRR / kWm^{-2} ± 15	TCOP / g ± 0.02
35	56.6	29.9	227	293	0.23
50	54.6	29.5	261	334	0.25
70	53.7	28.2	317	401	0.29

5.4. Conclusion of chapter 5

Different flame-retardant additives were tested to improve the fire properties of WPC material. Fire behavior was tested by cone calorimeter measurements. Furthermore, the mechanisms of action of these flame retardants inside WPC materials were investigated by carrying out TG-FTIR and FTIR measurements in the condensed phase.

All investigated flame retardants showed improvement in the fire behavior of WPC material. Their impacts are summarized in *5.13*. The lowest impact on flame retardancy was observed for the single flame retardants RP and EG, although EG showed the greatest potential for flame retardancy. It forms a layer made of graphite worms which acts as a highly effective thermal barrier. But disruption of the formed barrier worsened its effect and strongly decreased flame retardancy. The addition of APP, Dis or Str to WPC material achieved moderate results. All of these flame retardants reduced the HRR significantly. All act through a condensed-phase mechanism by cross-linking wood species to build up a barrier. The combination of APP and EG as well as APP and RP also achieved moderate results, and no further improvement in comparison to APP alone was observed. The best performance was achieved by Pax and the combination of RP and EG. Both flame-retardant formulations contain RP. RP alone was not able to significantly reduce the fire behavior of WPC material. But in combination with an oxygen source or a synergist it is able to form phosphates to cross-link residue. In Pax oxygen originates from additional additives inside the flame retardant. In RP + EG oxygen from the surrounding air comes in contact with the sample due to the good barrier properties of EG. Therefore EG and RP act synergistically because RP inhibits disruption of the residue.

Table 5.13: Comparison of flame-retarded impact for investigated flame retardants in WPC material

Flame retardant	Flame retardant loading	Condensed phase	Gas phase	Flame retardancy
EG	15 wt.%	X		Low
RP	5 wt.%		X	Low
Dis	10 wt.%	X		Medium
Str	15 wt.%	X		Medium
APP + EG	15 wt.%	X		Medium
APP + RP	10 wt.%	X	X	Medium
APP	15 wt.%	X		Medium
Pax	10.8 wt.%	X	X	High
RP + EG	10 wt.%	X		High

6. Flame retardancy of WPC decking boards

The investigations in the previous section focused only on the effects of materials. Other influencing factors were eliminated. In this section the fire behavior of WPC is investigated in relation to their use as decking boards. Decking boards are a product that introduces some important new parameters. The most important new parameter is the geometry of the samples. In addition, the influence of water uptake becomes important due to the field of application of decking boards in outdoor use.

6.1. Influence of geometry

WPC decking boards are available with hollow and solid profiles. The next section presents a study of the influence of these two types of decking boards and will give some deeper insights into the effects of a hollow shape. Referring to a product in end-use conditions also entails examining the effect of an incorporated surface profile.

6.1.1. General effects of hollow shape

To understand the differences between the burning of hollow and solid decking boards, first cone calorimeter investigations on model decking boards were carried out. A hollow (H2) and a solid decking board (S2) were manufactured with the material WPC(70). The samples were chosen to generate the same initial mass to eliminate every influence concerning different sample masses. The geometries used in this section 6.1.1 are given in *Figure 6.1*. A detailed description of all investigated geometries is presented in *Figure 3.2* of the experimental section.

Figure 6.1: Geometries S2 and H2 of WPC decking boards

Figure 6.2 presents the HRR and the EHC of the measurements. The first difference obtained from the comparison of hollow and solid samples is an additional pHRR at about 200 s for WPC(70) H2. The additional pHRR goes back to the effect which already caused the pHRR at the end of burning. Thermal conductivity inside the cavities of the hollow sample is poor. The thermal conductivity of air is about ten times lower than that of WPC material. The value of thermal conductivity at room temperature for air was derived from the literature [99] and the thermal conductivity of WPC material was measured to be around 0.35 $Wm^{-1}K^{-1}$. The cavities cause thermal feedback and generate an additional pHRR. Afterwards the burning front needs to breach the cavities. The HRR of WPC(70) H2 decreased in comparison to the solid sample. This decrease is caused by insulating effects due to the air cushion inside the cavities.

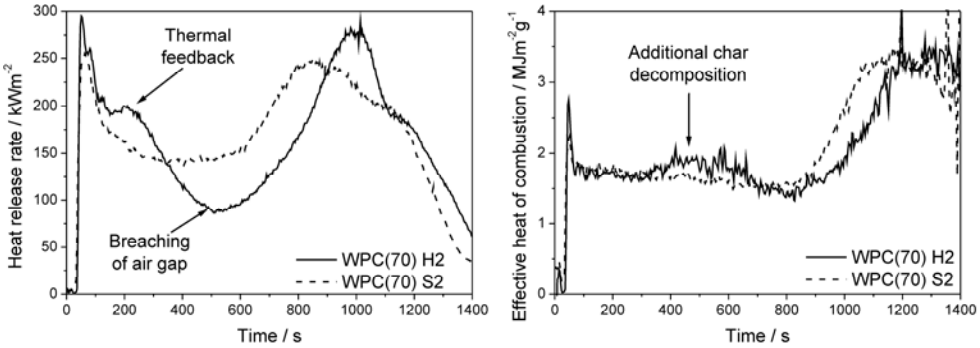

Figure 6.2: HRR and EHC for comparison of solid (S2) and hollow (H2) decking boards

The last pHRR of WPC(70) H2 is increased in comparison to WPC(70) S2. Exact values are given in *Table 6.1*. The decrease in last pHRR indicates that the residue from the solid board is able to insulate underlying material better than that from the hollow form.

The EHC offers some differences between the hollow and solid samples as well. An increased 1.pEHC was found for the sample of the hollow form. 1.pEHC is attributed to a change in the heating rate inside the sample. Thermal feedback increased the heating rate inside the sample because of the limited heat conduction to the back side. Due to the thin top layer of the sample, the influences of thermal feedback already occurred at the beginning of measurement. Furthermore, an additional pEHC occurred with a maximum at about 500 s (*Table 6.1*, *Figure 6.2*). When the pyrolysis front reached the cavity the progress of fire propagation slowed down because the pyrolysis front had to cross this gap. At this time the top layer of the sample was already burned and only char was left. But the thermal feedback still trapped heat inside the top layer. The result is additional char decomposition, which was detectable by an additional pEHC.

Table 6.1: Values of cone calorimeter measurements for WPC(70) H2 and WPC(70) S2 at an irradiance of 50 kWm^{-2} (values for pEHC(500s) are averaged from 400 s to 600 s to reduce the error)

	Last pHRR / kWm^{-2} ± 8	**1.pEHC / MJm^{-2}g^{-1} ± 0.1**	**pEHC(500s) / MJm^{-2}g^{-1} ± 0.03**
WPC(70) H2	284	2.63	1.87
WPC(70) S2	257	2.23	1.64

6.1.2. Influence of hollow shape concerning fire risks of commercially available decking boards

In a next step investigations were continued on commercially available decking boards and their fire risks compared. The geometries of commercially available decking boards are

optimized with regard to their mechanical properties and their cost-benefit ratio. For investigations of fire behavior three different samples were chosen: WPC(55)$_{talc}$ H1, WPC(60) H1 and WPC(50)$_{talc}$ S1. WPC(55)$_{talc}$ H1 and WPC(50)$_{talc}$ S1 have comparable material composition but different geometries, and WPC(55)$_{talc}$ H1 and WPC(60) H1 have the same geometry but different material compositions. A slight difference in material composition between WPC(55)$_{talc}$ H1 and WPC(50)$_{talc}$ S1 is due to the products on the market. The S1 and H1 geometries are plotted again in *Figure 6.3* as a reminder.

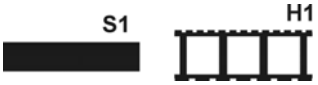

Figure 6.3: Geometries S1 and H1 of WPC decking boards

First cone calorimeter measurements were performed. One main difference between WPC(55)$_{talc}$ H1 and WPC(50)$_{talc}$ S1 is an increased THE for the solid sample (*Table 6.2*) because the solid sample contains a higher amount of combustible material. The time of burning for WPC(50)$_{talc}$ S1 is increased as well. Therefore solid decking boards are able to feed a fire for a longer time than hollow decking boards and present a higher risk in terms of long-duration fires.

Table 6.2: Values of cone calorimeter measurements for samples with different geometries

	THE / MJm^{-2} ± 8	**Burning time / s ± 100**	**1.pHRR / kWm^{-2} ± 8**	**Last pHRR / kWm^{-2} ± 8**	**Residue / wt.% ± 1**
WPC(60) H1	307	1660	353	182	18.9
WPC(55)$_{talc}$ H1	283	2010	343	185	26.8
WPC(50)$_{talc}$ S1	454	3490	381	133	30.1

Minor differences are a slightly increased 1.pHRR of WPC(50)$_{talc}$ S1 in comparison to WPC(55)$_{talc}$ H1 due to the slightly increased amount of PP. Furthermore WPC(55)$_{talc}$ H1 has an increased last pHRR because the total amount of residue is higher for WPC(50)$_{talc}$ S1 than for WPC(55)$_{talc}$ H1. The increase in the total amount of residue is also the reason why the percentage of residue increases for WPC(50)$_{talc}$ S1 (*Table 6.2*). Apart from the difference in the last pHRR, the HRR curves of WPC(50)$_{talc}$ S1 and WPC(55)$_{talc}$ H1 show similar shapes (*Figure 6.4*). The risk of igniting other objects while WPC decking boards are burning is similar for both. A difference occurred for WPC(60) H1. It shows a strong additional pHRR at about 500 s. The pHRR is not attributed to the thermal feedback of the cavities. It goes back to the collapse of the top layer. The top layer of the hollow decking board was no longer able to bear its own weight. The protective char layer was destroyed and the HRR increased. The increased heat release at the beginning also increases the fire risk of the sample because ignition of other objects is more probable. The top layer caves in

if the wood content of the WPC is not high enough. WPC(70) H2 had a comparable geometry and showed no collapse. Another possibility for avoiding collapse of the top layer in the cone calorimeter measurements is the addition of talc. As already mentioned in chapter 4, talc forms a shell around the residue and stabilizes it. The mechanical properties of a residue containing talc improve.

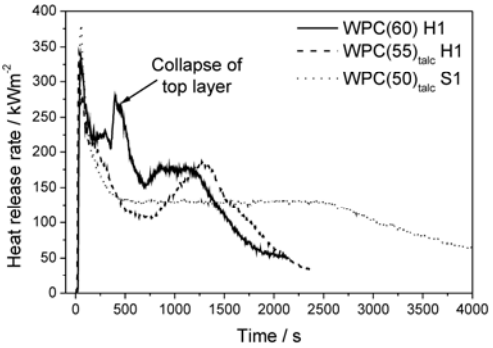

Figure 6.4: Cone calorimeter measurement for commercially available hollow and solid samples at an irradiance of 50 kWm^{-2}

Apart from increase in the HRR, the subsidence of the top layer also increased the production of CO and smoke. *Figure 6.5* shows a comparison of the smoke and CO production of WPC(60) H1 and WPC(55)$_{talc}$ H1. Results for the same materials with only simple geometries of plates of 3 mm thickness are also shown. Samples as plates avoid the effects of geometry. For plates no difference was observed between the samples with and without talc. But hollow samples of WPC(60) showed increased values.

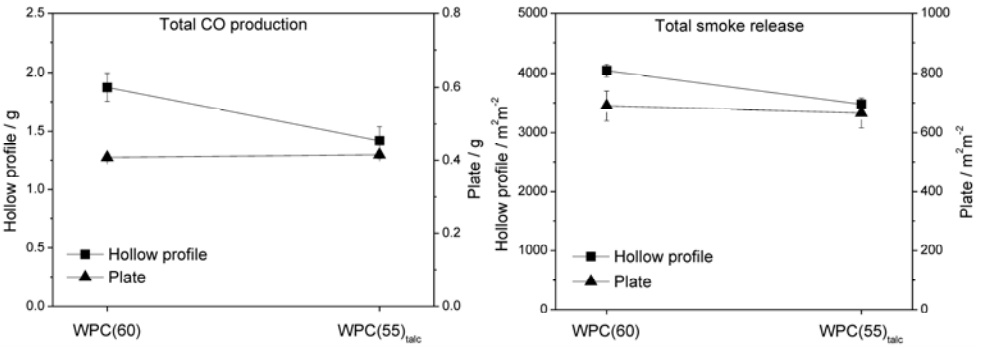

Figure 6.5: TCOP and TSR for WPCs with and without talc for hollow profiles and plates (lines serve only as a visual aid and do not represent values for WPCs with other talc contents)

Another important parameter of flooring material is flame spread. If flames spread across the floor quickly they can immediately ignite other objects far away from the ignition source.

Flame spread was measured with RPT. The sample was ignited with a methane burner at the edge of the decking board. (*Figure 6.6)* shows the burned length of the samples over time. The shape of the curve of burned length was comparable for all samples. The burned length increases over time, but over time the slope of the curve decreases. The solid sample (WPC(50)$_{talc}$ S1) achieved a lower burned length than the investigated hollow samples. Both of the hollow samples (WPC(60) H1 and WPC(55)$_{talc}$ H1) showed no differences and obtained similar results. In general it is concluded that the flame spreads more slowly across solid decking boards than hollow ones.

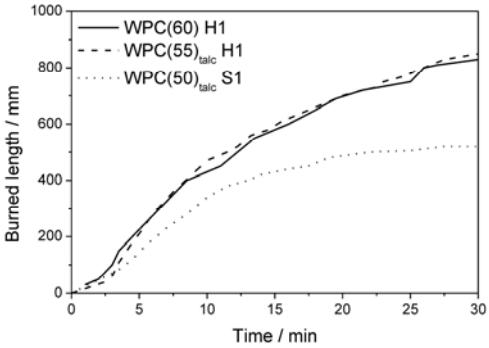

Figure 6.6: Radiant panel test of hollow and solid samples

Flame spread is a response of areas which are not burning to the energy released during the combustion of areas which are burning. If the energy is high enough to ignite other parts the fire will spread. The energy released is due, first, to the combustion of the material itself. Second, in the RPT an external heat source is added. The external heat source is the reason why the slope of the curves of measured burned length decreases. The burner is placed at the edge of the sample. Its impact on unburned material decreases as the burning front moves away from the burner. In addition, the applied heat flux of the heater decreases over sample length.

The impact of the flame of the burning sample itself is displayed in the cone calorimeter measurements. Most important is the HRR at the beginning of the cone calorimeter measurement, because the flame at the edge of the burning front has the highest impact. The HRR at the beginning of the cone calorimeter measurements (0 – 250 s) was similar for all samples (*Figure 6.4*). Due to comparable material compositions for all samples, the thermal properties of the investigated samples are also similar. But the different geometries (H1 and S1) allow different heat uptakes. Solid samples are able to take up much more heat due to their increased sample masses. They are furthermore able to conduct more thermal energy away from the claimed section. The cavities inside the hollow decking boards, again, hinder heat conduction inside the samples.

Subsidence of the top layer in RPT measurements was observed for both of the hollow samples, WPC(55)$_{talc}$ H1 and WPC(60) H1. But for WPC(60) H1 it was more distinct. However, caving in had hardly any influence on the burned length in RPT because it

occurred after about 600 s at a fixed place. At this time the burning front is already too far away from the subsidence to have a major impact.

In general, it is concluded that solid decking boards S1 show lower fire risk in terms of flame spread than hollow decking boards H1.

6.1.3. Variation of hollow geometries

To gain a deeper insight into the effect of the hollow shape, additional measurements were performed with varied hollow-shaped geometries. First the width of the cavities and then the height of the cavities were varied. The WPC material was chosen to be WPC(70), showing no collapse of the charred top layer. The geometries studied in this section are summarized in *Figure 6.7*.

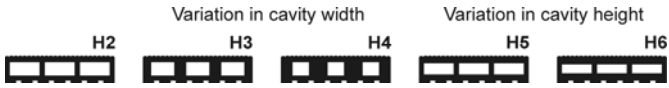

Figure 6.7: Geometries H2, H3, H4, H5 and H6 of WPC decking boards

Figure 6.8 presents the cone calorimeter results for variation of cavity width. The main effect in HRR was a decrease in the last pHRR for decreasing cavity widths. A decreased cavity width allows more initial mass to be stored inside the sample. The increased sample mass allows the production of an increased total amount of residue, which is able to act as a better barrier. In parallel, the increase in initial mass increased the burning time of the sample. The 2.pHRR at about 200 s also decreased with decreasing width of the cavities. The 2.pHRR is related to decreased heat conductivity inside the cavities. The reduced cavity width goes along with an increase in the thickness of the bars inside the cavities. Thicker bars between the cavities allow better heat conduction from the top of the sample to the bottom. Less heat is trapped inside the top layer and the 2.pHRR decreases. The EHC showed a decrease in 2.pEHC for decreasing width of cavities as well. The 2.pEHC was related to additional char decomposition in the top layer due to an increased temperature. The increased heat conduction reduces the thermal feedback and therefore reduces the temperature inside the top layer, which reduces the additional char decomposition as well.

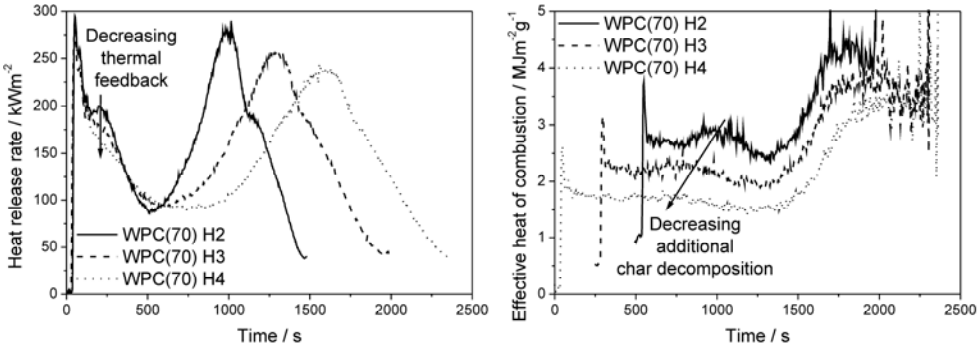

Figure 6.8: Influence of different cavity width in HRR and EHC (cavity width of H2 = 28 mm, of H3 = 22 mm and of H4 = 16 mm)

Variations in cavity heights are shown in *Figure 6.9*. Again, a decrease in the last pHRR occurs for samples with decreased cavity heights. This decrease relies on the increased initial mass as was discussed above. The 2.pHRR was decreased to a shoulder for the geometries H5 and H6. H5 and H6 show decreased cavity heights in comparison to H7. Therefore H5 and H6 have a top layer which is increased in thickness. The thicker top layer is able to create an increased total amount of residue. It acts as a better barrier while reaching the 2.pHRR. This better barrier resulted in a decreased HRR. The EHC shows no changes. Heat conduction inside the samples was affected only marginally by varying the cavity heights. The 2.pEHC showed no change.

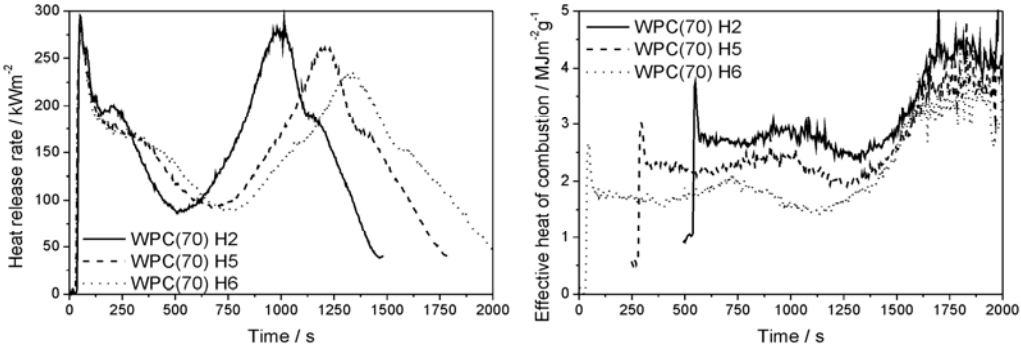

Figure 6.9: Influence of different cavity heights in HRR and EHC (cavity height of H2 = 13 mm, of H5 = 11 mm and of H6 = 9 mm)

6.1.4. Effect of surface profile

For this study different surface profiles were incorporated onto WPC samples. The samples were plates of 3 mm thickness with an additional surface profile of 2 mm. The samples are discussed in detail in the experimental section (*Figure 3.3*). The material was WPC(70), as already used for other investigations concerning geometry.

Measurements of samples with different surface profiles show a difference only in the last pHRR and in the burning time. The same differences were also observed by just varying the initial mass of the samples without adding a surface profile (*Figure 6.10*). It is concluded that surface profiles have hardly any influence on the burning behavior of a WPC. Their only impact is the storage of additional combustible material.

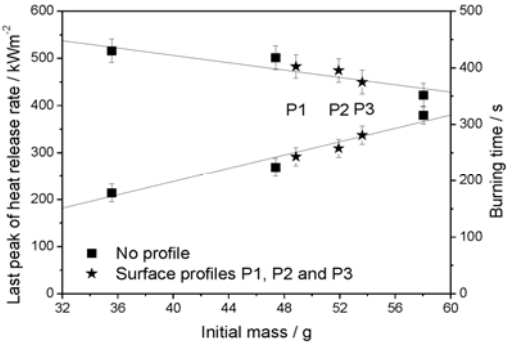

Figure 6.10: Influence of surface profile by comparing samples with and without surface profiles (lines serve as visual aids)

6.2. Influence of moisture

WPC decking boards are mainly used for terraces or balconies and therefore have their main field of application in outdoor use. The materials come in contact with water, so because they are a wood composite WPCs are able to take up much more water than other polyolefin materials. In our studies WPC(60) was able to take up 16 wt.% of moisture. The general effect of moisture is already well known. The endothermic reaction of water evaporation cools the sample and the water vapor dilutes pyrolysis gases [100]. In thin samples water evaporation and pyrolysis occur simultaneously and water has already evaporated before ignition. In thicker samples a drying zone is formed which moves in front of the pyrolysis zone [101].

Moist decking boards were tested in a cone calorimeter. Four different moisture contents were tested: 5 wt.%, 10 wt.% and 16 wt.% of moisture and a dry sample. Cone calorimeter results confirmed the effect of water discussed above. Cooling and flame gas dilution reduced burning at the beginning, which is seen in the reduction of the 1.pHRR and in an increase in burning time (*Table 6.3* and *Figure 6.11*). The end of burning is not affected at all; values for the last pHRR are the same for all samples. By this time the water is already completely evaporated from the sample. Neither did the THE show any change. Moist samples contained the same amount of combustible material as dry samples.

Table 6.3: Values of cone calorimeter measurements at 50 kWm^{-2} for WPC(60) containing different amounts of moisture

	1.pHRR / kWm^{-2} ± 5	**2.pHRR / kWm^{-2} ± 3**	**Last pHRR / kWm^{-2} ± 8**	**1.pEHC / MJm^{-2}g^{-1} ± 0.18**	**THE / MJm^{-2} ± 8**
WPC(60) dry	358	330 ± 25	191	3.6	300
WPC(60) 5% moist.	339	220	191	3.1	311
WPC(60) 10% moist.	275	220	189	2.3	314
WPC(60) 16% moist.	273	218	186	2.3	309

Hollow decking boards made of WPC(60) showed a collapse of the top layer while burning. The same effect was observed for the dry sample of WPC(60). An additional pHRR arose at about 400 s. For samples with 5 wt.% moisture, the collapse was shifted to later times. The pHRR, which was attributed to the collapse, occurred at about 650 s. Samples with 10 wt.% and more moisture did not cave in at all. Water must have changed the decomposition mechanism of wood, leading to a residue with enhanced mechanical properties. For samples which show no collapse of the top layer, a pHRR attributed to thermal feedback from the cavities was observed at about 330 s. Due to the delayed collapse for WPC(60) with 5 wt.% moisture, a pHRR due to thermal feedback was observed here as well. The pHRR of thermal feedback is further increased, because at this time hardly any water evaporated. Water evaporation originated from a drying zone located underneath the pyrolysis zone. When thermal feedback occurred, the pyrolysis zone was located directly above the cavities. This means that the drying zone was inside the cavities, where only a small amount of water was stored inside the bars. A lack of water evaporation is seen in the EHC as well. In general water evaporation reduces the EHC because it adds a mass loss without contributing to the HRR. A lack of water evaporation causes an additional pEHC. The pEHC due to lack of water evaporation is marked in Figure 9. Values of the 1.pEHC of moist samples (*Table 6.3*) are decreased further than could be explained by just taking the mass loss of water evaporation into account. Additional cooling of the sample at the beginning also contributes to reduction of the 1.pEHC. The 1.pEHC originates from an increased heating rate inside the WPCs before formation of a protective residue (chapter 4.2). Cooling reduces the heating rate and therefore reduces the 1.pEHC.

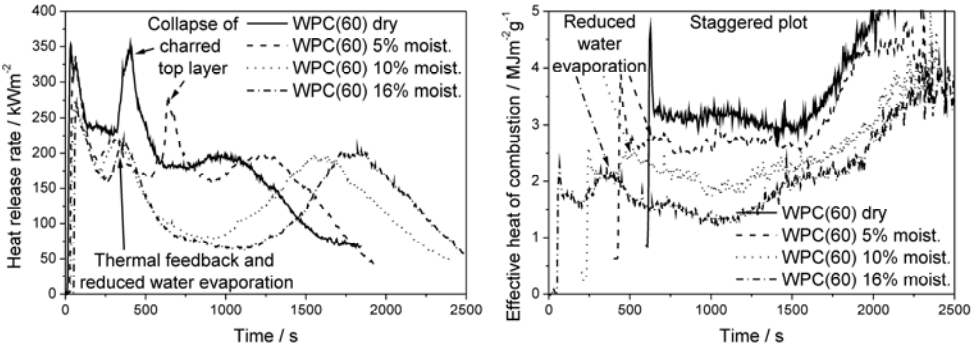

Figure 6.11: Cone calorimeter measurements to investigate the influence of moisture on the burning behavior of WPC decking boards. The plot of EHC is shown staggered. Shifts are 200, 400 and 600 s for the x-axis and 0.3, 0.6 and 0.9 $MJm^{-2}g^{-1}$ for the y-axis.

Further investigations were carried out on samples in the form of plates to eliminate the effect of geometry. Both hollow decking boards and plates showed a decrease in TSR and TCOP for increasing moisture contents (*Figure 6.12*). The reason is the change in the thermal decomposition mechanism of wood, which was already notable in the formation of a residue with enhanced mechanical properties. Furthermore, the decrease for hollow decking boards is much stronger than for plates. For hollow decking boards an additional effect occurred. The collapse of the charred top layer caused an increase in TCOP and TSR as well, which was already discussed above. Accordingly, the avoidance of collapse decreased the TCOP and TSR. For hollow decking boards containing 5 wt.% moisture the collapse was less distinct, hence values lie between those of the dry sample and the samples with higher moisture contents.

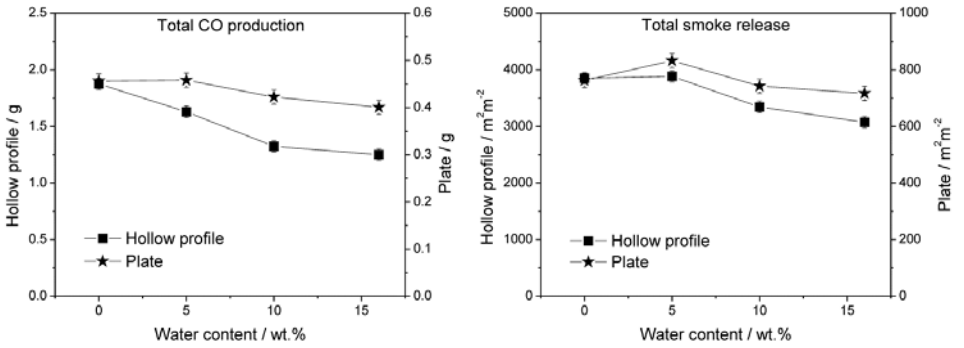

Figure 6.12: Comparison of CO and smoke production for WPC with different moisture contents. Samples are decking boards and plates. (Lines are visual aids.)

6.3. Influence of flame retardants

Apart from the investigations of various flame retardants in WPCs in chapter 5 with respect only to the material, different flame retardant formulations were also tested as hollow decking boards in end use geometry. Measurements were carried out with cone calorimeter and RPT.

Cone calorimeter results of WPC(50)$_{talc}$-APP and WPC(50)$_{talc}$-Str confirmed the outcome of investigations of chapter 5. An increased amount of residue due to cross-linking formed a better barrier than in WPC(55)$_{talc}$ and reduced the HRR (*Figure 6.13* and *Table 6.4*). Additional cross-linking made a positive contribution to preventing the subsidence of the top layer because it improves the mechanical properties of charred residue. Furthermore the THE is reduced in comparison to WPC(55)$_{talc}$ because of the exchange of combustible material by the flame retardant and due to the storage of combustible material in the residue due to cross-linking. WPC(50)$_{talc}$-Str also showed a decrease in TCOP.

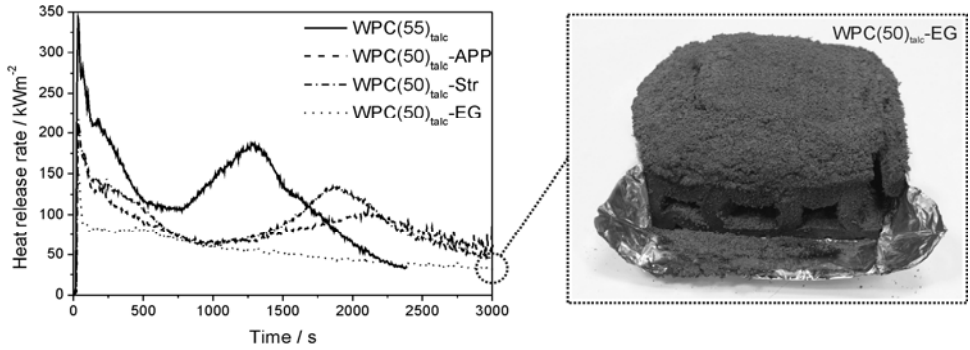

Figure 6.13: Heat release rates of WPC decking boards with different flame retardants and a picture of the residue of WPC(50)$_{talc}$-EG after cone calorimeter measurement

WPC(50)$_{talc}$-EG showed a different behavior than was observed in section 5.1.2. Decking boards flame-retarded with EG showed only one peak in their HRRs at about 30 s (*Figure 6.13*). Afterwards the HRR dropped down and flaming combustion switched mainly to glowing combustion. After the measurements, all investigated samples containing EG showed unburned material remaining at the bottom of the sample. *Figure 6.13* also shows a picture of the residue after cone calorimetric measurements at 50 kWm^{-2}, which indicates that not all WPC material was consumed. Furthermore FTIR-ATR measurements identified peaks of unburned PP and wood. The reason for changed burning behavior is a different residue formation. During investigations of WPC(50)$_{talc}$-EG in section 5.1.2, residue showed a loose structure and the expansion of graphite worms disrupted the formed residue. Decking boards made of WPC(50)$_{talc}$-EG formed a continuous graphite layer on top of the sample without disrupting the residue. A barrier of loose residue is easy to break. Evaporating pyrolysis gases and flames were able to break holes inside the formed barrier, worsening its thermal protection properties. The residue of decking boards made of WPC(50)$_{talc}$-EG did not break during measurements and therefore provides better thermal barrier protection of the underlying material.

For WPC(50)$_{talc}$-EG decking boards the temperature underneath the graphite layer was not high enough to decompose WPC material. But it was high enough to further expand the graphite worms. During investigations of WPC(50)$_{talc}$-EG material in section 5.1.2 the temperature underneath the graphite layer was high enough to decompose WPC material and promote combustion. But in principle a loose graphite structure would offer better thermal barrier properties than compact structures if the graphite layer were not disrupted by evaporating pyrolysis gases.

Comparing the 1.pHRRs, the WPC(50)$_{talc}$-EG material in section 5.1.2 offers lower values than WPC(50)$_{talc}$-EG in decking boards (*Table 5.3* compared to *Table 6.4*). For 50 kWm^{-2} the difference amounted to about 70%. A loose structure of graphite worms includes a larger volume of gaps inside the layer than in a compact structure. Gaps increase thermal barrier properties. Intumescent flame-retardant systems are also designed to form a ballooned structure of char to increase thermal barrier properties [102].

In summary, cone calorimeter measurements show that all flame-retarded samples reduce the fire risk of long-duration fires and the risk of igniting other objects by burning WPCs in comparison to WPC material without flame retardants. The lowest fire risks were obtained by decking boards made of WPC(50)$_{talc}$-EG.

Table 6.4: Results of cone calorimetric measurement for flame-retarded decking boards

Sample at heat flux	**THE / MJm^{-2} ± 8**	**Residue / wt.% ± 1.3**	**1.pHRR / kWm^{-2} ± 7**	**Last pHRR / kWm^{-2} ± 7**	**TCOP / g ± 0.2**	**t_{ig} / s ± 15%**
$WPC(55)_{talc}$ at 50 kWm^{-2}	283	26.8	343	185	1.4	16
$WPC(50)_{talc}$-APP at 35 kWm^{-2}	216	44.9	158	86	2.0	59
$WPC(50)_{talc}$-APP at 50 kWm^{-2}	235	41.5	210	105	1.8	23
$WPC(50)_{talc}$-APP at 70 kWm^{-2}	248	38.2	272	141	1.7	14
$WPC(50)_{talc}$-Str at 35 kWm^{-2}	218	41.0	164	98	0.8	62
$WPC(50)_{talc}$-Str at 50 kWm^{-2}	240	38.4	214	129	0.8	21
$WPC(50)_{talc}$-Str at 70 kWm^{-2}	256	34.8	270	176	1.1	13
$WPC(50)_{talc}$-EG at 35 kWm^{-2}	85	76.8	117	-	1.3	61
$WPC(50)_{talc}$-EG at 50 kWm^{-2}	145	61.7	155	-	2.7	24
$WPC(50)_{tal}$-EG at 70 kWm^{-2}	194	52.5	201	-	2.2	13

The radiant panel test also showed a reduced fire risk for flame spread of flame-retarded decking boards in comparison to unprotected samples. The results are given in *Figure 6.14*. It shows burned lengths of the samples as a function of time. The slowest flame spread was obtained from $WPC(50)_{talc}$-EG. The burned length after 30 min amounted to 370 ± 10 mm. Both $WPC(50)_{talc}$-APP and $WPC(50)_{talc}$-Str achieved similar results for flame spread, which lay above the values for $WPC(50)_{talc}$-EG. The burned length after 30 min amounted to 480 ± 10 mm for $WPC(50)_{talc}$-APP and 470 ± 10 mm for $WPC(50)_{talc}$-Str, respectively. Classification of the samples according to DIN EN 13501 would lead to class C_{fl} for $WPC(50)_{talc}$-EG and class D_{fl} for $WPC(50)_{talc}$-APP and $WPC(50)_{talc}$-Str. In comparison, $WPC(50)_{talc}$ failed RPT according to DIN EN 13501 and could only achieve class E_{fl}. Closer inspection of the burned length of all samples in *Figure 6.14* reveals similar values at the beginning of the test up to 3 min.

Differences for different materials do not occur until after 3 min. At the beginning of measurement the applied heat flux is dominated by the burner inside RPT and approximately similar for all investigated materials. The applied heat flux to the unburned part of the sample is the sum of the heat flux of the burner, the heat flux of the heater and the heat flux of the flame in parts of the sample that are already burning. The impact of the burner becomes smaller as the burning front moves forward. None of the flame retardants is able to act before the samples are already heated up. EG needs to reach a temperature close to the start of decomposition of the WPC material to expand, and both APP and Str can act only if the sample is already burning. Ignition (t_{ig}) of the samples is affected only slightly by adding these flame retardants (*Table 6.4*). Only if the samples are already burning does a difference for different flame retardants appear. Flame retardants reduce the heat release of burning WPC samples. This reduces the applied heat flux on unburned regions of the samples and thus the flame spread.

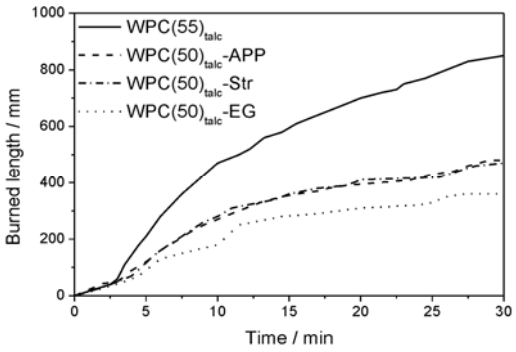

Figure 6.14: Radiant panel tests of flame-retarded WPC decking boards

RPT measurements of investigated flame-retarded samples show that further reduction of flame spread must be realized by increasing the time to ignition of the samples. Strong reduction in the HRR for $WPC(50)_{talc}$-EG was not able to reduce flame spread at the beginning of the test. Impeding ignition would permit the material to reduce flame spread even at the beginning of RPT, with the additional applied heat flux from the external burner.

6.4. Correlation between radiant panel test and cone calorimeter

Measurements of flame spread with RPT are much more extensive than performing measurements with cone calorimeter. Predicting the results for flame spread with cone calorimeter measurements would help save money and time.

RPT measures the flame spread of a material. The literature presents different possibilities for predicting flame spread with the cone calorimeter. Two possibilities are to use pHRR or pHRR divided by time to ignition as a direct correlation parameter [103]. PHRR is often used as simplification for measured HRR during the cone calorimeter test. HRR is directly correlated to the heat flux exposed from the flame of a burning sample. Time to ignition inserts another important parameter for flame spread by assessing ignitability.

Figure 6.15 presents the burned length of various samples after 10, 20 and 30 min in the RPT in comparison to the pHRR (left) and pHRR / t_{ig} (right) in cone calorimeter measurement.

Both parameters show a good correlation for samples with the same geometry. For samples of hollow shape H1 a fitting line for different measurements is plotted on the figure. For these samples burned length increases linearly with increasing pHRR or pHRR / t_{ig}, respectively. Solid decking boards yielded different results. For pHRR all of the measured values of burned length after 10, 20 and 30 min do not fit with the results for hollow decking boards. For pHRR / t_{ig} the values for burned length after 10 min showed strong correlation, but, again, after 20 and 30 min the values diverged from those of hollow decking boards. As already discussed in 6.1, geometry plays an important role for thermal conduction and heat uptake inside the samples. The pHRR is not able to express the thermal properties inside the sample. It is only a proportion for the heat flux of the flame. Time to ignition did not show a direct correlation to thermal properties inside the sample either, but it is affected by thermal properties [87]. Especially for flame spread, thermal properties of the sample are very important — as already discussed in section 6.1.

If the thermal properties of the samples are the same, the pHRR and pHRR / t_{ig} are good possibilities for predicting the flame spread. If the thermal properties differ, pHRR does not correlate at all with RPT, and pHRR / t_{ig} shows only a minor correlation. Measurements of the thermal conductivity and heat capacity showed that they differ only slightly for investigated WPC formulations. This means that geometry is the only residual parameter with a major influence on thermal conduction inside the sample.

The slope of the fitting lines for samples with good correlation increases for increasing test times in the RPT. This means the impact of the pHRR on the burned length increases. Apart from the heat flux of the flame, external heat fluxes are also set to the samples inside the RPT. Due to the setup of the measurement, external heat flux decreases with increasing burned length and thus the impact of the heat flux of the flame becomes more relevant. Furthermore, at the beginning of the RPT flame spread is dominated by the pilot flame which ignites the sample. After 10 min the burner for the pilot flame is switched off. This explains the greater difference between measurements after 10 and 20 min. Afterwards the difference between 20 and 30 min is much smaller.

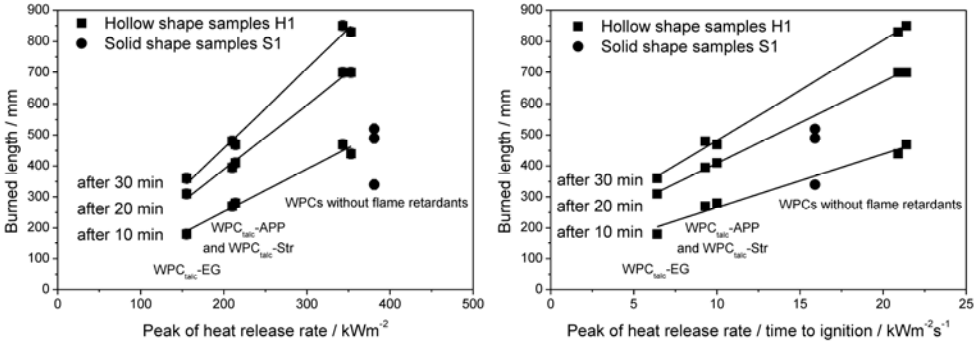

Figure 6.15: Correlation between burned length from radiant panel test and pHRR as well as pHRR / t_{ig} from cone calorimeter measurement for different samples

6.5. Conclusion of chapter 6

The flame retardancy of products made of WPC offer new important factors influencing fire behavior other than the flame retardancy of WPC material alone. Here WPC decking boards were investigated according to the main field of application of WPC material. Fire behavior was studied by cone calorimetric measurements and measurements of RPT.

The most important influence on burning behavior, apart from material properties, was the geometry of the samples. Decking boards exhibit solid and hollow geometries. Hollow decking boards reduce the amount of combustible material and therefore reduce the risk of long duration fires. But by incorporating cavities inside the decking boards, heat conduction from the top to the bottom and the amount of heat which can be stored inside the decking board are reduced. This increases the flame spread for hollow decking boards in comparison to solid ones. By increasing the thickness of the bars between the cavities in hollow geometries, the heat flow increases and flame spread is reduced. Therefore optimized cavity geometries should contain thick bars. Cavity height plays only a minor role. Furthermore, hollow decking boards bear the risk of the top layer caving in during burning. Subsidence destroys the residue layer and boosts combustion. Subsidence is prevented by adding flame retardants that act by cross-linking the residue. Furthermore, the addition of talc also reduced the risk of subsidence.

With respect to its use as decking boards in flooring applications, $WPC(50)_{talc}$-EG turned out to show the best properties in flame retardancy of the investigated materials. The results for $WPC(50)_{talc}$-EG deviated from those in chapter 5. After formation of a continuous layer of expanded graphite, the resulting thermal barrier was able to prevent underlying material in cone calorimeter tests from being combusted.

For all of the flame-retarded WPC decking boards with similar geometries investigated, it was possible to predict flame spread in RPT using cone calorimetric data, specifically pHRR or pHRR / t_{ig}.

Since WPC decking boards are used in outdoor applications, the moisture uptake of decking boards becomes important. Moisture reduces the HRR of the samples due to an endothermic reaction of water evaporation and flame gas dilution. Furthermore, moisture changes the thermal decomposition mechanism of wood, leading to modified residue and reduced CO production.

7. Conclusion

In this work the fire behavior of WPCs was investigated and optimized in relation to its fire properties. In a first step among investigations of the basic mechanisms of burning of WPC material, the impact of material composition and thermal properties was investigated. Therefore measurements with cone calorimeter and PCFC were performed as well as numerical simulations with FDS. In a next step different flame retardant additives were tested to improve the fire behavior of WPC material and examine its mechanisms of action. Investigations based on TG-FTIR measurements and FTIR measurements in the condensed phase were carried out as well as cone calorimeter tests. In the last part special attention was drawn to the flame retardancy of WPC decking boards, which represent a product in end-use conditions. Apart from cone calorimeter measurements RPTs were also performed, which present a test for flooring materials.

WPCs offer the same burning behavior as pure wood samples, with an increased heat release. Heat release goes mainly back to the PP inside the samples. PP has a heat of combustion more than four times higher than wood. In general PP burns much more vigorously than wood. Accordingly, WPC burns even more vigorously as the ratio of PP to wood increases. In contrast, substituting wood with other wood species has only a minor influence, as does the addition of talc. Numerical simulations of cone calorimeter measurements identified that the specific heat of WPC material and the heat of combustion of PP content has the greatest impact on WPC burning.

All of the investigated flame retardants improved the burning behavior of WPC material. The lowest impact was achieved by the flame retardants EG and RP, although EG showed the highest potential for flame retardancy. EG forms a very effective thermal barrier on top of WPC samples, but continuous disruption of the residue worsens the barrier formed. Disruption is accompanied by the expansion of graphite worms. RP acts over a condensed-phase and a gas-phase mechanism, but neither is able to achieve good flame retardancy in WPC material. APP, Dis and Str all act all over a condensed-phase mechanism by cross-linking wood species. This results in increased residue formation, which produces an increased thermal barrier. All achieved good results in their flame-retardant actions. Combinations of APP and EG as APP and RP achieved good flame-retardant impacts as well. But performance is not increased in comparison to WPC samples containing only APP. For combinations of APP and EG, the disruption of the residue that goes along with the addition of EG was partly avoided. But high amounts of APP are necessary to embed expanded graphite worms in a cross-linked residue. This sampled amount of EG was too low to activate its full potential. The best results were obtained for Pax and the combination of EG and RP. Both flame-retardant formulations are based on a synergistic effect between RP and other components to form phosphates. The formation of phosphates is possible only if RP comes in contact with oxygen. In Pax ingredients are added which present an oxygen source. In contrast, EG decreases the flames of the burning sample so that oxygen from the surrounding air is able to contact the sample due to the good thermal barrier properties of EG. In return, phosphates formed from RP embed expanded graphite and hinder the residue from being disrupted.

Measurements of flame-retarded WPC decking boards by APP and Str achieved similar results as the fire tests for material investigations. But WPC-EG yielded different results.

Here graphite worms formed a continuous layer above the sample without disrupting the residue. Therefore WPC-EG presents the best investigated material composition to flame-retard WPC with respect to a flooring application. Apart from the impact of material, the geometry of decking boards is also important for their fire behavior. WPC decking boards are available in solid and hollow shapes. Hollow decking boards reduce the amount of combustible material and therefore present a lower risk of long-duration fire. But the incorporation of cavities decreases the heat flow from the top to the bottom, resulting in an increase of flame spread in comparison to solid WPC decking boards. Furthermore, hollow decking boards present the risk of the top layer caving in during combustion, destroying the formed char layer and accelerating combustion. Subsidence is avoided by cross-linking the formed residue. Furthermore, the addition of talc also provided positive effects on preventing subsidence. In outdoor applications moisture uptake becomes important. During burning moisture evaporation cools the sample and dilutes the flame gases, resulting in a reduction of the HRR. Furthermore moisture changes the thermal decomposition of wood, as wood decomposition depends strongly on the heating rate inside the sample. Moist samples show reduced values of CO and smoke production. Additionally, the formed residue offers increased mechanical properties to prevent the subsidence of hollow samples.

8. Future work

Due to very few publications on the flame retardancy of WPCs, this thesis sets the basis for the development of flame-retarded WPC materials. The topic offers different possibilities for continuing work.

The investigations discussed in this thesis are based on measurements on a small scale up to sample dimensions of about one meter. Up to now investigations on an even larger scale are lacking. Studying the burning behavior of a complete balcony could be realized either by real measurements or by numerical simulations.

The thesis also focused on WPC products in end-use conditions. Apart from studying WPC decking boards, other applications could be analyzed as well. Nowadays WPC materials are also used as façade claddings. As opposed to flooring, façades present a vertical application. Upward flame spread differs from horizontal flame spread, so that further investigations would be necessary to draw conclusions on the burning of WPC facade cladding.

9. Abbreviations

WPC	Wood-plastic composites
PE	Polyethylene
PP	Polypropylene
$\dot{q}$	Heat flux
ε	Emissivity
σ	Stefan-Boltzmann constant
T	Temperature
h_c	Surface convective heat transfer
C_v	Heat capacity at constant volume
C_p	Heat capacity at constant pressure
ρ	Density
t	Time
t_{ig}	Time to ignition
k	Rate constant of pyrolysis
R	Universal gas constant
A	Pre-exponential factor
E_A	Activation energy
APP	Ammonium polyphosphate
RP	Red phosphorus
EG	Expandable graphite
Dis	Disflamoll TP LXS 51064
Pax	Paxymer
Str	Struktol SA 0832
TG	Thermogravimetric analysis
FTIR	Fourier-transform infrared spectrometer
ATR	Attenuated total reflection
PCFC	Pyrolysis combustion flow calorimeter
HRR	Heat release rate
THE	Total heat evolved

TCOP	Total CO production
EHC	Effective heat of combustion
RPT	Radiant panel test
SEM	Scanning electron microscopy
FDS	Fire dynamics simulator
MLR	Mass loss rate
DTG	Differential thermogravimetric analysis
pHRR	Peak of heat release rate
pEHC	Peak of effective heat of combustion

10. Presentations and Publications

Henrik Seefeldt & Ulrike Braun

"Flame retardancy of ammonium polyphosphate protected wood plastic composites"

Poster presentation at European Conference on Composite Materials 2010 in Budapest

Henrik Seefeldt, Ulrike Braun & Anja Hofmann

“Influence of structure, wood content, moisture and additives on the burning behaviour of wood plastic composites”

Lecture and conference contribution at Fire and Materials 2011 in San Francisco

Henrik Seefeldt & Ulrike Braun

“Burning behaviour of wood plastic composite decking boards in end use conditions: the effect of geometry, material composition and moisture”

Journal of Fire Science 2012; 30 (1): 41-54

Henrik Seefeldt & Ulrike Braun

“A new flame retardant for wood material tested in wood-plastic composites”

Macromolecular Materials and Engineering 2012;

DOI: 10.1002/mame.201100382

Annette Naumann, Henrik Seefeldt, Ina Stephan, Ulrike Braun & Mathias Noll

“Material resistance of flame retarded WPCs against fungal decay”

Polymer degradation and stability 2012;

DOI: 10.1016/j.polymdegradstab.2012.03.031

Henrik Seefeldt, Ulrike Braun & Manfred H. Wagner

“Residue stabilization in fire retardancy of wood-plastic composites: combination of ammonium polyphosphate, expandable graphite and red phosphorus”

Macromolecular chemistry and physics;

DOI: 10.1002/macp.201200119

11. References

[1] Chawla KK, Composite Materials: Science and Engineering, Springer, Birmingham **1998**

[2] Woodrow B and Szlawieniec-Haw M, World Fire Statistics 27, Geneva Association Information Newsletter, Geneva **2011**

[3] Di Nenno PJ, Drysdale D, Beyler CL, Walton WD, Custer RLP, Hall JR and Watts JM, Appendices, SFPE Handbook of Fire Protection Engineering Third Edition, A40-A42, National Fire Protection Association, Massachusetts **2002**

[4] Zaikov GE and Lomakin SM, Ecological Issue of Polymer Flame Retardancy, Journal of Applied Polymer Science **2002**; 86 (10): 2449-2462

[5] Green J, An Overview of the Fire Retardant Chemicals Industry, Past - Present - Future, Fire and Materials **1995**; 19 (5): 197-204

[6] Lyon RE, Heat Release Kinetics, Fire and Materials **2000**; 24 (4): 179-186

[7] Lyon RE, Janssens ML and Mark HF, Encyclopedia of Polymer Science & Technology, Wiley, **2004**

[8] Factor A, Char Formation in Aromatic Engineering Polymers, Fire and Polymers 425, 274-287, American Chemical Society, **1990**

[9] Warnatz J, Maas U and Dibble RW, Combustion Physical and Chemical Fundamentals, Modeling and Simulation, Experiments, Pollutant Formation, Springer, Heidelberg **1998**

[10] Grønli MG and Melaaen MC, Mathematical Model for Wood Pyrolysis Comparison of Experimental Measurements with Model Predictions, Energy & Fuels **2000**; 14 (4): 791-800

[11] Richard E L, Pyrolysis Kinetics of Char Forming Polymers, Polymer Degradation and Stability **1998**; 61 (2): 201-210

[12] Mulholland GW, Section 2 / Chapter 13 Smoke production and properties, SFPE Handbook of Fire Protection Engineering 258-268, National Fire Protection Association, Quincy **1995**

[13] Léonard S, Mulholland GW, Puri R and Santoro RJ, Generation of Co and Smoke During Underventilated Combustion, Combustion and Flame **1994**; 98 (1-2): 20-34, IN23-IN24

[14] Troitzsch J, Plastics Flammability Handbook, Carl Hanser Verlag, München **2004**

[15] Green J, Mechanisms for Flame Retardancy and Smoke Suppression -a Review, Journal of Fire Sciences **1996**; 14 (6): 426-442

[16] Camino G, Costa L and Luda di Cortemiglia MP, Overview of Fire Retardant Mechanisms, Polymer Degradation and Stability **1991**; 33 (2): 131-154

[17] Hornsby PR, Fire Retardant Fillers for Polymers, International Materials Reviews **2001**; 46 (4): 199-210

[18] Jimenez M, Duquesne S and Bourbigot S, Intumescent Fire Protective Coating: Toward a Better Understanding of Their Mechanism of Action, Thermochimica Acta **2006**; 449 (1-2): 16-26

[19] Weil ED, Levchik SV, Ravey M and Zhu W, A Survey of Recent Progress in Phosphorus-Based Flame Retardants and Some Mode of Action Studies, Phosphorus, Sulfur, and Silicon and the Related Elements **1999**; 144 (1): 17-20

[20] Horrocks AR, Developments in Flame Retardants for Heat and Fire Resistant Textiles - the Role of Char Formation and Intumescence, Polymer Degradation and Stability **1996**; 54 (2-3): 143-154

[21] Levchik SV and Weil ED, Overview of Recent Developments in the Flame Retardancy of Polycarbonates, Polymer International **2005**; 54 (7): 981-998

[22] Bourbigot S, Bras ML, Leeuwendal R, Shen KK and Schubert D, Recent Advances in the Use of Zinc Borates in Flame Retardancy of Eva, Polymer Degradation and Stability **1999**; 64 (3): 419-425

[23] Lu S-Y and Hamerton I, Recent Developments in the Chemistry of Halogen-Free Flame Retardant Polymers, Progress in Polymer Science **2002**; 27 (8): 1661-1712

[24] Weil ED and Levchik SV, Flame Retardants in Commercial Use or Development for Polyolefins, Journal of Fire Sciences **2008**; 26 (1): 5-43

[25] Rothon RN and Hornsby PR, Flame Retardant Effects of Magnesium Hydroxide, Polymer Degradation and Stability 54 (2-3): 383-385

[26] Hornsby PR, Wang J, Rothon R, Jackson G, Wilkinson G and Cossick K, Thermal Decomposition Behaviour of Polyamide Fire-Retardant Compositions Containing Magnesium Hydroxide Filler, Polymer Degradation and Stability **1996**; 51 (3): 235-249

[27] Hull TR, Witkowski A and Hollingbery L, Fire Retardant Action of Mineral Fillers, Polymer Degradation and Stability **2011**; 96 (8): 1462-1469

[28] Molnarne M, Mizsey P and Schröder V, Flammability of Gas Mixtures: Part 2: Influence of Inert Gases, Journal of Hazardous Materials **2005**; 121 (1-3): 45-49

[29] Camino G, Maffezzoli A, Braglia M, De Lazzaro M and Zammarano M, Effect of Hydroxides and Hydroxycarbonate Structure on Fire Retardant Effectiveness and Mechanical Properties in Ethylene-Vinyl Acetate Copolymer, Polymer Degradation and Stability **2001**; 74 (3): 457-464

[30] Hastie JW, Treasure of the Past Viii: Molecular Basis of Flame Inhibition, Journal of Research of the National Institute of Standards and Technology **2001**; 106 (4): 731-752

[31] Pawlowski KH and Schartel B, Flame Retardancy Mechanisms of Triphenyl Phosphate, Resorcinol Bis(Diphenyl Phosphate) and Bisphenol a Bis(Diphenyl Phosphate) in Polycarbonate/Acrylonitrile–Butadiene–Styrene Blends, Polymer International **2007**; 56 (11): 1404-1414

[32] Perret B, Pawlowski K and Schartel B, Fire Retardancy Mechanisms of Arylphosphates in Polycarbonate (Pc) and Pc/Acrylonitrile-Butadiene-Styrene, Journal of Thermal Analysis and Calorimetry **2009**; 97 (3): 949-958

[33] Braun U, Bahr H, Sturm H and Schartel B, Flame Retardancy Mechanisms of Metal Phosphinates and Metal Phosphinates in Combination with Melamine Cyanurate in Glass-Fiber Reinforced Poly(1,4-Butylene Terephthalate): The Influence of Metal Cation, Polymers for Advanced Technologies **2008**; 19 (6): 680-692

[34] Lewin M, Synergistic and Catalytic Effects in Flame Retardancy of Polymeric Materials - an Overview, Journal of Fire Sciences **1999**; 17 (1): 3-19

[35] Fengel D and Wegener G, Wood Chemistry Ultrastructure Reactions, Walter de Gruyter & Co., Berlin **1984**

[36] Sjöström E, Wood Chemistry Fundamentals and Applications, Acadamic Press, San Diego **1993**

[37] Rowell RM, Handbook of Wood Chemistry and Wood Composites, CRC press, Milton Keynes **2005**

[38] Mohan D, Pittman CU and Steele PH, Pyrolysis of Wood/Biomass for Bio-Oil: A Critical Review, Energy & Fuels **2006**; 20 (3): 848-889

[39] Evans RJ and Milne TA, Molecular Characterization of the Pyrolysis of Biomass, Energy & Fuels **1987**; 1 (2): 123-137

[40] Qian L, Shurong W, Kaige W, Zhongyang L and Kefa C, Pyrolysis of Wood Species Based on the Compositional Analysis, Korean Journal of Chemical Engineering **2009**; 26 (2): 548-553

[41] Yoshio T and Kikuo S, Thermal Decomposition Products of Cellulose, Journal of Applied Polymer Science **1970**; 14 (8): 2003-2013

[42] Mamleev V, Bourbigot S, Le Bras M and Yvon J, The Facts and Hypotheses Relating to the Phenomenological Model of Cellulose Pyrolysis: Interdependence of the Steps, Journal of Analytical and Applied Pyrolysis **2009**; 84 (1): 1-17

[43] Wahyudiono, Sasaki M and Goto M, Recovery of Phenolic Compounds through the Decomposition of Lignin in near and Supercritical Water, Chemical Engineering and Processing: Process Intensification **2008**; 47 (9-10): 1609-1619

[44] Sain M, Park SH, Suhara F and Law S, Flame Retardant and Mechanical Properties of Natural Fibre-Pp Composites Containing Magnesium Hydroxide, Polymer Degradation and Stability **2004**; 83 (2): 363-367

[45] Clerc L, Ferry L, Leroy E and Lopez-Cuesta J-M, Influence of Talc Physical Properties on the Fire Retarding Behaviour of (Ethylene-Vinyl Acetate Copolymer/Magnesium Hydroxide/Talc) Composites, Polymer Degradation and Stability **2005**; 88 (3): 504-511

[46] Haurie L, Fernández AI, Velasco JI, Chimenos JM, Lopez Cuesta J-M and Espiell F, Synthetic Hydromagnesite as Flame Retardant. Evaluation of the Flame Behaviour in a Polyethylene Matrix, Polymer Degradation and Stability **2006**; 91 (5): 989-994

[47] Nie S, Hu Y, Song L, He Q, Yang D and Chen H, Synergistic Effect between a Char Forming Agent (Cfa) and Microencapsulated Ammonium Polyphosphate on the Thermal and Flame Retardant Properties of Polypropylene, Polymers for Advanced Technologies **2008**; 19 (8): 1077-1083

[48] Le Bras M, Duquesne S, Fois M, Grisel M and Poutch F, Intumescent Polypropylene/Flax Blends: A Preliminary Study, Polymer Degradation and Stability **2005**; 88 (1): 80-84

[49] Schartel B, Braun U, Schwarz U and Reinemann S, Fire Retardancy of Polypropylene/Flax Blends, Polymer **2003**; 44 (20): 6241-6250

[50] Matkó S, Toldy A, Keszei S, Anna P, Bertalan G and Marosi G, Flame Retardancy of Biodegradable Polymers and Biocomposites, Polymer Degradation and Stability **2005**; 88 (1): 138-145

[51] Levchik SV, Camino G, Costa L and Levchik GF, Mechanism of Action of Phosphorus-Based Flame Retardants in Nylon 6. I. Ammonium Polyphosphate, Fire and Materials **1995**; 19 (1): 1-10

[52] Green J, A Review of Phosphorus-Containing Flame Retardants, Journal of Fire Sciences **1992**; 10 (6): 470-487

[53] Bourbigot S, Bras ML, Duquesne S and Rochery M, Recent Advances for Intumescent Polymers, Macromolecular Materials and Engineering **2004**; 289 (6): 499-511

[54] Almeras X, Le Bras M, Poutch F, Bourbigot S, Marosi G and Anna P, Effect of Fillers on Fire Retardancy of Intumescent Polypropylene Blends, Macromolecular Symposia **2003**; 198 (1): 435-448

[55] Bourbigot S, Bras ML and Delobel R, Carbonization Mechanisms Resulting from Intumescence Association with the Ammonium Polyphosphate-Pentaerythritol Fire Retardant System, Carbon **1993**; 31 (8): 1219-1230

[56] Shriver DF, Atkins PW and Langford CH, Inorganic Chemistry, Oxford University Press, Oxford **1994**

[57] Braun U and Schartel B, Effect of Red Phosphorus and Melamine Polyphosphate on the Fire Behavior of Hips, Journal of Fire Sciences **2005**; 23 (1): 5-30

[58] Braun U and Schartel B, Flame Retardant Mechanisms of Red Phosphorus and Magnesium Hydroxide in High Impact Polystyrene, Macromolecular Chemistry and Physics **2004**; 205 (16): 2185-2196

[59] Peters EN, Flame-Retardant Thermoplastics. I. Polyethylene–Red Phosphorus, Journal of Applied Polymer Science **1979**; 24 (6): 1457-1464

[60] Granzow A, Ferrillo RG and Wilson A, The Effect of Elemental Red Phosphorus on the Thermal Degradation of Poly(Ethylene Terephthalate), Journal of Applied Polymer Science **1977**; 21 (6): 1687-1697

[61] Wang Z, Han E and Ke W, Influence of Expandable Graphite on Fire Resistance and Water Resistance of Flame-Retardant Coatings, Corrosion Science **2007**; 49 (5): 2237-2253

[62] Duquesne S, Delobel R, Le Bras M and Camino G, A Comparative Study of the Mechanism of Action of Ammonium Polyphosphate and Expandable Graphite in Polyurethane, Polymer Degradation and Stability **2002**; 77 (2): 333-344

[63] Modesti M, Lorenzetti A, Simioni F and Camino G, Expandable Graphite as an Intumescent Flame Retardant in Polyisocyanurate-Polyurethane Foams, Polymer Degradation and Stability **2002**; 77 (2): 195-202

[64] Duquesne S, Le Bras M, Bourbigot S, Delobel R, Poutch F, Camino G, Eling B, Lindsay C and Roels T, Analysis of Fire Gases Released from Polyurethane and Fire-Retarded Polyurethane Coatings, Journal of Fire Sciences **2000**; 18 (6): 456-482

[65] Meng X-Y, Ye L, Zhang X-G, Tang P-M, Tang J-H, Ji X and Li Z-M, Effects of Expandable Graphite and Ammonium Polyphosphate on the Flame-Retardant and Mechanical Properties of Rigid Polyurethane Foams, Journal of Applied Polymer Science **2009**; 114 (2): 853-863

[66] Ehrenstein GW, Riedel G and Trawiel P, Thermal Analysis of Plastics Theory and Practice, Hanser, München **2004**

[67] Materazzi S, Thermogravimetry - Infrared Spectroscopy (Tg-Ftir) Coupled Analysis, Applied Spectroscopy Reviews **1997**; 32 (4): 385-404

[68] Babrauskas V, Development of the Cone Calorimeter—a Bench-Scale Heat Release Rate Apparatus Based on Oxygen Consumption, Fire and Materials **1984**; 8 (2): 81-95

[69] Babrauskas V and Peacock RD, Heat Release Rate: The Single Most Important Variable in Fire Hazard, Fire Safety Journal **1992**; 18 (3): 255-272

[70] Huggett C, Estimation of Rate of Heat Release by Means of Oxygen Consumption Measurements, Fire and Materials **1980**; 4 (2): 61-65

[71] Walters RN, Hackett SM and Lyon RE, Heats of Combustion of High Temperature Polymers, Fire and Materials **2000**; 24 (5): 245-252

[72] Schartel B, Pawlowski KH and Lyon RE, Pyrolysis Combustion Flow Calorimeter: A Tool to Assess Flame Retarded Pc/Abs Materials?, Thermochimica Acta **2007**; 462 (1-2): 1-14

[73] Lyon RE and Walters RN, Pyrolysis Combustion Flow Calorimetry, Journal of Analytical and Applied Pyrolysis **2004**; 71 (1): 27-46

[74] Lyon RE and Walters RN, A Microscale Combustion Calorimeter, Final Report DOT/FAAAR-01/117, 2002

[75] Cogen JM, Lin TS and Lyon RE, Correlations between Pyrolysis Combustion Flow Calorimetry and Conventional Flammability Tests with Halogen-Free Flame Retardant Polyolefin Compounds, Fire and Materials **2009**; 33 (1): 33-50

[76] DIN EN ISO 9239-1:2002, Prüfung Zum Brandverhalten Von Bodenbeläge Teil1: Bestimmung Der Brandverhaltens Bei Beanspruchung Mit Einem Wärmestrahler

[77] DIN EN 13501-1:2007+A1:2009, Klassifizierung Von Bauprodukten Und Bauarten Zu Ihrem Brandverhalten –

Teil 1: Klassifizierung Mit Den Ergebnissen Aus Den Prüfungen Zum Brandverhalten Von Bauprodukten

[78] McGrattan K, Klein B, Hostikka S and Floyd J, Fire Dynamics Simulator (Version 5) User's Guide, National Institute of Standards and Technology Special Publication **2007**; 1019 (5): 200

[79] McGrattan K, Baum H, Rehm R, Mell W and McDermott R, Fire Dynamics Simulator (Version 5) Technical Reference Guide, National Institute of Standards and Technology Special Publication **2007**; 1018 (5): 94

[80] Ryder NL, Sutula JA, Schemel CF, Hamer AJ and Brunt VV, Consequence Modeling Using the Fire Dynamics Simulator, Journal of Hazardous Materials **2004**; 115 (1-3): 149-154

[81] Prasad K, Krämer R, Marsh N, Nyden M, Ohlemiller T and Zammarano M Numerical Simulation of Fire Spread on Polyurethane Foam Slabs, 11th international conference on fire and materials, London **Year**

[82] ISO 5660-1:2002, Reaction-to-Fire Tests - Heat Release, Smoke Production and Mass Loss Rate Part 1: Heat Release Rate (Cone Calorimeter Method)

[83] Lindholm J, Brink A and Hupa M, Influence of Decreased Sample Size on Cone Calorimeter Results, Fire and Materials **2011**; 36 (1): 63-73

[84] Zhang X, Hendro W, Fujii M, Tomimura T and Imaishi N, Measurements of the Thermal Conductivity and Thermal Diffusivity of Polymer Melts with the Short-Hot-Wire Method, International Journal of Thermophysics **2002**; 23 (4): 1077-1090

[85] Suleiman BM, Larfeldt J, Leckner B and Gustavsson M, Thermal Conductivity and Diffusivity of Wood, Wood Science and Technology **1999**; 33 (6): 465-473

[86] Di Blasi C, Modeling Chemical and Physical Processes of Wood and Biomass Pyrolysis, Progress in Energy and Combustion Science **2008**; 34 (1): 47-90

[87] Spearpoint MJ and Quintiere JG, Predicting the Burning of Wood Using an Integral Model, Combustion and Flame **2000**; 123 (3): 308-325

[88] Beaumont O and Schwob Y, Influence of Physical and Chemical Parameters on Wood Pyrolysis, Industrial & Engineering Chemistry Process Design and Development **1984**; 23 (4): 637-641

[89] Pettersen Roger C, The Chemistry of Solid Wood 207, 57-126, American Chemical Society, **1984**

[90] Levchik SV and Weil ED, Overview of the Recent Literature on Flame Retardancy and Smoke Suppression in Pvc, Polymers for Advanced Technologies **2005**; 16 (10): 707-716

[91] Lum RM, Antimony Oxide–Pvc Synergism: Laser Pyrolysis Studies of the Interaction Mechanism, Journal of Polymer Science: Polymer Chemistry Edition **1977**; 15 (2): 489-497

[92] Basfar AA, Effect of Various Combinations of Flame-Retardant Fillers on Flammability of Radiation Cross-Linked Poly(Vinyl Chloride) (Pvc), Polymer Degradation and Stability **2003**; 82 (2): 333-340

[93] Gupta M, Yang J and Roy C, Specific Heat and Thermal Conductivity of Softwood Bark and Softwood Char Particles, Fuel **2003**; 82 (8): 919-927

[94] Rinaldi R and Schüth F, Acid Hydrolysis of Cellulose as the Entry Point into Biorefinery Schemes, ChemSusChem **2009**; 2 (12): 1096-1107

[95] Suárez-García F, Martínez-Alonso A and Tascón JMD, A Comparative Study of the Thermal Decomposition of Apple Pulp in the Absence and Presence of Phosphoric Acid, Polymer Degradation and Stability **2002**; 75 (2): 375-383

[96] Scheirs J, Camino G and Tumiatti W, Overview of Water Evolution During the Thermal Degradation of Cellulose, European Polymer Journal **2001**; 37 (5): 933-942

[97] Levchik SV, Levchik GF, Camino G and Costa L, Mechanism of Action of Phosphorus-Based Flame Retardants in Nylon 6. Ii. Ammonium Polyphosphate/Talc, Journal of Fire Sciences **1995**; 13 (1): 43-58

[98] Bras ML, Wilkie CA, Bourbigot S, Duquesne S and Jama C, Fire Retardancy of Polymers New Applications of Mineral Fillers, The Royal Society of Chemistry, **2005**

[99] Montgomery RB, Viscosity and Thermal Conductivity of Air and Diffusivity of Water Vapor in Air, Journal of Meteorology **1947**; 4 (6): 193-196

[100] Zhigang L and Kim AK, A Review of Water Mist Fire Suppression Systems-Fundamental Studies, Journal of Fire Protection Engineering **1999**; 10 (3): 32-50

[101] Bryden KM and Hagge MJ, Modeling the Combined Impact of Moisture and Char Shrinkage on the Pyrolysis of a Biomass Particle [Small Star, Filled], Fuel **2003**; 82 (13): 1633-1644

[102] Halpern Y, Mott DM and Niswander RH, Fire Retardancy of Thermoplastic Materials by Intumescence, Industrial & Engineering Chemistry Product Research and Development **1984**; 23 (2): 233-238

[103] Petrella RV, The Assessment of Full-Scale Fire Hazards from Cone Calorimeter Data, Journal of Fire Sciences **1994**; 12 (1): 14-43

12. Appendix

The appendix contains the source code of the FDS simulation:

```
&HEAD CHID='WPC_Cone_Calorimeter',
&MESH IJK=36,24,30, XB=-0.18,0.18,-0.12,0.12,-0.042,0.258 /
&TIME T_END=2000., WALL_INCREMENT = 1, DT = 0.01 /
&DUMP DT_PL3D=10000000. /

&SURF ID='hood', VEL=0.06, COLOR='IVORY BLACK' /

&SURF ID = 'Cone',
     RGB = 255,102,0,
     TMP_FRONT = 781.0 /

&SURF ID = 'backing'
     STRETCH_FACTOR = 1.
     CELL_SIZE_FACTOR = 0.5
     MATL_ID = 'ceramic_wool'
     THICKNESS = 0.02 /

&SURF ID = 'alu_foil'
     STRETCH_FACTOR = 1.
     CELL_SIZE_FACTOR = 0.5
     MATL_ID = 'alu'
     THICKNESS = 0.001 /

&SURF ID = 'WPC'
     STRETCH_FACTOR = 1.
     CELL_SIZE_FACTOR = 0.5
     MATL_ID(1,1:5) = 'water', 'talc', 'poly', 'cell', 'pp' ,
     MATL_MASS_FRACTION(1,1:5)= 0.02, 0.049, 0.1595, 0.3305, 0.441 ,
```

```
    THICKNESS = 0.022, /

&MATL ID = 'water'
    DENSITY = 1000.
    CONDUCTIVITY = 0.6
    SPECIFIC_HEAT = 4.19
    N_REACTIONS = 1
    A = 1E22
    E = 1.62E+05
    NU_WATER = 1.0
    HEAT_OF_REACTION = 2260. /

&MATL ID = 'talc',
    SPECIFIC_HEAT_RAMP = 'cp_wpc',
    CONDUCTIVITY = 0.35,
    DENSITY = 1200.00 /

&MATL ID = 'poly',
    SPECIFIC_HEAT_RAMP = 'cp_wpc',
    CONDUCTIVITY = 0.35,
    DENSITY = 1200.00,
    HEAT_OF_COMBUSTION = 0.99E004,
    N_REACTIONS = 1,
    NU_FUEL = 0.8,
    NU_RESIDUE = 0.2,
    RESIDUE = 'Char'
    A = 5.7E6
    E = 1.01E5 /

&MATL ID = 'cell',
    SPECIFIC_HEAT_RAMP = 'cp_wpc',
```

```
    CONDUCTIVITY = 0.35,
    DENSITY = 1200.00,
    HEAT_OF_COMBUSTION = 0.99E004,
    N_REACTIONS = 1,
    NU_FUEL = 0.8,
    NU_RESIDUE = 0.2,
    RESIDUE = 'Char'
    A = 4.0E12
    E = 1.8E5 /

&MATL ID = 'pp',
    SPECIFIC_HEAT_RAMP = 'cp_wpc',
    CONDUCTIVITY = 0.35 ,
    DENSITY = 1200.00,
    HEAT_OF_COMBUSTION = 3.61E004,
    N_REACTIONS = 1,
    NU_FUEL = 0.95,
    NU_RESIDUE = 0.05,
    RESIDUE = 'talc'
    A = 2.0E20
    E = 3.2E5 /

&MATL ID = 'Char'
    SPECIFIC_HEAT_RAMP = 'cp_char'
    CONDUCTIVITY = 0.1,
    DENSITY = 300 /

&MATL ID = 'ceramic_wool'
    SPECIFIC_HEAT = 1.0,
    CONDUCTIVITY = 1.0,
    DENSITY = 140. /
```

```
&MATL ID = 'alu'
      SPECIFIC_HEAT = 0.9
      CONDUCTIVITY = 235.0
      DENSITY = 2700. /
```

functions of heat capacity and thermal conductivity

```
&RAMP ID = 'cp_wpc', T =   0.0, F = 1.04 /
&RAMP ID = 'cp_wpc', T = 099.0, F = 1.37 /
&RAMP ID = 'cp_wpc', T = 121.0, F = 1.43 /
&RAMP ID = 'cp_wpc', T = 142.0, F = 1.73 /
&RAMP ID = 'cp_wpc', T = 150.0, F = 2.05 /
&RAMP ID = 'cp_wpc', T = 160.0, F = 2.92 /
&RAMP ID = 'cp_wpc', T = 164.0, F = 3.9  /
&RAMP ID = 'cp_wpc', T = 168.0, F = 1.65 /
&RAMP ID = 'cp_wpc', T = 171.0, F = 1.4  /
&RAMP ID = 'cp_wpc', T = 227.0, F = 1.4  /

&RAMP ID = 'cp_char', T =   0.0, F = 0.95 /
&RAMP ID = 'cp_char', T = 125.0, F = 1.14 /
&RAMP ID = 'cp_char', T = 180.0, F = 1.06 /
```

cone heater

```
&OBST XB=-0.1000,0.1000,-0.1000,0.1000,0.0300,0.0500, SURF_ID='Cone'/ plate1
(bottom)
&OBST XB=-0.0900,0.0900,-0.0900,0.0900,0.0500,0.0700, SURF_ID='Cone'/ plate2
&OBST XB=-0.0800,0.0800,-0.0800,0.0800,0.0700,0.0900, SURF_ID='Cone'/ plate3
&OBST XB=-0.0700,0.0700,-0.0700,0.0700,0.0900,0.1100, SURF_ID='Cone'/ plate4
&OBST XB=-0.0600,0.0600,-0.0600,0.0600,0.1100,0.1300, SURF_ID='Cone'/ plate5
&OBST XB=-0.0500,0.0500,-0.0500,0.0500,0.1300,0.1500, SURF_ID='Cone'/ plate6
```

&OBST XB=-0.0400,0.0400,-0.0400,0.0400,0.1500,0.1700, SURF_ID='Cone'/ plate7 (top)

&HOLE XB=-9.0000000E-002,9.0000000E-002,-9.0000000E-002,9.0000000E-002,3.0000000E-002,5.0000000E-002/ hole1

&HOLE XB=-8.0000000E-002,8.0000000E-002,-8.0000000E-002,8.0000000E-002,5.0000000E-002,7.0000000E-002/ hole2

&HOLE XB=-7.0000000E-002,7.0000000E-002,-7.0000000E-002,7.0000000E-002,7.0000000E-002,9.0000000E-002/ hole3

&HOLE XB=-6.0000000E-002,6.0000000E-002,-6.0000000E-002,6.0000000E-002,9.0000000E-002,1.1000000E-001/ hole4

&HOLE XB=-5.0000000E-002,5.0000000E-002,-5.0000000E-002,5.0000000E-002,1.1000000E-001,1.3000000E-001/ hole5

&HOLE XB=-4.0000000E-002,4.0000000E-002,-4.0000000E-002,4.0000000E-002,1.3000000E-001,1.5000000E-001/ hole6

&HOLE XB=-3.0000000E-002,3.0000000E-002,-3.0000000E-002,3.0000000E-002,1.5000000E-001,1.7000000E-001/ hole7

exhaust hood

&OBST XB = -0.1,0.1,-0.1,0.1,0.24,0.258, SURF_ID='INERT'/ hood

&VENT XB = -0.1,0.1,-0.1,0.1,0.24,0.24, SURF_ID='hood'/ hood

sample holder

&OBST XB = -0.05,0.05,-0.05,0.05,-0.042,-0.022, SURF_ID = 'backing', COLOR='YELLOW' /

&OBST XB = -0.05,0.05,-0.051,-0.05,-0.042,-0.022, SURF_ID = 'alu_foil', COLOR='BLACK' /

&OBST XB = -0.05,0.05,0.05,0.051,-0.042,-0.022, SURF_ID = 'alu_foil', COLOR='BLACK' /

&OBST XB = -0.051,-0.05,-0.05,0.05,-0.042,-0.022, SURF_ID = 'alu_foil', COLOR='BLACK' /

&OBST XB = 0.05,0.051,-0.05,0.05,-0.042,-0.022, SURF_ID = 'alu_foil', COLOR='BLACK' /

sample

```
&OBST XB = -0.05,0.05,-0.05,0.05,-0.022,0.0, SURF_ID = 'WPC', COLOR='BROWN' /

boundaries

&VENT MB = 'ZMIN', SURF_ID = 'OPEN' /
&VENT MB = 'ZMAX', SURF_ID = 'OPEN' /

&TAIL /
```

13. Danksagung

Ich möchte mich an dieser Stelle bei allen Menschen bedanken, die mir bei der Erstellung meiner Doktorarbeit mit Rat und Tat zur Seite gestanden haben.

Mein Dank gilt Frau Dr. U. Braun und Frau Dr. A. Hofmann für die Initiierung dieser Arbeit im Rahmen der BAM Innovationsoffensive. Herrn Prof. Dr. M.H. Wagner und Herrn Prof. Dr. M. Maskos danke ich für die Begutachtung meiner Arbeit und Herrn Prof. Dr. W. Reimers für die Übernahme des Vorsitzes des Promotionsausschusses.

Ganz besonders möchte ich mich noch einmal bei Frau Dr. U. Braun für ihre wunderbare Betreuung in jeglicher Hinsicht bedanken.

Des weiteren bedanke ich mich bei Herrn Dr. Schulte und der Firma Werzalit für die finanzielle Unterstützung, die Bereitstellung der Probenmaterialien, sowie der kooperativen Zusammenarbeit.

Mein Dank gilt auch Herrn Dr. B. Schartel für die freundliche Zusammenarbeit und dafür, dass ich problemlos die Messgeräte seiner Arbeitsgruppe nutzen durfte. Des weiteren bedanke ich mich dafür, dass ich die Möglichkeit hatte an zwei Seminarfahrten mit ihm Teil nehmen zu dürfen.

Ich möchte mich außerdem bei allen Kollegen aus den früheren Fachgruppen 6.3 und 7.3 für ein überaus freundliches Arbeitsklima und ihre Hilfsbereitschaft bedanken. Ganz besonders danke ich dabei: Herrn H. Bahr, Frau B. Perret, Frau E. Wawrzyn, Frau M. Despinasse, Herrn F. Kempel, Frau T. Raspe, Herrn D. Neubert, Herrn E. Dümichen, Herrn P. Klack, Frau K. Brademann-Jock, Herrn B. Klaffke, Frau G. Wu, Frau B. Dittrich, Herrn S. Brehme, Herrn A. Hörold, Frau S. Krüger, Herrn J. Deubel und Frau K. Bajer.

Insbesondere bedanke ich mich bei meinen Eltern, meiner Familie und meinen Freunden für Rückhalt in jeder Lebenslage.